High-time-resolution chemical composition and source apportionment of $PM_{2.5}$ in northern Chinese cities: implications for policy

Yong Zhang[1,2,3], Jie Tian[1,2,4], Qiyuan Wang[1,2,3,4*], Lu Qi[5], Manousos Ioannis Manousakas[5], Yuemei Han[1,4], Weikang Ran[1,2], Yele Sun[6], Huikun Liu[1,2,4], Renjian Zhang[6], Yunfei Wu[6], Tianqu Cui[5], Kaspar Rudolf Daellenbach[5], Jay Gates Slowik[5], André S. H. Prévôt[5], Junji Cao[6*]

[1] State Key Laboratory of Loess and Quaternary Geology, Institute of Earth Environment, Chinese Academy of Sciences, Xi'an 710061, China
[2] National Observation and Research Station of Regional Ecological Environment Change and Comprehensive Management in the Guanzhong Plain, Shaanxi, Xi'an 710061, China
[3] University of Chinese Academy of Sciences, Beijing 100049, China
[4] Center for Excellence in Quaternary Science and Global Change, Xi'an 710061, China
[5] Laboratory of Atmospheric Chemistry, Paul Scherrer Institute (PSI), Villigen 5232, Switzerland
[6] Institute of Atmospheric Physics, Chinese Academy of Sciences, Beijing 100029, China

Correspondence: wangqy@ieecas.cn (Qiyuan Wang), jjcao@mail.iap.ac.cn (Junji Cao).

Abstract: Fine particulate matter ($PM_{2.5}$) pollution is still one of China's most important environmental issues, especially in northern cities during wintertime. In this study, intensive real-time measurement campaigns were conducted in Xi'an, Shijiazhuang, and Beijing to investigate the chemical characteristics and source contributions of $PM_{2.5}$ and explored the formation ~~progress~~ of heavy pollution for policy implications. The chemical compositions of $PM_{2.5}$ in three cities were all dominated by organic aerosol (OA) and nitrate (NO_3^-). Results of source apportionment analyzed by hybrid environmental receptor model (HERM) showed that the ~~secondary nitrate plus sulfate~~secondary formation source contributed higher to $PM_{2.5}$ compared to other primary sources. Biomass burning was the dominant primary source in three pilot cities. The contribution of coal combustion to $PM_{2.5}$ is non-negligible in Xi'an and Shijiazhuang but is no longer an important contributor in the capital city of Beijing due to the execution of a strict coal-banning policy. The potential formation mechanisms of secondary aerosol in three cities were further explored by establishing the correlations between the ~~secondary nitrate plus sulfate~~secondary formation source and aerosol liquid water content (ALWC), and O_x ($O_3 + NO_2$), respectively. The results showed that photochemical oxidation and aqueous-phase reaction were two important pathways of secondary aerosol formation. According to sources variations, air pollution events that occurred in campaigns were classified into three types: biomass combustion dominated, ~~secondary nitrate plus sulfate~~secondary formation source dominated, and a combination of primary and secondary sources. Additionally, this study compared the changes in chemical composition and source contributions of $PM_{2.5}$ in past decades. The results suggested that the clean energy replacements for rural household should be

urgently encouraged to reduce the primary source emissions in northern China, and collaborative control on ozone and particulate matter need to be continuously promoted to weaken the atmosphere oxidation capacity for the sake of reducing secondary aerosol formation.

1. Introduction

Fine particulate matter ($PM_{2.5}$, aerodynamic diameter <= 2.5 μm) is of large concern because of its adverse effects on both natural environment (Kuniyal and Guleria, 2019; Kuo et al., 2013) and human health (Pöschl, 2005; Shen et al., 2021; Zeng and He, 2019). With the soaring economic growth and urbanization in China, $PM_{2.5}$ pollution has been a most serious environmental issue in recent decades (Chan and Yao, 2008; He et al., 2002; Pui et al., 2014; Zhang et al., 2013). The most impressive case is that an extremely severe haze pollution episode occurred in eastern and central China in January 2013 with peak value of $PM_{2.5}$ concentration over 500 μg m^{-3}. This month had been reported as the haziest month in the past 60 years in Beijing, China (Wang et al., 2014; Huang et al., 2014). Thereafter, aiming to improve air quality, the China central government ~~implemented~~ issued the Air Pollution Prevention and Control Action Plan (APCAP) in September 2013 (http://www.gov.cn/zwgk/2013-09/12/content_2486773.htm, in Chinese), and the Three-year Action Plan to Fight Air Pollution (TAPFAP) in June 2018 (http://www.gov.cn/zhengce/content/2018-07/03/content_5303158.htm, in Chinese). With the implementation of strict pollution controls, air quality in northern China has improved significantly over the past decade (Wang et al., 2020a, 2017; Li et al., 2020). Previous studies show that $PM_{2.5}$ concentration decreased notably in past two decades, and the composition of organic aerosol (OA), black carbon (BC) and sulfate (SO_4^{2-}) decreased as well, while the ammonium (NH_4^+) slightly increased and nitrate (NO_3^-) increased obviously. In ~~perspective~~ terms of $PM_{2.5}$ sources, contribution of secondary source increased obviously while contribution of industrial emission and coal combustion decreased due to elimination of industries and enterprises with high pollutant emissions, promotion of desulfurization in industrial facilities, replacement of clean energy, and optimization of industrial and energy structures (Lu et al., 2021; Ma et al., 2022;Tao et al., 2017; Wang et al., 2019). However, there is still a significant gap between the $PM_{2.5}$ concentration in northern China and its latest recommendations on air quality guideline (5 μg m^{-3}) by the World Health Organization (https://apps.who.int/iris/bitstream/handle/10665/345329/9789240034228-eng.pdf, page 78). In addition, severe $PM_{2.5}$ pollutions still frequently occurred in northern China during wintertime (Guo et al., 2021; Li et al., 2017a, 2021b). To figure out the causes behind the pollutions and further improve ~~furtherly~~ air quality in northern China, it is essential to use online high-time-resolution source apportionment technology to understand the chemical composition and source contribution of $PM_{2.5}$ in those pollution events.

Recently, more research on measurements of $PM_{2.5}$ and its source apportionments were conducted using online high-time-resolution technologies (Li et al., 2017c; Wang et al., 2021a; Elser et al., 2015). Compared to traditional offline filter-based approach, online methods characterize the short-time variation of $PM_{2.5}$. It allows for distinguishing the rapid changes and evolutions of chemical components, and is particularly profitable to gain knowledge on the formations of heavy air pollution or episode events (Liu et al., 2016; Ouyang et al., 2019; Zheng et al., 2016; Elser et al., 2015). For instance, Lv et al. (2021) employed a Positive matrix factorization (PMF) model with high-time-resolution online $PM_{2.5}$ data to accurately quantify and distinguish the source distributions in Beijing during two haze episodes in January 2019. Liu et~~.~~ al. (2019) recognized the main drivers of haze event occurred in winter Beijing in 2016 according to high-time-resolution source apportionment of $PM_{2.5}$ with multiple models. Furthermore, Wang et al. (2021b) found that vehicle emission contributed most to $PM_{2.5}$ during pollution episodes in downtown Lanzhou based on high-resolution online data source apportionment. Currently, to fully understand and solve heavy pollution events in winter that troubles local governments in northern cities of China (Wang et al., 2022b; Xu et al., 2022; Zhou et al., 2022), more advanced online measurement, and source apportionment is a better choice (Tao et al., 2015). It should be pointed out that previous researches were mainly focused on individual cities, and those results have some limitations in guiding the improvement of air quality in the entire northern region of China. Therefore, it is necessary to conduct comparative research among multiple cities.

Considering the differences in geographical location, population, economy, industrial/energy structure, air quality, and depth of air pollution control measures among different cities, three cities in northern China including Beijing, Shijiazhuang and Xi'an were chosen as pilot research subjects. The cities of Beijing and Shijiazhuang are located ~~to~~ in the North China Plain, which is one of the most polluted regions in China (Chan and Yao, 2008). Beijing is the capital of China and its air quality has significantly improved under the implementation of the strictest clean air policy since 2013 (Li et al., 2021a; Pang et al., 2021; Vu et al., 2019; Zhang et al., 2020). However, the city was still plagued by pollution events in wintertime (Wang et al., 2020b; Yang et al., 2022c; Zhou et al., 2022). Shijiazhuang was recognized as one of the most serious air pollution cities worldwide (Liu et al., 2018b; Huang et al., 2019). Its air quality had also improved under the implementation of the Clean Air Plan, whereas its annual $PM_{2.5}$ concentration was still unable to meet the China's National Ambient Air Quality Standards (NAAQS-II) of 35 $\mu g\ m^{-3}$ until 2021 (Fig. S1). Xi'an is located ~~to~~ in the Fenwei Plain, which is a region that suffered from heavy pollution and was designated as a key region for TAPFAP in 2018 (Cao and Cui, 2021). Compared with Beijing and Shijiazhuang, high-intensity air pollution controls in Xi'an started late due to a lack of financial support. And the annual $PM_{2.5}$

concentration in Xi'an could not meet the NAAQS-II until 2021 as well (Fig. S1). Meanwhile, it is still unclear ~~to~~ about the actual causes of the pollution, either topography, meteorological conditions, or local emissions (Chen et al., 2021; Tian et al., 2022; Wang et al., 2015, 2022b). In this study, we conducted intensive real-time observation of $PM_{2.5}$ chemical components in Xi'an, Shijiazhuang, and Beijing during wintertime. The objectives are 1) to determine the characteristics of $PM_{2.5}$ and its chemical components in the three typical northern China cities during wintertime; 2) to quantify the source contribution and explore the potential formation mechanism of secondary aerosols; 3) to explore the unique causes of heavy pollution events in different cities; and 4) to provide suggestions on establishment of efficient policies for air quality continuous improvement. This study provides scientific guidance for developing policy on air quality improvement for northern China cities.

2. Methods

2.1 Sampling sites and periods

In this study, intensive online measurements of $PM_{2.5}$ were conducted at three pilot cities of Xi'an, Shijiazhuang, and Beijing during wintertime (Fig. 1). The sampling sites in Xi'an and Beijing are located at two Chinese Academy of Sciences (CAS) stations. The one in Xi'an is the Guanzhong Plain Ecological Environment Change and Comprehensive Treatment National Observation and Research Station, Institute of Earth Environment (IEE) (34.24°N, 108.87°E), and another one in Beijing is Tower Branch of the Institute of Atmospheric Physics (IAP) (39.98°N, 116.39°E). Both two sites are surrounded by commercial and residential buildings without intense industrial emissions nearby. Previous studies indicated that these two sites were influenced by biomass and coal burning for heating and cooking during wintertime as well as usual local traffic emissions (Tian et al., 2021; Xu et al., 2021). The sampling site in Shijiazhuang is situated in the courtyard of Hebei Sailhero Environmental Protection High-tech Co., Ltd. (38.04°N, 114.65°E), which is surrounded by pharmaceutical and machine-building industries and close to the streets. The intensive campaigns were continuously conducted for ~1 month in each city (i.e., 12 December 12th 2020 to January 7th 2021 in Xi'an, December 20th 2021 to January 24th 2022 in Shijiazhuang, and January 17th 2021 to February 20th 2021 in Beijing).

2.2 Online measurements of $PM_{2.5}$ chemical components

2.2.1 Organic aerosol and inorganic ions

Concentrations of OA, NO_3^-, SO_4^{2-}, ammonium (NH_4^+), and chloride (Cl^-) in $PM_{2.5}$ at a 15-minute time resolution

were monitored by a quadrupole aerosol chemical speciation monitor (Q-ACSM, Aerodyne Research Inc., Billerica, Massachusetts, USA) equipped with a $PM_{2.5}$ lens. The detailed operational principles and calibration method of the Q-ACSM are described elsewhere (Ng et al., 2011; Hu et al., 2017). First, the sampled ambient air stream passed through a PM_{10} impactor inlet and a Nafion® dryer (MD-700-24F-3; Perma Pure, Inc., Lakewood, NJ, USA) with a flowrate of 5 L min^{-1} before entering the Q-ACSM chamber. Then, the pre-treatment particles passed through a 100 μm critical orifice at 0.1 L min^{-1} and were focused into a narrow beam by an aerodynamic intermediate pressure lens. The focused particle beam was flash vaporized by a capture vaporizer (CV) at ~600 C°. The vaporized compounds were then ionized by an electron impactor (EI) ionization source at 70 eV and subsequently analyzed by the quadrupole mass spectrometer.

Based on calibration system consists of an atomizer (Model 9302, TSI Inc., Shoreview, MN, USA), a differential mobility analyzer (DMA, TSI model 3080, TSI Inc.), and a condensation particle counter (CPC, TSI model 3772, TSI Inc.), ammonium nitrate (NH_4NO_3) and ammonium sulfate ($(NH_4)_2SO_4$) aerosol were used for calibration. The raw data of Q-ACSM were analyzed by the ACSM local tool (V1.5.3.5, Aerodyne Research Inc., Billerica, Massachusetts, USA) compiled with Igor Pro 6.37 (Wavemetrics, Lake Oswego, OR, USA). The response factors (RFs) for NO_3^- in Xi'an, Shijiazhuang, and Beijing were set as 2.03×10^{-11}, and 5.9×10^{-11}, 2.20×10^{-11}, respectively, and the relative ionization efficiencies (RIEs) for NH_4^+ and SO_4^{2-} were set as 8.06 and 0.83 in Xi'an, 5.82 and 0.30 in Shijiazhuang, 6.31 and 0.38 in Beijing, respectively. Other RIEs for NO_3^-, OA, and Cl^- were set as default values of 1.4, 1.1, and 1.3, respectively (Ng et al., 2011). In addition, the collection efficiency (CE) value of Q-ACSM equipped with a $PM_{2.5}$ lens was recommended as 1 based on laboratory simulation experiments by Xu et al. (2017). Finally, the chemical components monitored by Q-ACSM was corrected by the results of offline filter sampling experiments during the same periods (Fig. S2).

2.2.2 Black carbon

BC concentration in $PM_{2.5}$ was obtained by an Aethalometer (Model AE33, Magee Scientific Inc., Berkeley, CA, USA) with a 1-minute time resolution. The AE33 monitors the light attenuation of seven wavelengths (λ = 370, 470, 525, 590, 660, 880, and 940 nm), and the light attenuation at λ = 880 nm was used to calculate BC concentration (Wang et al., 2019; Drinovec et al., 2015). Briefly, the ambient air was first sampled on a filter tape inside the instrument through a $PM_{2.5}$ cyclone (SCC-1.829, BGI Inc., USA) at a flowrate of 5 L min^{-1}. The entering particles were divided into two sample spots on the filter through two channels with different follows. Then the light

attenuation transmitted through two parallel spots was detected. For quality accuracies of monitoring, the sampled particles were desiccated with a Nafion® dryer (MD-700-24F-3; Perma Pure, Inc., Lakewood, NJ, USA) before entering the AE33. Furthermore, a real-time loading effect compensation algorithm based on two spots measurement was used to eliminate the nonlinear loading effects of the Aethalometer. A detailed description of the Model AE33 principle can be found in Drinovec et al. (2015).

2.2.3 Elements

Twenty-four elements, including Si, K, Ca, V, Cr, Mn, Fe, Co, Ni, Cu, Zn, Ga, As, Se, Ag, Cd, Sn, Ba, Au, Hg, Th, Pb, and Pd in $PM_{2.5}$, were analyzed by a Xact625 Ambient Metals Monitor (Cooper Environmental Services, Tigard, Oregon, USA) with a 1-hour time resolution. Si, K, Ca, Cr, Mn, Fe, Ni, Cu, Zn, As, Se, Ba, and Pb were selected for further analysis in Xi'an and Beijing, while other elements were excluded due to most of their concentration below the method detection limit. In Shijiazhuang, S, Cl, and Ti were analyzed by replacement of Ga, Ag and Au, respectively. Finally, Si, K, Ca, Ti, Cr, Mn, Fe, Ni, Cu, Zn, As, Se, Ba, and Pb were selected for further analysis. The description and detection principles of Xact625 were introduced by Furger et al. (2020) and Rai et al. (2020). In brief, the ambient air stream was firstly sampled on a Teflon filter tape inside the instrument through a $PM_{2.5}$ cyclone inlet at a constant flow rate of 16.7 L min^{-1}, and then the sample was automatically analyzed by nondestructive energy-dispersive X-ray fluorescence (XRF) to determine the mass of the species. For quality control and assurance, the Xact625 performed automatic internal quality control by testing the Pd rod every hour to ensure the stability of the instrument. Energy calibration was performed daily from 00:00 to 00:15 and a range calibration from 00:15 to 00:30 local standard time (LST) to monitor any possible shift and instability of the XRF (Liu et al., 2019). During our sampling periods, the concentration of Pd varies within 3 standard deviations (Fig. S3), illustrating the reliable and stable performance of the Xact625.

2.2.4 Complementary data

Online hourly concentrations of $PM_{2.5}$ and gas pollutants (i.e., NO_x, NO_2, CO, SO_2, and O_3) were acquired from the National Air Quality Monitoring Station (https://air.cnemc.cn:18007/). Meteorological parameters, including wind speed (WS), wind direction (WD), relative humidity (RH), and temperature (T) were obtained from National Meteorological Station (http://data.cma.cn/). The detailed information for complementary data was listed in Table S1.

2.3 Data analysis

2.3.1 $PM_{2.5}$ mass reconstruction

Chemical closure was utilized to assess whether chemical compositions can be representative of $PM_{2.5}$. The sum of OA, NO_3^-, SO_4^{2-}, NH_4^+, Cl^-, BC, mineral dust (MD), and trace elements (TE) was considered as the reconstructed $PM_{2.5}$, where MD and TE were calculated as follows (Chow et al., 2015).

$$[MD] = 2.20\times[Al] + 2.49\times[Si] + 1.63\times[Ca] + 2.42\times[Fe] + 1.94\times[Ti] \quad (1)$$

$$[TE] = [K] + [Cr] + [Mn] + [Ni] + [Cu] + [Zn] + [As] + [Se] + [Ba] + [Pb] \quad (2)$$

where [ ] represents the chemical species concentration; [Al] and [Ti] were calculated by the concentration of Ca ([Al] = 4.3×[Ca] and [Ti] = 0.25×[Ca]) (Wei et al., 1991). Good correlations between online and reconstructed $PM_{2.5}$ mass (slope = 0.87–1.10, R^2 = 0.82–0.93) in three pilot cities (Fig. S4) indicated that our measurements could detect major components of $PM_{2.5}$. The $PM_{2.5}$ concentration used in the following discussion referred to the reconstructed $PM_{2.5}$ concentration.

2.3.2 Hybrid environment receptor model

Source apportionment of $PM_{2.5}$ was analyzed with a bilinear model named the hybrid environment receptor model (HERM). HERM is developed by the IEECAS and the University of Nevada, Las Vegas (Chen and Cao, 2018). Like other receptor models, the speciation of pollutants at a receptor site can be separated into emission sources and the chemical compositions of the sources. To solve the mass balance of $PM_{2.5}$, the bilinear HERM in matrix notation is defined as follows

$$C_{mn} = \sum_{i=1}^{I} F_{mi} G_{in} + Q_{mn} \quad (3)$$

where C_{mn} is the measured concentration of chemical species m during time n; F_{mi} is the source profile, that is the fractional quantity of species m in source i emission; G_{in} represents the contribution of source i during time n; and Q_{mn} is the model residual for species m concentration measured during time n. Based on an iterative conjugate gradient algorithm, the HERM solves G_{in} and unknown F_{mi} by minimizing the Q_{mn}, which is defined as follows.

$$Q_{mn} = \sum_{m=1}^{M} \sum_{n=1}^{N} \frac{(C_{mn} - \sum_{i=1}^{I} F_{mi} G_{in})^2}{\sigma_{C_{mn}}^2 + \sum_{i=1}^{I} (\sigma_{F_{mi}}^2 G_{in}^2 + \delta_{mi} \sigma_{C_{mn}}^2)} \quad (4)$$

where M, N, and I are the number of samples, chemical species, and sources, respectively; $\sigma_{F_{mi}}$ represents the error in the variability in the constrained factor profile. δ_{mi} was set to 0 or 1 depending on whether the i^{th} factor profile is constrained or unconstrained, respectively.

The HERM input data included the concentration and uncertainty data of chemical species. 19 chemical species in

Xi'an and Shijiazhuang and 20 chemical species in Beijing were selected for source apportionment, respectively. Details of selected chemical species and its uncertainty calculation was described in Text S1 in the Supplement. A range from two to ten factors solutions was investigated by HERM with completely unconstrained factor profiles to search for optimal solutions. The detailed diagnostics can be seen in Text S2 in the Supplement. A six-factor solution for Xi'an and Shijiazhuang and an eight-factor solution for Beijing were found to be the optimal solution based on multiple criteria including 1) variations in Q/Q_{exp} which can be used to choose the optimal number of resolved factors, 2) physical meaningfulness of distinct factor profiles and explained variation (EV) values of variables, 3) good correlations between sources contribution and external and internal tracers, and 4) agreement between the measured and modeled $PM_{2.5}$ mass. More detailed information on the final selected factor profiles and contributions is presented in Sect. 3.2.

2.3.3 Aerosol liquid water content

Aerosol liquid water content (ALWC) was calculated by ISORROPIA-II thermodynamic equilibrium model (http://isorropia.eas.gatech.edu/) based on data of $PM_{2.5}$ chemical species (including NO_3^-, SO_4^{2-}, NH_4^+, and Cl^-) and meteorological parameters including relative humidity (RH) and temperature (T), more model information can be found in Fountoukis and Nenes (2007). It should be noted that the ISORROPIA-II model does not consider the contribution of the organic, as inorganic aerosols are the most hygroscopic species and dominant contributor to ALWC (Huang et al., 2020).

3. Results and discussion

3.1 –Characteristics of $PM_{2.5}$ and its chemical components

Figure 1 illustrates the mass composition of $PM_{2.5}$ in three pilot cities during the sampling periods, and their concentrations levels are summarized in Table S4. The average $PM_{2.5}$ concentrations in Xi'an, Beijing, and Shijiazhuang were 77±47 μg m^{-3}, 64±57 μg m^{-3}, and 60±39 μg m^{-3}, respectively. It is noted that the average $PM_{2.5}$ concentrations in Xi'an, Beijing, and Shijiazhuang did not meet the second level of the NAAQS, indicating that it is necessary to establish more particular and efficient pollution reduction measures. As shown in Fig. 1, the chemical compositions of $PM_{2.5}$ were similar in Beijing and Shijiazhuang (Fig. 1b and c) which was mainly composed of OA (26.9–34.2%), followed by NO_3^- (23.6–26.5%), SO_4^{2-} (11.8–15.0%), NH_4^+ (11.8–14.8%), MD (7.4–10.1%), BC (2.9–6.5%), and Cl^- (1.1–4.8%). However, in Xi'an, MD contributed in comparison more to $PM_{2.5}$ (17.3%), while SO_4^{2-}

had a smaller contribution (6.8%). This could be explained by more construction activities and MD transport from the Loess Plateau to Xi'an (Long et al., 2016; Yan et al., 2015). Meanwhile, the lowest sulfur oxidation ratio (SOR) was observed in Xi'an (0.18 ± 0.08, see Table S5), indicating weak efficiency of the second generation of SO_4^{2-}. The sum of SO_4^{2-}, NO_3^-, and NH_4^+ accounted for 39.0–53.0% of $PM_{2.5}$ in three pilot cities, highlighting the importance of the secondary inorganic components in northern China. In addition, the fractions of BC, Cl^-, and TE in $PM_{2.5}$ were lower in Beijing than those in the other two cities, which can be explained by the stricter local control policies on solid fuels combustion and tightening the industrial emission standards in and near the capital city of China (Li et al., 2021a; Pang et al., 2021).

To ~~have a~~ better understanding ~~of~~ the impact of the chemical components, the mass fraction of each component was plotted as a function of the $PM_{2.5}$ mass concentration (Fig. 2a–c). The two dominant components of $PM_{2.5}$ were OA (25.7–38.0%) and MD (19.9–37.1%) while the $PM_{2.5}$ concentrations were below 40 μg m^{-3}. The faction of OA in $PM_{2.5}$ was the highest in Shijiazhuang and Beijing, while MD contributed most to $PM_{2.5}$ in Xi'an. This is potentially related to more emissions and higher backgrounds of local dust. With ~~increasing~~ increases of the $PM_{2.5}$ mass concentration, the fractions of chemical components in Xi'an and Shijiazhuang changed notably. The factions of OA and NO_3^- increased the most and reached the peaks of 40.1% and 28.7%, respectively, when the $PM_{2.5}$ concentration reached ~196 μg m^{-3} in Xi'an. On the contrary, NO_3^- and SO_4^{2-} were two dominant drivers of increasing $PM_{2.5}$ concentrations in Shijiazhuang, showing peak contributions of 32.5% and 18.7%, respectively, when the $PM_{2.5}$ concentration was over 100 μg m^{-3}. Compared to Xi'an and Shijiazhuang, Beijing had relatively stable fractions of each chemical component with increasing $PM_{2.5}$ concentrations. Particularly, the fractions of OA and NO_3^- contributed dominantly with averages of 33.3±3.0% and 25.3±2.5%, respectively, when the $PM_{2.5}$ > 40 μg m^{-3}.

3.2 Source apportionment of $PM_{2.5}$

Six potential sources, including biomass burning, fugitive dust, industrial emission, coal combustion, vehicle emission, and ~~secondary nitrate plus sulfate~~secondary formation source, were resolved by the HERM analysis. In Beijing, ~~secondary nitrate plus sulfate~~secondary formation source was furtherly divided into secondary nitrate plus OA and secondary sulfate plus OA. A special pollution source of firework was separated due to the Chinese Spring Festival (from New Year's Eve to January 3rd in the lunar calendar). Figures S6–S8 present the sources profiles and contributions in Xi'an, Shijiazhuang, and Beijing, respectively. Biomass burning features high Explained Variation (EV) for the two tracers Cl^- (33–58%) and K (30–44%) in the three cities (Ni et al., 2017; Zhao et al., 2021). The

fugitive dust is characterized by high EV values for Si (60–90%) and Ca (34–54%), which are the dominant chemical species in the fugitive dust profiles in northern China (Shen et al., 2016; Zhao et al., 2006). The fractions of industrial emission vary among the cities, showing high EV for Ni (55% and 87%) and Cr (25% and 70%) in Xi'an and Shijiazhuang, and high EV for Cr (26%), Mn (40%), and Pb (27%) in Beijing. Ni is possibly emitted from the semiconductor industry (Simka et al., 2005). Cr, Mn, and Pb could originate from the steel manufacturing and incinerator fly ash (Duan and Tan, 2013; Ledoux et al., 2017). Coal combustion is characterized by high EV values for As (38–75%), Se (40–50%), and Pb (31–57%). These elements are enriched in coals, which are reliable indicators of coal combustion (Tian et al., 2013; Xu et al., 2012). The vehicle non-exhaust emissions could be identified by the elements Ba, Cu, Ca, Fe, and Mn. Cu and Ba can be released from brake and tire wear of vehicles (Adachi and Tainosho, 2004; Thorpe and Harrison, 2008). Moreover, Fe and Mn could be emitted from the combustion of lubricating oil and fuel additives (Ålander et al., 2005; Lewis et al., 2003). Relatively high EV values for Ba (68%), Cu (36%), and Ca (35%) are seen in Xi'an, significantly high EV values of Mn (68%), Fe (65%), Cu (53%), and Ba (80%) are characterized in Shijiazhang and relatively high EV values of Fe (34%) and Cu (39%) are featured in Beijing, respectively. Moreover, moderate EV values for BC (18–27%) and OA (13–22%) are commonly regarded as contributions of vehicles engine exhaust, while the temporal variations of VE are well correlated with gaseous NO_x or NO_2 in three cities (R^2 = 0.45–0.78), which is the good tracer of traffic-related emissions (Huang et al., 2017; Li et al., 2017b). The secondary sources resolved by HERM are different among the three cities. In Xi'an and Shijiazhuang, ~~the source of secondary nitrate plus sulfate~~this factor are characterized by high EV values for SO_4^{2-} (62–75%), NO_3^- (55–53%), NH_4^+ (60–56%) and a medium EV value for OA (23–29%), which showed good correlations with SO_4^{2-} (R^2 = 0.85–0.90) and NO_3^- (R^2 = 0.85–0.92) (Dai et al., 2020; Tian et al., 2022). In addition, The OA concentration in this factor was calculated by EV value of OA, which was close to the secondary OA (SOA) concentration estimated by BC-trace method (see Text S3 and Table S6). This means that SOA was mixed in this factor, therefore, this factor was identified as secondary formation source. In Beijing, two secondary sources were resolved. The first one was characterized by high EV value for NO_3^-(58%), NH_4^+ (42%) and medium values for OA (21%), another one was characterized by high EV value for SO_4^{2-}(58%), and medium values for OA (16%), NH_4^+ (30%). The OA concentration in those two factors was also comparable to that estimated by BC-trace method (see Text S3). So, those two sources were identified as secondary nitrate plus OA and secondary sulfate plus OA~~the secondary sources of nitrate and sulfate show high EV values of 58% and 65%~~, respectively. The combination of secondary nitrate plus OA and secondary sulfate plus OA~~secondary nitrate and secondary sulfate~~ is equivalent to the ~~secondary nitrate plus sulfate~~secondary formation source for next discussion. Additionally, the source of firework

emission is characterized by high EV values of Ba (83%), Cu (45%), and K (38%), which are recognized as common indication in fireworks (Rai et al., 2020; Tian et al., 2014).

The modeled $PM_{2.5}$ mass was well correlated with the reconstructed $PM_{2.5}$ mass (R^2 = 0.99, slope = 0.90–1.01, Fig. ~~S9~~S10) in three pilot cities, indicating the established models are reasonable. As shown in Fig. 1d and e, the contributions of primary sources (i.e., the sum of biomass burning, fugitive dust, industrial emission, coal combustion, and vehicle emission) in $PM_{2.5}$ were significantly higher than those of the ~~source of secondary nitrate plus sulfate~~secondary formation source in Xi'an and Shijiazhuang, indicating the $PM_{2.5}$ in these two cities are mainly influenced by the primary source emissions during wintertime. Particularly, biomass burning and coal combustion were two dominant contributors to $PM_{2.5}$ with contributions of 24.6% and 15.1%, respectively, in Xi'an; and 24.4% and 16.0%, respectively, in Shijiazhuang. These suggest that controls of solid fuel combustion are critical to reducing $PM_{2.5}$ pollution in these cities. In contrast, the contribution of ~~secondary nitrate plus sulfate~~secondary formation source to $PM_{2.5}$ in Beijing was highly dominant (> 50%), potentially attributed to strict control of primary emissions under the execution of a series of pollution control policies (Lv et al., 2016; Pang et al., 2021), and more regional transportation of secondary pollutants (Liu et al., 2019; Wang and Zhao, 2018). Among the primary sources, the contributions of biomass burning and vehicle emission were only 18.4% and 11.3%, respectively, further reflecting the benefits of reductions of all primary emissions. Due to the Chinese Spring Festival, the contribution of firework (7.9%) to $PM_{2.5}$ ranked second in primary sources (Fig. ~~S10~~S11). Which indicates more refined control schemes need to be encouraged to deal with such special event in the future. It should be noted that contribution of fugitive dust was all lower than fraction of mineral dust in the three pilot cities (Fig. 1). This is because fugitive dust defined here mainly refers road and construction dust emission. While mineral dust represents material assumed oxides of mineral elements such as Al, Si, Ca, Ti and Fe (Chow et al., 2015). These mineral elements in $PM_{2.5}$ comes from more emission sectors including industry, crust, and transportation, construction, combustion (Liu et al., 2018a; Lu et al., 2014; Pant and Harrison, 2013; Shen et al., 2016).

Figures 2d–f shows variations of source contribution with increases in $PM_{2.5}$ mass concentrations in three pilot cities. The most two dominant sources were ~~secondary nitrate plus sulfate~~secondary formation source (32.1%) and fugitive dust (31.4%) in Xi'an, coal combustion (24.9%) and vehicle emission (21.3%) in Shijiazhuang, and ~~secondary nitrate plus sulfate~~secondary formation source (24.3%) and fugitive dust (23.8%) in Beijing, when the $PM_{2.5}$ mass concentration <40 μg m^{-3}. In Xi'an, when the $PM_{2.5}$ mass concentrations exceeded 180 μg m^{-3}, the contribution of

biomass burning raised mostly and reached the peak of 38.4%, demonstrating that biomass burning plays an important role in worsening of air quality in Xi'an. On the contrary, the contributions of ~~secondary nitrate plus sulfate~~secondary formation source increased mostly in comparison to other sources in Shijiazhuang and Beijing, indicating the $PM_{2.5}$ pollution was mainly dominated by the secondary aerosol formations during the wintertime. And the peak contributions of secondary nitrate and sulfate were 66.5% and 74,7% while the $PM_{2.5}$ mass concentration increased to 113 μg m^{-3} and 223 μg m^{-3} in Shijiazhuang and Beijing, respectively.

3.3 Formation of secondary aerosols

Using the high-time-resolution data, we further explored the possible formation mechanisms of ~~secondary nitrate plus sulfate~~secondary formation source. The concentration of ~~secondary nitrate plus sulfate~~secondary formation source is standardized by dividing background corrected CO (ΔCO) to ~~–~~weaken impact of planetary boundary layer height (PBLH) (DeCarlo et al., 2010). In this study, ΔCO is defined as the 1.25th percentile of CO concentration during the campaign, which are 0.17, 0.15, and 0.16 ppm in Xi'an, Shijiazhuang, and Beijing, respectively. O_x (NO_2 + O_3) is an indicator of the photochemical oxidation degree (Wood et al., 2010). The function between ~~secondary nitrate plus sulfate~~secondary formation source/ΔCO ratio and O_x during the daytime (i.e., 08:00–17:00 LST) (Fig. ~~S11~~S12) was plotted to explain the effect of photochemical oxidations in three pilot cities. As shown in Fig. 3, good linear correlations of ~~secondary nitrate plus sulfate~~secondary formation source/ΔCO and O_x (R^2 = 0.83–0.99) suggest that photochemical oxidations play an important role in the formation of secondary aerosol during the daytime. Compared to the low-level O_x, formation of secondary aerosol significantly enhanced at high-level O_x (>50 ppb) in Xi'an and Beijing, characterized by larger slopes of 17.2 and 38.9, respectively (Fig. 3a and c). Furthermore, the highest atmospheric oxidation capacity was found in Beijing, inferring by the highest fraction of O_3 to O_x. This is consistent with the highest contribution of ~~secondary nitrate plus sulfate~~secondary formation source to $PM_{2.5}$ in Beijing during the daytime (Fig. ~~S12a~~S13a–c).

The aqueous-phase reaction is another important pathway for secondary aerosol formation in the atmosphere (Wang et al., 2018; Xue et al., 2014). ALWC is considered an indicator of an aqueous-phase reaction (Ervens et al., 2011). Considering that the aqueous-phase reaction occurs both during the daytime and nighttime characterized by good correlations between secondary formation source/ΔCO and ALWC (R^2 = 0.81–0.98, Fig. S14). The correlations of ~~secondary nitrate plus sulfate~~secondary formation source/ΔCO ratio and ALWC during ~~nighttime~~ all sampling periods ~~(18:00–07:00 the next day LST, Fig. S11)~~ were re-established in three pilot cities to assess the implications

of aqueous-phase chemistry for secondary aerosol production. As shown in Fig. 4, ~~The~~ the secondary formation source~~nitrate plus sulfate~~/ΔCO showed a significant linear correlation to ALWC (R^2 = 0.~~81~~92–0.~~95~~99) when RH < 80% ~~(Fig. 4)~~, indicating an obvious effect of aqueous-phase reaction on the secondary aerosol formation during the ~~nighttime~~sampling periods. However, when RH >80%, the secondary formation source~~nitrate plus sulfate~~/ΔCO showed no notable increase with ALWC in Shijiazhuang (Fig. 4b), whereas a tiny increase with ALWC in Beijing (Fig. 4c). The higher ALWC at RH > 80% probably inhibits secondary aerosol formation due to the decrease in aerosol acidity (Huang et al., 2019; Meng et al., 2014). Khan et al. (2008) found that NO_3 radicals can rapidly generate from the reaction between NO_2 and O_3 with unsaturated organic species during nighttime. The value of $O_3 \times NO_2$ can thus represent its production reaction rate or be used as a proxy for the NO_3 radical. The highest NO_3 radical production rate was found in Beijing, followed by Xi'an and Shijiazhuang, when RH<80%. This could be used to explain the highest contribution of secondary formation source~~nitrate plus sulfate~~ to $PM_{2.5}$ in Beijing during the daytime and nighttime (Fig. S1~~2~~3~~d f~~). Moreover, the results showed that both photochemical oxidation and aqueous-phase reaction play more important roles in Beijing, where the primary sources have been better controlled. This reflects that pollution control policies need to be focused on the suppression of secondary formations.

3.4 Elaborations of different episode cases

During the sampling periods, the concentration of $PM_{2.5}$ and its chemical components ~~simply~~ accumulated within a short period in a few cases (Fig.~~S13a~~S15a–c). We define such a rapid rise in $PM_{2.5}$ mass concentration as a pollution episode. As shown in Table 1, meteorological conditions, the concentration levels of gaseous pollutants, chemical compositions, and source contributions of $PM_{2.5}$ during pollution episodes in three pilot cities are summarized. The episodes were accompanied by low wind speed (< 2 m s^{-1}), leading to weak dispersions of ~~the~~ fresh emissions and accumulated pollutants (Chen et al., 2020b). OA and NO_3^- were ~~The~~ the two dominant chemical components in $PM_{2.5}$ during all pollution episode cases ~~were OA and NO_3^-,~~ with fractions of 26–40% and 23–32%, respectively. Their high abundances could be explained by the significant reduction of SO_2 emissions ~~by~~ because of the prohibiting of burning bulk coals and executing the "Coal-to-Natural Gas" policy in recent years (Meng et al., 2022). In this study, eight pollution episodes (donated as EP1-EP8) were classified into three types: The first type was dominated by biomass burning (30–40%) (EP1, EP4, and EP8). The second type was dominated by ~~secondary nitrate plus sulfate~~secondary formation source (61–70%) (EP5, EP6, and EP7). The two remaining pollution episodes were mutually contributed by both primary and secondary sources (EP2 and EP3), in which ~~secondary nitrate plus sulfate~~secondary formation source (34–39%) and biomass burning (23–24%) were the two dominant contributors to $PM_{2.5}$.

To ~~profoundly understand~~gain insights into the ~~progress~~ process of pollution episodes, three typical pollution events were chosen for detailed discussion (i.e., EP2 in Xi'an, EP4 in Shijiazhuang, and EP7 in Beijing) based on the validity and integrity of the data and the representativeness of the selected pollution events. The two-stage evolution was distinguished for EP4 as an example of the first type of episode (Fig. S16). ~~For the first type of episode represented by EP4 (Fig. S14), a two-stages evolution was distinguished.~~ At Stage 1, the $PM_{2.5}$ mass concentrations rapidly increased from 7 to 82 μg m^{-3} under stable weather conditions inferring by low wind speed (1.8±0.8 m s^{-1}, Fig. ~~S14b~~S16b), in which the concentrations (fractions) of biomass burning increased from 0.6 μg m^{-3} (7%) to 36.7 μg m^{-3} (55%) due to heating ~~demand~~ activities during nighttime. Meanwhile, the chemical composition was relatively stable and dominated by OA (31±5%) and NO_3^-(21±5%). At Stage 2, the $PM_{2.5}$ mass concentration continuously increased to 105 μg m^{-3} in a few hours along with the most notable abundance of the source of ~~secondary nitrate plus sulfate~~secondary formation source, which concentration (contribution) rapidly increased from 2.3 μg m^{-3} (4%) to 54.4 μg m^{-3} (52%) (Fig. ~~S14g~~ S16g and h). This is due to the aqueous-phase reactions effect inferring by the rapid increase in ALWC (from 16 μg m^{-3} to 78 μg m^{-3}, Fig. ~~S14e~~S16c) and RH (from 51% to 79%, Fig. ~~S14a~~S16a).

In contrast, a three-stage~~s~~ evolution was discriminated for the second type of episode, using EP7 as an example (Fig. ~~S15~~S17). At Stage 1, the $PM_{2.5}$ concentration gradually increased from 11 to 30 μg m^{-3}, as well as NO_2 (from 15 to 59 μg m^{-3}, Fig. ~~S15d~~S17d) due to the boosts of the predominant contributions of vehicle emission and biomass burning (Fig. ~~S15g~~ S17g and h). In the meantime, the contribution of coal combustion also slowly increased along with SO_2 (Fig. ~~S15d~~ S17d and h). At Stage 2, under the lowest average wind speed in the study period (0.7±0.4 m s^{-1}, Fig. ~~S15b~~S17b), the $PM_{2.5}$ mass concentrations moderately increased from 30 to 91 μg m^{-3} with relatively stable chemical composition and source contribution (Fig. ~~S15f~~ S17f and h). Compared to Stage 1, the fractions of NO_3^- increased mostly from 9±3% to 23±3%, this is probably influenced by photochemical oxidations inferring by relative high O_x and NO_2 concentration (Fig. ~~S15c~~ S17c and d). At Stage 3, the $PM_{2.5}$ mass concentration rapidly rose to 142 μg m^{-3} and then remained stable. Furthermore, the ~~In which~~ greatest increase of sources ~~the~~ concentrations (~~fractions~~contribution) ~~of~~ was ~~secondary nitrate plus sulfate~~secondary formation source ~~increased mostly~~ from 18.9 μg m^{-3} (48%) to 120.6 μg m^{-3} (80%). This might be due to the occurrence of an aqueous-phase reaction, which was indicated by the elevation of RH and ALWC (Fig. ~~S15a~~ S17a and c).

Figure S16 illustrates the third type of episode using EP2 as an example, ~~while~~ in which a four-stages evolution was resolved. At Stage 1, the $PM_{2.5}$ mass concentration (14±3 μg m^{-3}) was relatively low and dominated by the

contributions of ~~secondary nitrate plus sulfate~~secondary formation source (43±17%) and fugitive dust (24±8%), as well as MD (28±7%) and OA (26±7%). At Stage 2, the $PM_{2.5}$ mass concentrations promptly increased from 21 to 82 μg m^{-3}, with the two dominant chemical components of OA (21.7 μg m^{-3}) and NO_3^- (17.1 μg m^{-3}). The $PM_{2.5}$ increases can be also ~~contributed~~ attributed to the raise of ~~secondary nitrate plus sulfate~~secondary formation source (25.3 μg m^{-3}) and biomass burning (14.4 μg m^{-3}). The enhancement of secondary aerosol was probably generated through the aqueous-phase reaction evidenced by the increase of ALWC and NO_2 (Fig. ~~S16c~~ S18c and d). At Stage 3, $PM_{2.5}$ mass continuously increased to 139 μg m^{-3} with a dominant increase of primary sources emission including biomass burning (29.0 μg m^{-3}), vehicle emission (21.5 μg m^{-3}) and coal combustion (16.5 μg m^{-3}) along with the increases of SO_2 and NO_2 as well (Fig. ~~S16~~ S18d). The three primary sources contributed >60% of the total resolved sources. Meanwhile, the ~~secondary nitrate plus sulfate~~secondary formation source also increased slowly through aqueous-phase reaction inferring by increase of ALWC (Fig. ~~S16c~~S18c). At the final Stage 4, the $PM_{2.5}$ mass concentration maintained relatively stable with an average of 142±11 μg m^{-3}, dominated by ~~sources of secondary nitrate plus sulfate~~secondary formation source (34±6%) and biomass burning (28±6%); and chemical components of OA (36±4%) and NO_3^- (25±1%).

In summary, the pollution events occurred in Xi'an was mainly derived by stronger emissions of primary sources under adverse meteorological conditions, even though the aqueous-phase reaction also contribute to secondary aerosol formation. In contrast, pollution events occurred in Shijiazhuang and Beijing were mainly influenced by formation of secondary aerosols through both of aqueous-phase reaction and photochemical oxidation. What's more, ~~in which~~ aqueous-phase reaction plays a more important role than photochemical oxidation. Hence, to further improve the air quality in the north of China, primary source emissions should be prioritized for control in the northwest region, with a focus on biomass burning and coal combustion. In the North China Plain, the priority should be given to reduc~~ing~~e emissions of the precursors from secondary sources, with a focus on NO_x and volatile organic compounds (VOCs).

3.5 Policy implications

In past decades, the air quality in China improved notably under the implementation of air pollution control policies including APCAP and TAPFAP. The $PM_{2.5}$ mass in Xi'an, Shijiazhuang and Beijing were the lowest during campaigns compared with those in last decades (Table ~~S6~~S7). The variations of the chemical composition and the source contribution of $PM_{2.5}$ in the three pilot cities are displayed in Fig. 5. As shown, the dominant chemical components

of $PM_{2.5}$ changed from OA and SO_4^{2-}, to OA and NO_3^- (Fig. 5a–c). This could be attributed to the reduction in coal consumption due to clean energy replacement and the increase of vehicle ownership, which~~. This~~ lead a decrease of the SO_2 and an increase of NO_2 (Wang et al., 2013). Since the atmospheric oxidation reaction (i.e., aqueous-phase reaction and photochemical oxidation) of the precursors (i.e., NO_2, VOCs) is the primary source for the OA and NO_3^- in the atmosphere (Feng et al., 2018; Li et al., 2022; Tao et al., 2016; Yang et al., 2022b; Ziemann and Atkinson, 2012), and it is impossible to avoid, thus, the precursors of OA and NO_3^- should be reduced from the combustion and transportation sectors (Fermo et al., 2021; Liu et al., 2022; Wang et al., 2021c; Zhang et al., 2019). In addition, the fraction of NH_4^+ in $PM_{2.5}$ increased with an alarming rate. This is coincidentally in a similar trend of NH_3. Studies have reported that controls of NH_4^+ is more effective than that of NO_x in the reduction of $PM_{2.5}$ mass concentrations (Gu et al., 2021; Zheng et al., 2022). Therefore, collaborative control measures for the emissions of precursors including NO_x, VOCs, and NH_3 are necessary.

As shown Table ~~S7~~ S8 and Fig. 5d-f, coal combustion decreased remarkably due to the coal-related policies implementation including the strength of emissions standards for coal-fired power plants, the change of energy sources from coal to natural gas in some industrials, and the coal burning was forbidden in the main urban areas (Shen, 2016; Yang and Teng, 2018). The similar trend was also founded in the results of $PM_{2.5}$ source apportionment in Beijing released by Beijing Municipal Ecology and Environment Bureau (Fig. S19). Meanwhile, the contribution of industrial emission and vehicle emission decreased slightly because of the improvement of industrial emission standards (He et al., 2020; Wang et al., 2020a) and the traffic-related policy implementation such as the strength of vehicle emission standards, improvement of fuel quality, and elimination of high-emission-vehicles. This resulted in the reduction of the precursor gases and $PM_{2.5}$ from vehicles (Feng et al., 2021; Fontaras et al., 2012; Jin et al., 2012). However, the emission of biomass burning did not show a significant reduction in recent years, and its contribution increased from 9% in 2014 to 25% in 2020 (Xi'an), from 3% in 2015 to 24% in 2022 (Shijiazhuang), and from 6% in 2013 to 18% in 2021 (Beijing) (Fig. 5d-f). This is likely because biomass burning is an open source, which makes it more difficult to control compare with other primary sources. Biomass used for residential heating in rural areas is still frequently occurred (Ren, 2021; Tian et al., 2022; Yang et al., 2022a; Zhang et al., 2017). Hence, the clean energy revolution should be promoted urgently especially in the entire regions in northwest China. Moreover, the contributions of secondary formation source~~s~~ increased, it is potentially explained by the high reduction rate of primary emissions and the improvement of atmospheric oxidation capacity (Chen et al., 2020a; Feng et al., 2020). Therefore, more control measures should focus on weakening the ~~atmosphere~~atmospheric oxidation capacity, such

as reduction of O_3 formation, to reduce the formation of secondary pollutants which are now identified as the most critical drivers of pollution. Considering those factors, it is also important to promote the mitigation of *both* $PM_{2.5}$ and O_3.

4. Conclusion

The intensive real-time measurement campaigns about $PM_{2.5}$ chemical components were conducted in Xi'an, Shijiazhuang, and Beijing during the wintertime respectively. Chemical compositions of $PM_{2.5}$ in the three cities were all dominated by OA (26.9–34.2%) and NO_3^- (23.6–26.5%). Six sources of $PM_{2.5}$ in Xi'an and Shijiazhuang were resolved by HERM and their contributions were similar, with a descending order of ~~secondary nitrate plus sulfate~~secondary formation source (32.2–37.6%), biomass burning (24.4–24.6 %), coal combustion (15.1–16.0%), vehicle emission (12.2–12.5 %), industrial emission (5.5–7.7%) and fugitive dust (4.4–7.8%). However, the secondary nitrate (29.0%) and the secondary sulfate (23.0%) were separately resolved and relatively more important in Beijing. In addition, the contribution of firework (7.9%) to $PM_{2.5}$ was found during the Chinese Spring Festival.

The possible formation mechanism of ~~secondary nitrate plus sulfate~~secondary formation source in three pilot cities was explored. The results showed that secondary aerosols were generated by both photochemical oxidation and aqueous-phase reaction. Meanwhile, the formation rate of secondary aerosols in Beijing was higher than that in Xi'an and Shijiazhuang. Furthermore, the eight pollution episodes within the sampling periods were categorized three types and characterized respectively. The dominant chemical compositions of $PM_{2.5}$ were OA (26–40%) and NO_3^- (23–32%) during all pollution episodes. Furthermore, ~~secondary nitrate plus sulfate~~secondary formation source and biomass burning were two major derivers of the pollution.

The dominant chemical components of $PM_{2.5}$ in pilot cities have changed from OA and SO_4^{2-} to OA and NO_3^- under the implementation of a clean air plan in past decades. This indicates that reduction of precursors including NO_2 and VOCs should be a key task in the future. In addition, the contribution of biomass burning increased, especially in Xi'an. This indicates that clean energy for heating activities in rural areas in northwest China is still insufficient. Furthermore, to weaken the ~~atmosphere~~ atmospheric oxidation capacity for reducing the contribution of ~~secondary nitrate plus sulfate~~secondary formation source, it is necessary to promote the collaborative control on ozone and particulate matter.

Data availability. Data used to support the findings in this study are archived at the Institute of Earth Environment,

Chinese Academy of Sciences, and are publicly available at https://doi.org/10.5281/zenodo.~~7336744~~8106655.

Competing interest. The authors declare that they have no conflict of interest.

Author contributions. QW, YH, JC designed the campaigns. WR and YZ conducted the field measurements. YZ, JT, HL, LQ and TC performed data analysis and interpretation. MM, KRD, JGS and ASHP were involved supervision and review. YZ wrote the paper with contributions from all co-authors.

Acknowledgments. The authors are grateful to the staff from Guanzhong Plain, Eco-environmental Change and Comprehensive Treatment, National Observation and Research Station; Tower Branch of Institute of Atmospheric Physics, Chinese Academy Sciences; and Hebei Sailhero Environmental Protection High-tech Co., Ltd. for their assistance with field sampling.

Financial support. This work was financially supported by the Sino-Swiss Cooperation on Air Pollution for Better Air (7F-09802.01.02) from the Swiss Agency for Development and Cooperation (SDC), the National Key R&D Program of China (2022YFF0802501), and the Youth Innovation Promotion Association of the Chinese Academy of Sciences (2019402). Natural Science Basic Research Program of Shaanxi (2022JQ-267)

References:

Adachi, K. and Tainosho, Y.: Characterization of heavy metal particles embedded in tire dust, Environ. Int., 30, 1009–1017, https://doi.org/10.1016/j.envint.2004.04.004, 2004.

Ålander, T., Antikainen, E., Raunemaa, T., Elonen, E., Rautiola, A., and Torkkell, K.: Particle emissions from a small Two-Stroke engine: Effects of fuel, lubricating oil, and exhaust aftertreatment on particle characteristics, Aerosol Sci. Technol., 39, 151–161, https://doi.org/10.1080/027868290910224, 2005.

Cao, J. J. and Cui, L.: Current status, characteristics and causes of particulate air pollution in the Fenwei Plain, China: A Review, J. Geophy. Res-Atmos., 126, https://doi.org/10.1029/2020JD034472, 2021.

Chan, C. K. and Yao, X.: Air pollution in mega cities in China, Atmos. Environ., 42, 1–42, https://doi.org/10.1016/j.atmosenv.2007.09.003, 2008.

Chen, L.-W. A. and Cao, J. J.: $PM_{2.5}$ source apportionment using a hybrid environmental receptor model, Environ. Sci. Technol., 52, 6357–6369, https://doi.org/10.1021/acs.est.8b00131, 2018.

Chen, Q., Hua, X., Li, J. W., Chang, T., and Wang, Y.: Diurnal evolutions and sources of water-soluble chromophoric aerosols over Xi'an during haze event, in Northwest China, Sci. Total Environ., 786, 147412, https://doi.org/10.1016/j.scitotenv.2021.147412, 2021.

Chen, S., Wang, H., Lu, K., Zeng, L., Hu, M., and Zhang, Y.: The trend of surface ozone in Beijing from 2013 to 2019: Indications of the persisting strong atmospheric oxidation capacity, Atmos. Environ., 242, 117801, https://doi.org/10.1016/j.atmosenv.2020.117801, 2020a.

Chen, Z., Chen, D., Zhao, C., Kwan, M., Cai, J., Zhuang, Y., Zhao, B., Wang, X., Chen, B., Yang, J., Li, R., He, B., Gao, B., Wang, K., and Xu, B.: Influence of meteorological conditions on $PM_{2.5}$ concentrations across China: A review of methodology and mechanism, Environ. Int., 139, 105558, https://doi.org/10.1016/j.envint.2020.105558, 2020b.

Chow, J. C., Lowenthal, D. H., Chen, L.-W. A., Wang, X., and Watson, J. G.: Mass reconstruction methods for $PM_{2.5}$: a review, Air Qual. Atmos. Health, 8, 243–263, https://doi.org/10.1007/s11869-015-0338-3, 2015.

Dai, Q., Liu, B., Bi, X., Wu, J., Liang, D., Zhang, Y., Feng, Y., and Hopke, P. K.: Dispersion normalized PMF provides insights into the significant changes in source contributions to $PM_{2.5}$ after the COVID-19 outbreak, Environ. Sci. Technol., 54, 9917–9927, https://doi.org/10.1021/acs.est.0c02776, 2020.

DeCarlo, P. F., Ulbrich, I. M., Crounse, J., de Foy, B., Dunlea, E. J., Aiken, A. C., Knapp, D., Weinheimer, A. J., Campos, T., Wennberg, P. O., and Jimenez, J. L.: Investigation of the sources and processing of organic aerosol over the Central Mexican Plateau from aircraft measurements during MILAGRO, Atmos. Chem. Phys., 10, 5257–5280, https://doi.org/10.5194/acp-10-5257-2010, 2010.

Drinovec, L., Močnik, G., Zotter, P., Prévôt, A. S. H., Ruckstuhl, C., Coz, E., Rupakheti, M., Sciare, J., Müller, T., Wiedensohler, A., and Hansen, A. D. A.: The "dual-spo" Aethalometer: an improved measurement of aerosol black carbon with real-time loading compensation, Atmos. Meas. Tech., 8, 1965–1979, https://doi.org/10.5194/amt-8-1965-2015, 2015.

Duan, J. and Tan, J.: Atmospheric heavy metals and Arsenic in China: Situation, sources and control policies, Atmos. Environ., 74, 93–101, https://doi.org/10.1016/j.atmosenv.2013.03.031, 2013.

Elser, M., Huang, R.-J., Wolf, R., Slowik, J. G., Wang, Q.-Y., Canonaco, F., Li, G. H., Bozzetti, C., Daellenbach, K. R., Huang, Y., Zhang, R.-J., Li, Z.-Q., Cao, J. J., Baltensperger, U., El-Haddad, I., and Prévôt, A. S. H.: New insights into $PM_{2.5}$ chemical composition and sources in two major cities in China during extreme haze events using aerosol mass spectrometry, Aerosols/Field Measurements/Troposphere/Chemistry (chemical composition and reactions), https://doi.org/10.5194/acpd-15-30127-2015, 2015.

Ervens, B., Turpin, B. J., and Weber, R. J.: Secondary organic aerosol formation in cloud droplets and aqueous particles (aqSOA): a review of laboratory, field and model studies, Atmos. Chem. Phys., 11, 11069–11102, https://doi.org/10.5194/acp-11-11069-2011, 2011.

Feng, T., Bei, N., Zhao, S., Wu, J. rui, Li, X., Zhang, T., Cao, J., Zhou, W., and Li, G.: Wintertime nitrate formation during haze days in the Guanzhong basin, China: A case study, Environ. Pollut., 243, 1057–1067, https://doi.org/10.1016/j.envpol.2018.09.069, 2018.

Feng, T., Zhao, S., Zhang, X., Wang, Q., Liu, L., Li, G., and Tie, X.: Increasing wintertime ozone levels and secondary aerosol formation in the Guanzhong basin, central China, Sci. Total Environ., 12, 2020.

Feng, X., Zhang, X., He, C., and Wang, J.: Contributions of traffic and industrial emission reductions to the air quality improvement after the lockdown of Wuhan and neighboring Cities due to COVID-19, Toxics, 9, 358, https://doi.org/10.3390/toxics9120358, 2021.

Fermo, P., Artíñano, B., De Gennaro, G., Pantaleo, A. M., Parente, A., Battaglia, F., Colicino, E., Di Tanna, G., Goncalves da Silva Junior, A., Pereira, I. G., Garcia, G. S., Garcia Goncalves, L. M., Comite, V., and Miani, A.: Improving indoor air quality through an air purifier able to reduce aerosol particulate matter (PM) and volatile organic compounds (VOCs): Experimental results, Environ. Pollut., 197, 111131, https://doi.org/10.1016/j.envres.2021.111131, 2021.

Fontaras, G., Martini, G., Manfredi, U., Marotta, A., Krasenbrink, A., Maffioletti, F., Terenghi, R., and Colombo, M.: Assessment of on-road emissions of four Euro V diesel and CNG waste collection trucks for supporting air-quality improvement initiatives in the city of Milan, Sci. Total Environ., 426, 65–72, https://doi.org/10.1016/j.scitotenv.2012.03.038, 2012.

Fountoukis, C. and Nenes, A.: ISORROPIA II: a computationally efficient thermodynamic equilibrium model for K^+–Ca^{2+}–Mg^{2+}–NH_4^+–Na^+–SO_4^{2-}–NO_3^-–Cl^-–H_2O aerosols, Atmos. Chem. Phys., 7, 4639–4659, https://doi.org/10.5194/acp-7-4639-2007, 2007.

Furger, M., Rai, P., Slowik, J. G., Cao, J., Visser, S., Baltensperger, U., and Prévôt, A. S. H.: Automated alternating sampling of PM10 and PM2.5 with an online XRF spectrometer, Atmospheric Environment: X, 5, 100065, https://doi.org/10.1016/j.aeaoa.2020.100065, 2020.

Gu, B., Zhang, L., Van Dingenen, R., Vieno, M., Van Grinsven, H. J., Zhang, X., Zhang, S., Chen, Y., Wang, S., Ren, C., Rao, S., Holland, M., Winiwarter, W., Chen, D., Xu, J., and Sutton, M. A.: Abating ammonia is more cost-effective than nitrogen oxides for mitigating $PM_{2.5}$ air pollution, Science, 374, 758–762,

https://doi.org/10.1126/science.abf8623, 2021.

Guo, Y., Lin, C., Li, J., Wei, L., Yang, Y., Yang, Q., Li, D., Wang, H., and Shen, J.: Persistent pollution episodes, transport pathways, and potential sources of air pollution during the heating season of 2016–2017 in Lanzhou, China, Environ. Monit. Assess., 193, 852, https://doi.org/10.1007/s10661-021-09597-8, 2021.

He, J., Zhao, M., Zhang, B., Wang, P., Zhang, D., Wang, M., Liu, B., Li, N., Yu, K., Zhang, Y., Zhou, T., and Jing, B.: The impact of steel emissions on air quality and pollution control strategy in Caofeidian, North China, Atmos. Pollut. Res., 11, 1238–1247, https://doi.org/10.1016/j.apr.2020.04.012, 2020.

He, K., Huo, H., and Zhang, Q.: Urban air pollution in China: Current status, characteristics, and progress, Annu. Rev. Energy. Environ., 27, 397–431, https://doi.org/10.1146/annurev.energy.27.122001.083421, 2002.

Hu, W. wei, Campuzano-Jost, P., Day, D. A., Croteau, P., Canagaratna, M. R., Jayne, J. T., Worsnop, D. R., and Jimenez, J. L.: Evaluation of the new capture vapourizer for aerosol mass spectrometers (AMS) through laboratory studies of inorganic species, Atmos. Meas. Tech., 10, 2897–2921, https://doi.org/10.5194/amt-10-2897-2017, 2017.

Huang, R.-J., He, Y., Duan, J., Li, Y., Chen, Q., Zheng, Y., Chen, Y., Hu, W., Lin, C., Ni, H., Dai, W., Cao, J., Wu, Y., Zhang, R., Xu, W., Ovadnevaite, J., Ceburnis, D., Hoffmann, T., and O'Dowd, C. D.: Contrasting sources and processes of particulate species in haze days with low and high relative humidity in wintertime Beijing, Atmos. Chem. Phys., 20, 9101–9114, https://doi.org/10.5194/acp-20-9101-2020, 2020.

Huang, R.-J., Zhang, Y., Bozzetti, C., Ho, K.-F., Cao, J.-J., Han, Y., Daellenbach, K. R., Slowik, J. G., Platt, S. M., Canonaco, F., Zotter, P., Wolf, R., Pieber, S. M., Bruns, E. A., Crippa, M., Ciarelli, G., Piazzalunga, A., Schwikowski, M., Abbaszade, G., Schnelle-Kreis, J., Zimmermann, R., An, Z., Szidat, S., Baltensperger, U., Haddad, I. E., and Prévôt, A. S. H.: High secondary aerosol contribution to particulate pollution during haze events in China, Nature, 514, 218–222, https://doi.org/10.1038/nature13774, 2014.

Huang, X., Liu, Z., Liu, J., Hu, B., Wen, T., Tang, G., Zhang, J., Wu, F. kun, Ji, D., Wang, L., and Wang, Y.: Chemical characterization and source identification of $PM_{2.5}$ at multiple sites in the Beijing–Tianjin–Hebei region, China, Atmos. Chem. Phys., 17, 12941–12962, https://doi.org/10.5194/acp-17-12941-2017, 2017.

Huang, R.-J., Wang, Y., Cao, J., Lin, C., Duan, J., Chen, Q., Li, Y., Gu, Y., Yan, J., Xu, W., Fröhlich, R., Canonaco, F., Bozzetti, C., Ovadnevaite, J., Ceburnis, D., Canagaratna, M. R., Jayne, J., Worsnop, D. R., El-Haddad, I., Prévôt, A. S. H., and O'Dowd, C. D.: Primary emissions versus secondary formation of fine particulate matter in the most polluted city (Shijiazhuang) in North China, Atmos. Chem. Phys., 19, 2283–2298, https://doi.org/10.5194/acp-19-2283-2019, 2019.

Huang, X., Zhang, J., Luo, B., Luo, J., Zhang, W., and Rao, Z.: Characterization of oxalic acid-containing particles in summer and winter seasons in Chengdu, China, Atmos. Environ., 198, 133–141, https://doi.org/10.1016/j.atmosenv.2018.10.050, 2019.

Jin, T. sheng, Gao, J. jia, Fu, L. xin, Ai, Y., and Xu, X. H.: An evaluation of improvements in the air quality of Beijing arising from the use of new vehicle emission standards, Environ. Monit. Assess., 184, 2151–2159, https://doi.org/10.1007/s10661-011-2106-7, 2012.

Khan, M. A. H., Ashfold, M. J., Nickless, G., Martin, D., Watson, L. A., Hamer, P. D., Wayne, R. P., Canosa-Mas, C. E., and Shallcross, D. E.: Night-time NO_3 and OH radical concentrations in the United Kingdom inferred from hydrocarbon measurements, Atmos. Sci. Lett., 9, 140–146, https://doi.org/10.1002/asl.175, 2008.

Kuniyal, J. C. and Guleria, R. P.: The current state of aerosol-radiation interactions: A mini review, J. Aerosol Sci., 130, 45–54, https://doi.org/10.1016/j.jaerosci.2018.12.010, 2019.

Kuo, C.-Y., Cheng, F.-C., Chang, S.-Y., Lin, C.-Y., Chou, C. C. K., Chou, C.-H., and Lin, Y.-R.: Analysis of the major factors affecting the visibility degradation in two stations, J. Air Waste Manage., 63, 433–441, https://doi.org/10.1080/10962247.2012.762813, 2013.

Ledoux, F., Kfoury, A., Delmaire, G., Roussel, G., El Zein, A., and Courcot, D.: Contributions of local and regional anthropogenic sources of metals in $PM_{2.5}$ at an urban site in northern France, Chemosphere, 181, 713–724, https://doi.org/10.1016/j.chemosphere.2017.04.128, 2017.

Lewis, C. W., Norris, G. A., Conner, T. L., and Henry, R. C.: Source apportionment of Phoenix $PM_{2.5}$ aerosol with the Unmix receptor model, J. Air Waste Manage., 53, 325–338, https://doi.org/10.1080/10473289.2003.10466155, 2003.

Li, J., Du, H., Wang, Z., Sun, Y., Yang, W., He, J., Tang, X., and Fu, P.: Rapid formation of a severe regional winter haze episode over a mega-city cluster on the North China Plain, Environ. Pollut., 223, 605–615, https://doi.org/10.1016/j.envpol.2017.01.063, 2017a.

Li, J., Gao, W., Cao, L., Xiao, Y., Zhang, Y., Zhao, S., Liu, Z., Liu, Z., Tang, G., Ji, D., Hu, B., Song, T., He, L., Hu, M., and Wang, Y.: Significant changes in autumn and winter aerosol composition and sources in Beijing from 2012 to 2018: Effects of clean air actions, Environ. Pollut., 268, 115855, https://doi.org/10.1016/j.envpol.2020.115855, 2021a.

Li, K., Zhang, X., Zhao, B., Bloss, W. J., Lin, C., White, S., Yu, H., Chen, L., Geng, C., Yang, W., Azzi, M., George, C., and Bai, Z.: Suppression of anthropogenic secondary organic aerosol formation by isoprene, npj Clim. Atmos. Sci., 5, 12, https://doi.org/10.1038/s41612-022-00233-x, 2022.

Li, L., Tan, Q., Zhang, Y., Feng, M., Qu, Y., An, J., and Liu, X.: Characteristics and source apportionment of $PM_{2.5}$ during persistent extreme haze events in Chengdu, southwest China, Environ. Pollut., 230, 718–729, https://doi.org/10.1016/j.envpol.2017.07.029, 2017b.

Li, W., Shao, L. yi, Wang, W., Li, H., Wang, X., Li, Y., Li, W., Jones, T., and Zhang, D.: Air quality improvement in response to intensified control strategies in Beijing during 2013–2019, Sci. Total Environ., 744, 140776, https://doi.org/10.1016/j.scitotenv.2020.140776, 2020.

Li, X., Bei, N., Tie, X., Wu, J., Liu, S., Wang, Q., Liu, L., Wang, R., and Li, G.: Local and transboundary transport contributions to the wintertime particulate pollution in the Guanzhong Basin (GZB), China: A case study, Sci. Total Environ., 797, 148876, https://doi.org/10.1016/j.scitotenv.2021.148876, 2021b.

Li, Y., Sun, Y., Zhang, Q., Li, X., Li, M., Zhou, Z., and Chan, C. K.: Real-time chemical characterization of atmospheric particulate matter in China: A review, Atmos. Environ., 158, 270–304,

https://doi.org/10.1016/j.atmosenv.2017.02.027, 2017c.

Liu, J., Chen, Y., Chao, S., Cao, H., Zhang, A., Yang, Y.: Emission control priority of $PM_{2.5}$-bound heavy metals in different seasons: A comprehensive analysis from health risk perspective, Sci. Total Environ., 644, 20-30. https://doi.org/10.1016/j.scitotenv.2018.06.226, 2018a.

Liu, B., Cheng, Y., Zhou, M., Liang, D., Dai, Q., Wang, L., Jin, W., Zhang, L., Ren, Y., Zhou, J., Dai, C., Xu, J., Wang, J., Feng, Y., and Zhang, Y.: Effectiveness evaluation of temporary emission control action in 2016 in winter in Shijiazhuang, China, Atmos. Chem. Phys., 18, 7019–7039, https://doi.org/10.5194/acp-18-7019-2018, 2018b.

Liu, J., Chu, B., Jia, Y., Cao, Q., Zhang, H., Chen, T., Ma, Q., Ma, J., Wang, Y., Zhang, P., and He, H.: Dramatic decrease of secondary organic aerosol formation potential in Beijing: Important contribution from reduction of coal combustion emission, Sci. Total Environ., 832, 155045, https://doi.org/10.1016/j.scitotenv.2022.155045, 2022.

Liu, Y., Zheng, M., Yu, M., Cai, X., Du, H., Li, J., Zhou, T., Yan, C., Wang, X., Shi, Z., Harrison, R. M., Zhang, Q., and He, K.: High-time-resolution source apportionment of $PM_{2.5}$ in Beijing with multiple models, Atmos. Chem. Phys., 19, 6595–6609, https://doi.org/10.5194/acp-19-6595-2019, 2019.

Liu, Z., Wang, Y., Hu, B., Ji, D., Zhang, J., Wu, F., Wan, X., and Wang, Y.: Source appointment of fine particle number and volume concentration during severe haze pollution in Beijing in January 2013, Environ. Sci. Pollut. Res., 23, 6845–6860, https://doi.org/10.1007/s11356-015-5868-6, 2016.

Long, X., Li, N., Tie, X., Cao, J., Zhao, S., Huang, R., Zhao, M., Li, G., and Feng, T.: Urban dust in the Guanzhong Basin of China, part I: A regional distribution of dust sources retrieved using satellite data, Sci. Total Environ., 541, 1603–1613, https://doi.org/10.1016/j.scitotenv.2015.10.063, 2016.

Lu, J., Ge, P., Zhao, Y.: Recent development of effect mechanism of alloying elements in titanium alloy design, Rare Metal Mat. Eng., 43, 775-779. https://doi.org/10.1016/S1875-5372(14)60082-5, 2014.

Lu, W., Tian, Q., Xu, R., Qiu, L., Fan, Z., Wang, S., Liu, T., Huang, J., Li, Y., Wang, Y., Shi, C., Liu, Y., and Zhou, Y.: Ambient air pollution and hospitalization for chronic obstructive pulmonary disease: Benefits from Three-Year Action Plan, Ecotoxicol. Environ. Saf., 228, 113034, https://doi.org/10.1016/j.ecoenv.2021.113034, 2021.

Lv, B., Zhang, B., and Bai, Y.: A systematic analysis of $PM_{2.5}$ in Beijing and its sources from 2000 to 2012, Atmos. Environ., 124, 98–108, https://doi.org/10.1016/j.atmosenv.2015.09.031, 2016.

Lv, L., Chen, Y., Han, Y., Cui, M., Wei, P., Zheng, M., and Hu, J.: High-time-resolution $PM_{2.5}$ source apportionment based on multi-model with organic tracers in Beijing during haze episodes, Sci. Total Environ., 772, 144766, https://doi.org/10.1016/j.scitotenv.2020.144766, 2021.

Ma, Y., Huang, Y., Wu, J., E, J., Zhang, B., Han, D., and Ong, H. C.: A review of atmospheric fine particulate matters: chemical composition, source identification and their variations in Beijing, Energ. Source. Part A, 44, 4783–4807, https://doi.org/10.1080/15567036.2022.2075991, 2022.

675 Meng, H., Shen, Y., Fang, Y., and Zhu, Y.: Impact of the 'Coal-to-Natural Gas' Policy on Criteria Air Pollutants in
676 Northern China, Atmosphere, 13, 945, https://doi.org/10.3390/atmos13060945, 2022.

677 Meng, J., Wang, G., Li, J., Cheng, C., Ren, Y., Huang, Y., Cheng, Y., Cao, J., and Zhang, T.: Seasonal characteristics
678 of oxalic acid and related SOA in the free troposphere of Mt. Hua, central China: Implications for sources and
679 formation mechanisms, Sci. Total Environ., 493, 1088–1097, https://doi.org/10.1016/j.scitotenv.2014.04.086,
680 2014.

681 Ng, N. L., Herndon, S. C., Trimborn, A., Canagaratna, M. R., Croteau, P. L., Onasch, T. B., Sueper, D., Worsnop, D.
682 R., Zhang, Q., Sun, Y. L., and Jayne, J. T.: An Aerosol Chemical Speciation Monitor (ACSM) for Routine
683 Monitoring of the Composition and Mass Concentrations of Ambient Aerosol, Aerosol Sci. Technol., 45, 780–
684 794, https://doi.org/10.1080/02786826.2011.560211, 2011.

685 Ni, H., Tian, J., Wang, X., Wang, Q., Han, Y., Cao, J., Long, X., Chen, L.-W. A., Chow, J. C., Watson, J. G., Huang,
686 R.-J., and Dusek, U.: $PM_{2.5}$ emissions and source profiles from open burning of crop residues, Atmos. Environ.,
687 169, 229–237, https://doi.org/10.1016/j.atmosenv.2017.08.063, 2017.

688 Ouyang, J., Song, L.-J., Ma, L.-L., Luo, M., Dai, X.-X., Zhang, J.-T., and Xu, D.-D.: Quantification of secondary
689 particle loading during a heavy air pollution event in Beijing: A simplified method based on coal emission
690 indicators, Atmos. Environ., 215, 116896, https://doi.org/10.1016/j.atmosenv.2019.116896, 2019.

691 Pant, P. and Harrison, R.M.: Estimation of the contribution of road traffic emissions to particulate matter
692 concentrations from field measurements: A review, Atmos. Environ., 77, 78-97.
693 https://doi.org/10.1016/j.atmosenv.2013.04.028, 2013.

694 Pang, N., Gao, J., Zhu, G., Hui, L., Zhao, P., Xu, Z., Tang, W., and Chai, F.: Impact of clean air action on the $PM_{2.5}$
695 pollution in Beijing, China: Insights gained from two heating seasons measurements, Chemosphere, 263,
696 127991, https://doi.org/10.1016/j.chemosphere.2020.127991, 2021.

697 Pöschl, U.: Atmospheric Aerosols: Composition, Transformation, Climate and Health Effects, Angew. Chem. Int. Ed.,
698 44, 7520–7540, https://doi.org/10.1002/anie.200501122, 2005.

699 Pui, D. Y. H., Chen, S.-C., and Zuo, Z.: $PM_{2.5}$ in China: Measurements, sources, visibility and health effects, and
700 mitigation, Particuology, 13, 1–26, https://doi.org/10.1016/j.partic.2013.11.001, 2014.

701 Rai, P., Furger, M., Slowik, J. G., Canonaco, F., Fröhlich, R., Hüglin, C., Minguillón, M. C., Petterson, K.,
702 Baltensperger, U., and Prévôt, A. S. H.: Source apportionment of highly time-resolved elements during a
703 firework episode from a rural freeway site in Switzerland, Atmos. Chem. Phys., 20, 1657–1674,
704 https://doi.org/10.5194/acp-20-1657-2020, 2020.

705 Ren, Y.: Chemical components and source identification of $PM_{2.5}$ in non-heating season in Beijing: The influences
706 of biomass burning and dust, Atmos. Res., 8, 2021.

707 Shen, G.: Changes from traditional solid fuels to clean household energies – Opportunities in emission reduction of
708 primary $PM_{2.5}$ from residential cookstoves in China, Biomass——Bioenerg., 86, 28–35,
709 https://doi.org/10.1016/j.biombioe.2016.01.004, 2016.

Shen, W.-T., Yu, X., Zhong, S.-B., and Ge, H.-R.: Population Health Effects of Air Pollution: Fresh Evidence From China Health and Retirement Longitudinal Survey, Front. Public Health, 9, 779552, https://doi.org/10.3389/fpubh.2021.779552, 2021.

Shen, Z., Sun, J., Cao, J., Zhang, L., Zhang, Q., Lei, Y., Gao, J., Huang, R.-J., Liu, S., Huang, Y., Zhu, C., Xu, H., Zheng, C., Liu, P., and Xue, Z.: Chemical profiles of urban fugitive dust $PM_{2.5}$ samples in Northern Chinese cities, Sci. Total Environ., 569–570, 619–626, https://doi.org/10.1016/j.scitotenv.2016.06.156, 2016.

Simka, H., Shankar, S., Duran, C., and Haverty, M.: Fundamentals of Cu/Barrier-Layer Adhesion in Microelectronic Processing, MRS Proc., 863, B9.2, https://doi.org/10.1557/PROC-863-B9.2, 2005.

Tao, J., Zhang, L., Cao, J., and Zhang, R.: A review of current knowledge concerning $PM_{2.5}$ chemical composition, aerosol optical properties and their relationships across China, Atmos. Chem. Phys., 17, 9485–9518, https://doi.org/10.5194/acp-17-9485-2017, 2017.Tao, J., Zhang, L., Zhang, Z., Huang, R., Wu, Y., Zhang, R., Cao, J., and Zhang, Y.: Control of $PM_{2.5}$ in Guangzhou during the 16th Asian Games period: Implication for hazy weather prevention, Sci. Total Environ., 508, 57–66, https://doi.org/10.1016/j.scitotenv.2014.11.074, 2015.

Tao, Y., Ye, X., Ma, Z., Xie, Y., Wang, R., Chen, J., Yang, X., and Jiang, S.: Insights into different nitrate formation mechanisms from seasonal variations of secondary inorganic aerosols in Shanghai, Atmos. Environ., 145, 1–9, https://doi.org/10.1016/j.atmosenv.2016.09.012, 2016.

Thorpe, A. and Harrison, R. M.: Sources and properties of non-exhaust particulate matter from road traffic: A review, Sci. Total Environ., 400, 270–282, https://doi.org/10.1016/j.scitotenv.2008.06.007, 2008.

Tian, H. Z., Lu, L., Hao, J. M., Gao, J. J., Cheng, K., Liu, K. Y., Qiu, P. P., and Zhu, C. Y.: A Review of key hazardous trace elements in Chinese coals: Abundance, occurrence, behavior during coal combustion and their environmental impacts, Energ. Fuel., 27, 601–614, https://doi.org/10.1021/ef3017305, 2013.

Tian, J., Wang, Q., Zhang, Y., Yan, M., Liu, H., Zhang, N., Ran, W., and Cao, J.: Impacts of primary emissions and secondary aerosol formation on air pollution in an urban area of China during the COVID-19 lockdown, Environ. Int., 150, 106426, https://doi.org/10.1016/j.envint.2021.106426, 2021.

Tian, J., Wang, Q., Liu, H., Ma, Y., Liu, S., Zhang, Y., Ran, W., Han, Y., and Cao, J.: Measurement report: The importance of biomass burning in light extinction and direct radiative effect of urban aerosol during the COVID-19 lockdown in Xi'an, China, Atmos. Chem. Phys., 22, 8369–8384, https://doi.org/10.5194/acp-22-8369-2022, 2022.

Tian, Y. Z., Wang, J., Peng, X., Shi, G. L., and Feng, Y. C.: Estimation of the direct and indirect impacts of fireworks on the physicochemical characteristics of atmospheric PM_{10} and $PM_{2.5}$, Atmos. Chem. Phys., 14, 9469–9479, https://doi.org/10.5194/acp-14-9469-2014, 2014.

Vu, T. V., Shi, Z., Cheng, J., Zhang, Q., He, K., Wang, S., and Harrison, R. M.: Assessing the impact of clean air action on air quality trends in Beijing using a machine learning technique, Atmos. Chem. Phys., 19, 11303–11314, https://doi.org/10.5194/acp-19-11303-2019, 2019.

Wang, C., Li, X., Zhang, T., Tang, A., Cui, M., Liu, X., Ma, X., Zhang, Y., Liu, X., and Zheng, M.: Developing Nitrogen Isotopic Source Profiles of Atmospheric Ammonia for Source Apportionment of Ammonia in Urban

746 Beijing, Front. Environ. Sci., 10, 903013, https://doi.org/10.3389/fenvs.2022.903013, 2022a.

747 Wang, F., Yu, H., Wang, Z., Liang, W., Shi, G., Gao, J., Li, M., and Feng, Y.: Review of online source apportionment
748 research based on observation for ambient particulate matter, Sci. Total Environ., 762, 144095,
749 https://doi.org/10.1016/j.scitotenv.2020.144095, 2021a.

750 Wang, H. and Zhao, L.: A joint prevention and control mechanism for air pollution in the Beijing-Tianjin-Hebei
751 region in china based on long-term and massive data mining of pollutant concentration, Atmos. Environ., 174,
752 25–42, https://doi.org/10.1016/j.atmosenv.2017.11.027, 2018.

753 Wang, J., Zhao, B., Wang, S., Yang, F., Xing, J., Morawska, L., Ding, A., Kulmala, M., Kerminen, V.-M., Kujansuu,
754 J., Wang, Z., Ding, D., Zhang, X., Wang, H., Tian, M., Petäjä, T., Jiang, J., and Hao, J.: Particulate matter
755 pollution over China and the effects of control policies, Sci. Total Environ., 584–585, 426–447,
756 https://doi.org/10.1016/j.scitotenv.2017.01.027, 2017.

757 Wang, L., Wang, X., Gu, R., Wang, H., Yao, L., Wen, L., Zhu, F., Wang, W., Xue, L., Yang, L., Lu, K., Chen, J., Wang,
758 T., Zhang, Y., and Wang, W.: Observations of fine particulate nitrated phenols in four sites in northern China:
759 concentrations, source apportionment, and secondary formation, Atmos. Chem. Phys., 18, 4349–4359,
760 https://doi.org/10.5194/acp-18-4349-2018, 2018.

761 Wang, L. T., Wei, Z., Yang, J., Zhang, Y., Zhang, F. F., Su, J., Meng, C. C., and Zhang, Q.: The 2013 severe haze over
762 southern Hebei, China: model evaluation, source apportionment, and policy implications, Atmos. Chem. Phys.,
763 14, 3151–3173, https://doi.org/10.5194/acp-14-3151-2014, 2014.

764 Wang, M., Tian, P., Wang, L., Yu, Z., Du, T., Chen, Q., Guan, X., Guo, Y., Zhang, M., Tang, C., Chang, Y., Shi, J.,
765 Liang, J., Cao, X., and Zhang, L.: High contribution of vehicle emissions to fine particulate pollutions in
766 Lanzhou, Northwest China based on high-resolution online data source appointment, Sci. Total Environ., 798,
767 149310, https://doi.org/10.1016/j.scitotenv.2021.149310, 2021b.

768 Wang, P., Cao, J., Shen, Z., Han, Y., Lee, S., Huang, Y., Zhu, C., Wang, Q., Xu, H., and Huang, R.: Spatial and
769 seasonal variations of $PM_{2.5}$ mass and species during 2010 in Xi'an, China, Sci. Total Environ., 508, 477–487,
770 https://doi.org/10.1016/j.scitotenv.2014.11.007, 2015.

771 Wang, Q., Ye, J., Wang, Y., Zhang, T., Ran, W., Wu, Y., Tian, J., Li, L., Zhou, Y., Hang Ho, S. S., Dang, B., Zhang,
772 Q., Zhang, R., Chen, Y., Zhu, C., and Cao, J.: Wintertime Optical Properties of Primary and Secondary Brown
773 Carbon at a Regional Site in the North China Plain, Environ. Sci. Technol., 53, 12389–12397,
774 https://doi.org/10.1021/acs.est.9b03406, 2019.

775 Wang, Y., Wang, Q., Ye, J., Yan, M., Qin, Q., Prévôt, A. S. H., and Cao, J.: A Review of Aerosol Chemical
776 Composition and Sources in Representative Regions of China during Wintertime, Atmosphere, 10, 277,
777 https://doi.org/10.3390/atmos10050277, 2019.

778 Wang, Y., Zhang, Q. Q., He, K., Zhang, Q., and Chai, L.: Sulfate-nitrate-ammonium aerosols over China: response
779 to 2000–2015 emission changes of sulfur dioxide, nitrogen oxides, and ammonia, Atmos. Chem. Phys., 13,
780 2635–2652, https://doi.org/10.5194/acp-13-2635-2013, 2013.

781 Wang, Y., Yuan, Y., Wang, Q., Liu, C., Zhi, Q., and Cao, J.: Changes in air quality related to the control of coronavirus

in China: Implications for traffic and industrial emissions, Sci. Total Environ., 731, 139133, https://doi.org/10.1016/j.scitotenv.2020.139133, 2020a.

Wang, Y., Yu, M., Wang, Y., Tang, G., Song, T., Zhou, P., Liu, Z., Hu, B., Ji, D., Wang, L., Zhu, X., Yan, C., Ehn, M., Gao, W., Pan, Y., Xin, J., Sun, Y., Kerminen, V.-M., Kulmala, M., and Petäjä, T.: Rapid formation of intense haze episodes via aerosol–boundary layer feedback in Beijing, Atmos. Chem. Phys., 20, 45–53, https://doi.org/10.5194/acp-20-45-2020, 2020b.

Wang, Y., Liu, C., Wang, Q., Qin, Q., Ren, H., and Cao, J.: Impacts of natural and socioeconomic factors on $PM_{2.5}$ from 2014 to 2017, J. Environ. Manage., 284, 112071, https://doi.org/10.1016/j.jenvman.2021.112071, 2021c.

Wang, Z., Wang, R., Wang, J., Wang, Y., McPherson Donahue, N., Tang, R., Dong, Z., Li, X., Wang, L., Han, Y., and Cao, J.: The seasonal variation, characteristics and secondary generation of $PM_{2.5}$ in Xi'an, China, especially during pollution events, Environ. Res., 212, 113388, https://doi.org/10.1016/j.envres.2022.113388, 2022b.

Wei, F., Yang G., Jiang, D., Liu, Z., Sun, B.: Basic statistics and characteristics of background values of soil elements in China. Environ. Monit. in China (in Chinese) 7, 1–6. https://doi.org/10.19316/j.issn.1002-6002.1991.01.001, 1991.

Wood, E. C., Canagaratna, M. R., Herndon, S. C., Onasch, T. B., Kolb, C. E., Worsnop, D. R., Kroll, J. H., Knighton, W. B., Seila, R., Zavala, M., Molina, L. T., DeCarlo, P. F., Jimenez, J. L., Weinheimer, A. J., Knapp, D. J., Jobson, B. T., Stutz, J., Kuster, W. C., and Williams, E. J.: Investigation of the correlation between odd oxygen and secondary organic aerosol in Mexico City and Houston, Atmos. Chem. Phys., 10, 8947–8968, https://doi.org/10.5194/acp-10-8947-2010, 2010.

Xu, H. M., Cao, J. J., Ho, K. F., Ding, H., Han, Y. M., Wang, G. H., Chow, J. C., Watson, J. G., Khol, S. D., Qiang, J., and Li, W. T.: Lead concentrations in fine particulate matter after the phasing out of leaded gasoline in Xi'an, China, Atmos. Environ., 46, 217–224, https://doi.org/10.1016/j.atmosenv.2011.09.078, 2012.

Xu, J., Liu, D., Wu, X., Vu, T. V., Zhang, Y., Fu, P., Sun, Y., Xu, W., Zheng, B., Harrison, R. M., and Shi, Z.: Source apportionment of fine organic carbon at an urban site of Beijing using a chemical mass balance model, Atmos. Chem. Phys., 21, 2021.

Xu, P., Yang, Y., Zhang, J., Gao, W., Liu, Z., Hu, B., and Wang, Y.: Characterization and source identification of submicron aerosol during serious haze pollution periods in Beijing, J. of Environ. Sci., 112, 25–37, https://doi.org/10.1016/j.jes.2021.04.005, 2022.

Xu, W., Croteau, P., Williams, L., Canagaratna, M., Onasch, T., Cross, E., Zhang, X., Robinson, W., Worsnop, D., and Jayne, J.: Laboratory characterization of an aerosol chemical speciation monitor with $PM_{2.5}$ measurement capability, Aerosol Sci. Technol., 51, 69–83, https://doi.org/10.1080/02786826.2016.1241859, 2017.

Xue, J., Griffith, S. M., Yu, X., Lau, A. K. H., and Yu, J. Z.: Effect of nitrate and sulfate relative abundance in $PM_{2.5}$ on liquid water content explored through half-hourly observations of inorganic soluble aerosols at a polluted receptor site, Atmos. Environ., 99, 24–31, https://doi.org/10.1016/j.atmosenv.2014.09.049, 2014.

Yan, Y., Sun, Y. B., Weiss, D., Liang, L. J., and Chen, H. Y.: Polluted dust derived from long-range transport as a major end member of urban aerosols and its implication of non-point pollution in northern China, Sci. Total

Environ., 506–507, 538–545, https://doi.org/10.1016/j.scitotenv.2014.11.071, 2015.

Yang, D., Li, Z., Yue, Z., Liu, J. X., Zhai, Z., Li, Z., Gao, M., Hu, A. L., Zhu, W. J., Ding, N., Li, Z., Guo, S., Wang, X., Wang, L., and Wei, J.: Variations in sources, composition, and exposure risks of $PM_{2.5}$ in both pre-heating and heating seasons, Aerosol Air Qual. Res., 22, 14, https://doi.org/10.4209/aaqr.210333, 2022a.

Yang, S., Yuan, B., Peng, Y., Huang, S., Chen, W., Hu, W., Pei, C., Zhou, J., Parrish, D. D., Wang, W., He, X., Cheng, C., Li, X.-B., Yang, X., Song, Y., Wang, H., Qi, J., Wang, B., Wang, C., Wang, C., Wang, Z., Li, T., Zheng, E., Wang, S., Wu, C., Cai, M., Ye, C., Song, W., Cheng, P., Chen, D., Wang, X., Zhang, Z., Wang, X., Zheng, J., and Shao, M.: The formation and mitigation of nitrate pollution: comparison between urban and suburban environments, Atmos. Chem. Phys., 22, 4539–4556, https://doi.org/10.5194/acp-22-4539-2022, 2022b.

Yang, X. and Teng, F.: The air quality co-benefit of coal control strategy in China, Resour. Conserv. Recy., 129, 373–382, https://doi.org/10.1016/j.resconrec.2016.08.011, 2018.

Yang, X., Zheng, M., Liu, Y., Yan, C., Liu, J., Liu, J., and Cheng, Y.: Exploring sources and health risks of metals in Beijing $PM_{2.5}$: Insights from long-term online measurements, Sci. Total Environ., 814, 151954, https://doi.org/10.1016/j.scitotenv.2021.151954, 2022c.

Zeng, J. and He, Q.: Does industrial air pollution drive health care expenditures? Spatial evidence from China, J. Clean. Prod., 218, 400–408, https://doi.org/10.1016/j.jclepro.2019.01.288, 2019.

Zhang, Q., Zheng, Y., Tong, D., Shao, M., Wang, S., Zhang, Y., Xu, X., Wang, J., He, H., Liu, W., Ding, Y., Lei, Y., Li, J., Wang, Z., Zhang, X., Wang, Y., Cheng, J., Liu, Y., Shi, Q., Yan, L., Geng, G., Hong, C., Li, M., Liu, F., Zheng, B., Cao, J., Ding, A., Gao, J., Fu, Q., Huo, J., Liu, B., Liu, Z., Yang, F., He, K., and Hao, J.: Drivers of improved $PM_{2.5}$ air quality in China from 2013 to 2017, Proc. Natl. Acad. Sci. U.S.A., 116, 24463–24469, https://doi.org/10.1073/pnas.1907956116, 2019.

Zhang, Y., Vu, T. V., Sun, J., He, J., Shen, X., Lin, W., Zhang, X., Zhong, J., Gao, W., Wang, Y., Fu, T. M., Ma, Y., Li, W., and Shi, Z.: Significant changes in chemistry of fine particles in wintertime Beijing from 2007 to 2017: Impact of Clean Air Actions, Environ. Sci. Technol., 54, 1344–1352, https://doi.org/10.1021/acs.est.9b04678, 2020.

Zhang, Z., Gao, J., Zhang, L., Wang, H., Tao, J., Qiu, X., Chai, F., Li, Y., and Wang, S.: Observations of biomass burning tracers in $PM_{2.5}$ at two megacities in North China during 2014 APEC summit, Atmos. Environ., 169, 54–64, https://doi.org/10.1016/j.atmosenv.2017.09.011, 2017.

Zhao, P., Feng, Y., Zhu, T., and Wu, J.: Characterizations of resuspended dust in six cities of North China, Atmos. Environ., 40, 5807–5814, https://doi.org/10.1016/j.atmosenv.2006.05.026, 2006.

Zhao, S., Tian, H., Luo, L., Liu, H., Wu, B., Liu, S., Bai, X., Liu, W., Liu, X., Wu, Y., Lin, S., Guo, Z., Lv, Y., and Xue, Y.: Temporal variation characteristics and source apportionment of metal elements in $PM_{2.5}$ in urban Beijing during 2018–2019, Environ. Pollut., 268, 115856, https://doi.org/10.1016/j.envpol.2020.115856, 2021.

Zheng, G., Duan, F., Ma, Y., Zhang, Q., Huang, T., Kimoto, T., Cheng, Y., Su, H., and He, K.: Episode-Based Evolution Pattern Analysis of Haze Pollution: Method Development and Results from Beijing, China, Environ. Sci. Technol., 50, 4632–4641, https://doi.org/10.1021/acs.est.5b05593, 2016.

Zhang, R., Jing, J., Tao, J., Hsu, S.-C., Wang, G., Cao, J., Lee, C. S. L., Zhu, L., Chen, Z., Zhao, Y., and Shen, Z.: Chemical characterization and source apportionment of $PM_{2.5}$ in Beijing: seasonal perspective, Atmos. Chem. Phys., 13, 7053–7074, https://doi.org/10.5194/acp-13-7053-2013, 2013.

Zheng, M., Wang, Y., Yuan, L., Chen, N., and Kong, S.: Ambient observations indicating an increasing effectiveness of ammonia control in wintertime $PM_{2.5}$ reduction in Central China, Sci. Total Environ., 824, 153708, https://doi.org/10.1016/j.scitotenv.2022.153708, 2022.

Zhou, W., Lei, L., Du, A., Zhang, Z., Li, Y., Yang, Y., Tang, G., Chen, C., Xu, W., Sun, J., Li, Z., Fu, P., Wang, Z., and Sun, Y.: Unexpected increases of severe haze pollution during the post COVID‐19 Period: Effects of emissions, meteorology, and secondary production, J. Geophy. Res-Atmos., 127, https://doi.org/10.1029/2021JD035710, 2022.

Ziemann, P. J. and Atkinson, R.: Kinetics, products, and mechanisms of secondary organic aerosol formation, Chem. Soc. Rev., 41, 6582, https://doi.org/10.1039/c2cs35122f, 2012.

Table 1. Meteorological conditions, gas pollutants, chemical composition, and source contribution of $PM_{2.5}$ during pollution episodes in Xi'an, Shijiazhuang, and Beijing

Parameters	Xi'an		Shijiazhuang			Beijing		
	EP1	EP2	EP3	EP4	EP5	EP6	EP7	EP8
T (℃)	4.9 ± 2.6	1.5 ± 3.5	0.4 ± 3.4	-0.2 ± 3.3	-2.7 ± 3.3	0.3 ± 3.2	-1.6 ± 3.3	5.1 ± 3.6
RH (%)	52 ± 10	45 ± 10	61 ± 15	40 ± 13	75 ± 11	57 ± 19	45 ± 24	36 ± 10
WS ($m\ s^{-1}$)	0.5 ± 0.2	0.7 ± 0.3	1.4 ± 0.6	1.9 ± 0.8	1.4 ± 0.7	1.0 ± 0.6	1.1 ± 0.6	1.0 ± 0.6
Dominant WD[a]	WSW, WNW	WSW	NNW	NNW	NNW	NNE	NNW, NNE	NNE, ENE
CO ($mg\ m^{-3}$)	1.39 ± 0.40	1.15 ± 0.56	1.47 ± 0.62	0.60 ± 0.30	0.43 ± 0.33	1.04 ± 0.56	0.81 ± 0.32	1.00 ± 0.55
SO_2 ($\mu g\ m^{-3}$)	15 ± 3	15 ± 5	9 ± 4	8 ± 4	3 ± 1	6 ± 5	4 ± 3	6 ± 4
NO_2 ($\mu g\ m^{-3}$)	74 ± 22	63 ± 32	63 ± 14	47 ± 21	27 ± 11	54 ± 22	46 ± 17	42 ± 21
O_x (ppm)	47 ± 8	42 ± 10	36 ± 7	32 ± 6	27 ± 3	36 ± 6	33 ± 4	43 ± 9
ALWC ($\mu g\ m^{-3}$)	15 ± 11	8 ± 8	42 ± 37	12 ± 11	59 ± 448	28 ± 47	23 ± 8	11 ± 13
Dominant Chemical composition	OA (38%) NO_3^- (24%)	OA (34%) NO_3^- (24%)	NO_3^- (27%) OA (26%)	OA (30%) NO_3^- (23%)	NO_3^- (32%) OA (26%)	OA (32%) NO_3^- (26%)	OA (32%) NO_3^- (26%)	OA (40%) NO_3^- (23%)
Dominant source contribution[b]	BB (30%) SF (25%) CC (17%)	SF (34%) BB (24%) VE (16%)	SF (39%) BB (23%) CC (16%)	BB (40%) CC (16%) VE (16%)	SF (70%) BB (16%)	SF (62%) BB (13%)	SF (61%) BB (14%)	BB (38%) SF (27%) VE (15%)

[a] WSW : west-southwest; WNW : west-northwest; NNW : north-northwest; NNE : north-northeast; ENE : East-northeast

[b] BB: biomass burning; ~~SNpS~~SF: ~~secondary nitrate plus sulfate~~secondary formation source; CC: coal combustion; VE: vehicle emission

Figure captions:

Figure 1. Chemical composition and source apportionment results of $PM_{2.5}$ in three pilot cities of northern China during the sampling period.

Figure 2. Mass fractions of chemical components (a-c) and sources contribution (d-f) with reconstructed $PM_{2.5}$ concentration in Xi'an, Shijiazhuang, and Beijing.

Figure 3. Correlations of ~~secondary nitrate plus sulfate~~secondary formation source/ΔCO and O_x mixing ratio in (a) Xi'an, (b) Shijiazhuang, and (c) Beijing. Each point and its error bar represent the mean and standard deviation in each bin (ΔO_x = 5 ppb).

Figure 4. Correlation of ~~secondary nitrate plus sulfate~~secondary formation source/ΔCO and ALWC during ~~winter~~ sampling periods in (a) Xi'an, (b) Shijiazhuang, and (c) Beijing, respectively. The points and error bar represent the mean values and standard deviation values of ~~secondary nitrate plus sulfate~~secondary formation source/ΔCO and ALWC~~O_x~~ in each bin. In Xi'an, each bin is 5 μg m^{-3} (ΔALWC = 5 μg m^{-3}). In Shijiazhuang, each bin is 5 μg m^{-3} (ΔALWC = 5 μg m^{-3}) when ALWC ranged from 0 to 75μg m^{-3}, but 25 μg m^{-3} (ΔALWC = 25 μg m^{-3}) for ALWC ranged from 75 to 200 μg m^{-3} due to limitations in data. In Beijing, each bin is 5 μg m^{-3} (ΔALWC = 5 μg m^{-3}) when ALWC ranged from 0 to 50 μg m^{-3}, but 100 μg m^{-3} (ΔALWC = 100 μg m^{-3}) for ALWC ranged from 50 to 900 μg m^{-3} due to limitations in data.

Figure 5. Summary of $PM_{2.5}$ and its composition (a, b, c) and source contribution (d, e, f) in Xi'an, Shijiazhuang, and Beijing in winter in past decades. Where * represents the result of this study. The data and references used for this figure are listed in Table S5 and S7.

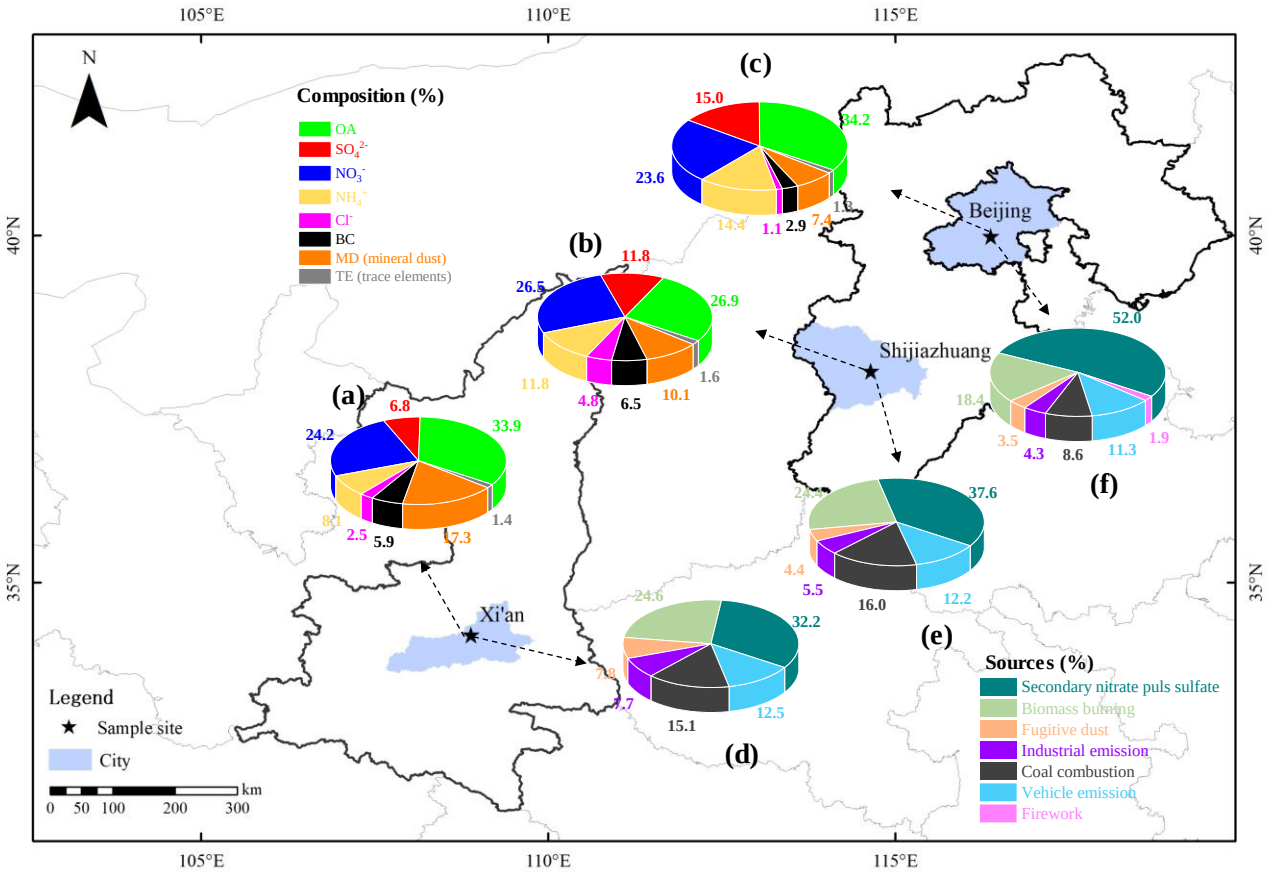
105°E
110°E
115°E
40°N
35°N
N
Composition (%)
OA
SO4 2-
NO3-
NH4+
Cl-
BC
MD (mineral dust)
TE (trace elements)
(a)
6.8
33.9
24.2
8.1
2.5
5.9
17.3
1.4
(b)
11.8
26.5
26.9
11.8
4.8
6.5
10.1
1.6
(c)
15.0
34.2
23.6
14.4
1.1
2.9
7.4
1.8
Beijing
Shijiazhuang
Xi'an
(d)
24.6
32.2
7.8
7.7
15.1
12.5
(e)
37.6
24.6
4.4
5.5
16.0
12.2
(f)
52.0
18.4
3.5
4.3
8.6
11.3
1.9
Legend
Sample site
City
km
0 50 100 200 300
Sources (%)
Secondary nitrate puls sulfate
Biomass burning
Fugitive dust
Industrial emission
Coal combustion
Vehicle emission
Firework

896

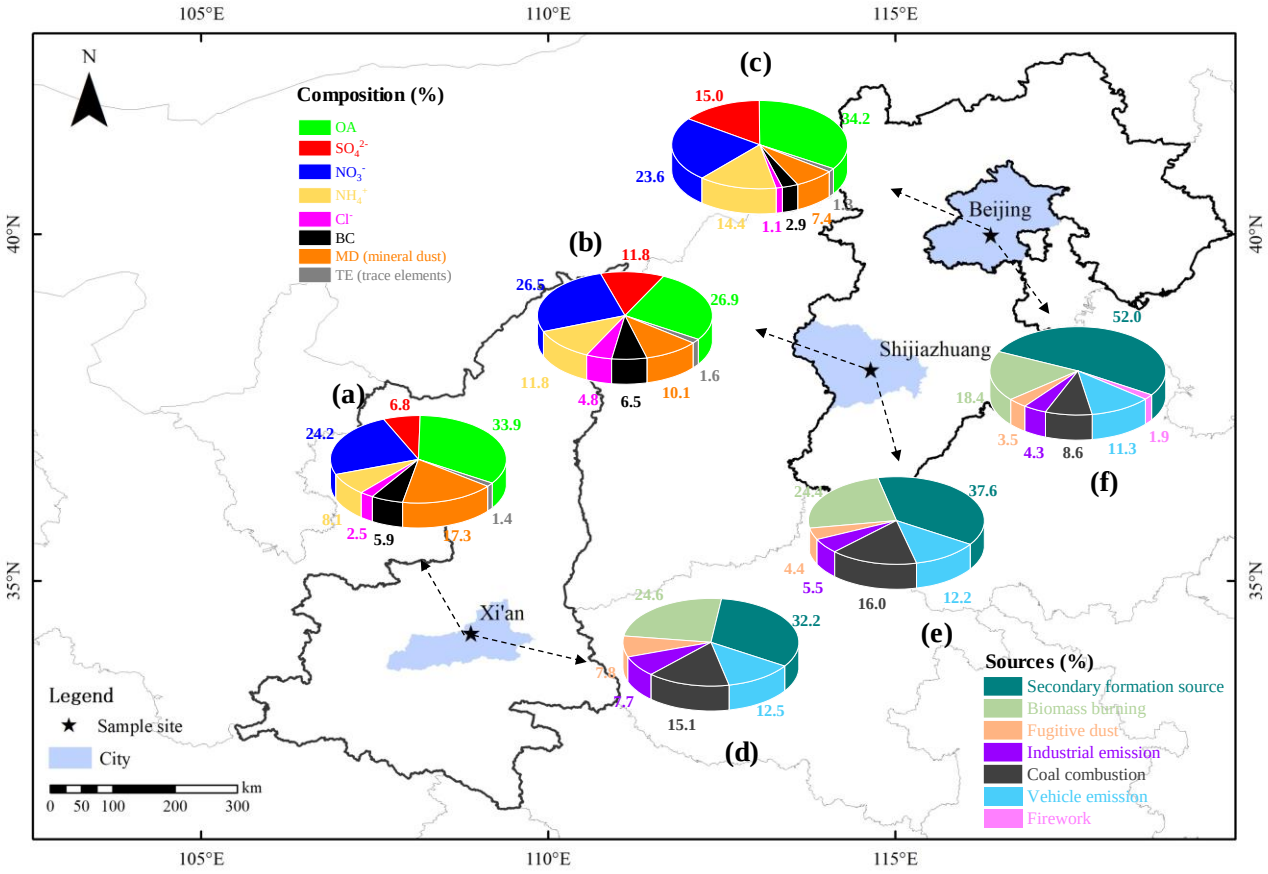

897

898 **Figure 1.** Chemical composition and source apportionment results of $PM_{2.5}$ in three pilot cities of northern China
899 during the sampling period.

900

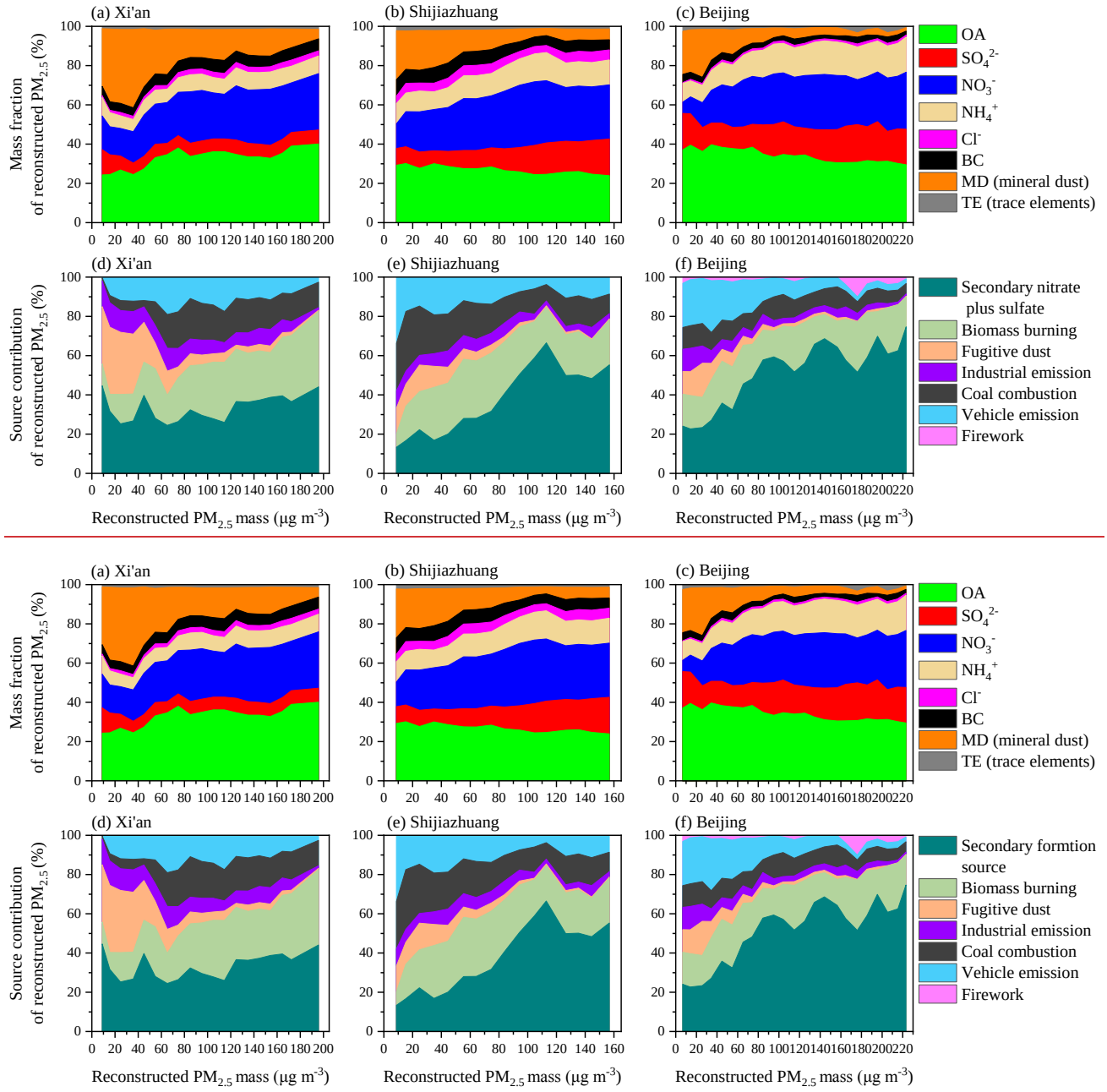

Figure 2. Mass fractions of chemical components (a-c) and sources contribution (d-f) with reconstructed $PM_{2.5}$ concentration in Xi'an, Shijiazhuang, and Beijing.

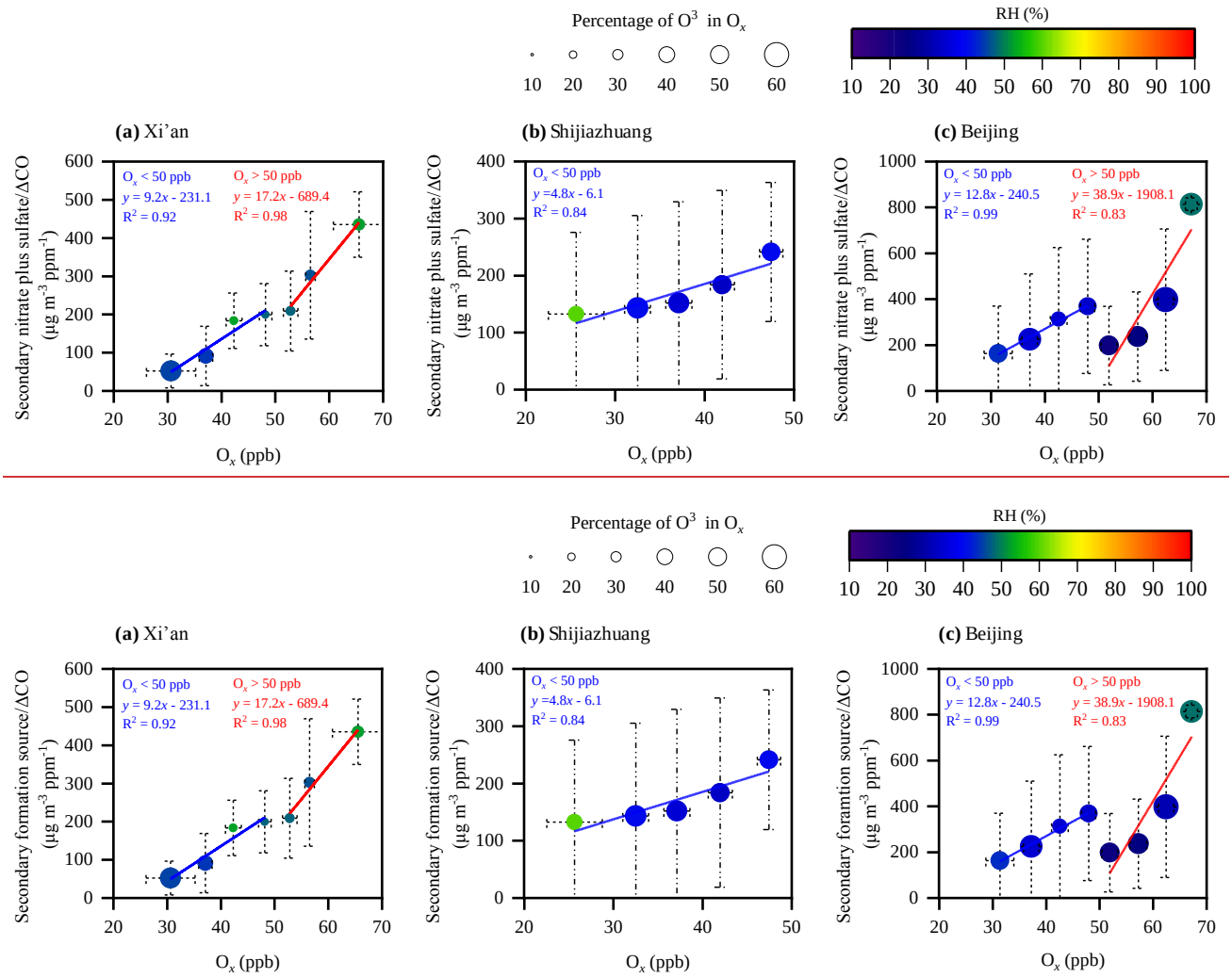

Figure 3. Correlations of ~~secondary nitrate plus sulfate~~secondary formation source/ΔCO and O_x mixing ratio in (a) Xi'an, (b) Shijiazhuang, and (c) Beijing. Each point and its error bar represent the mean and standard deviation in each bin (ΔO_x = 5 ppb).

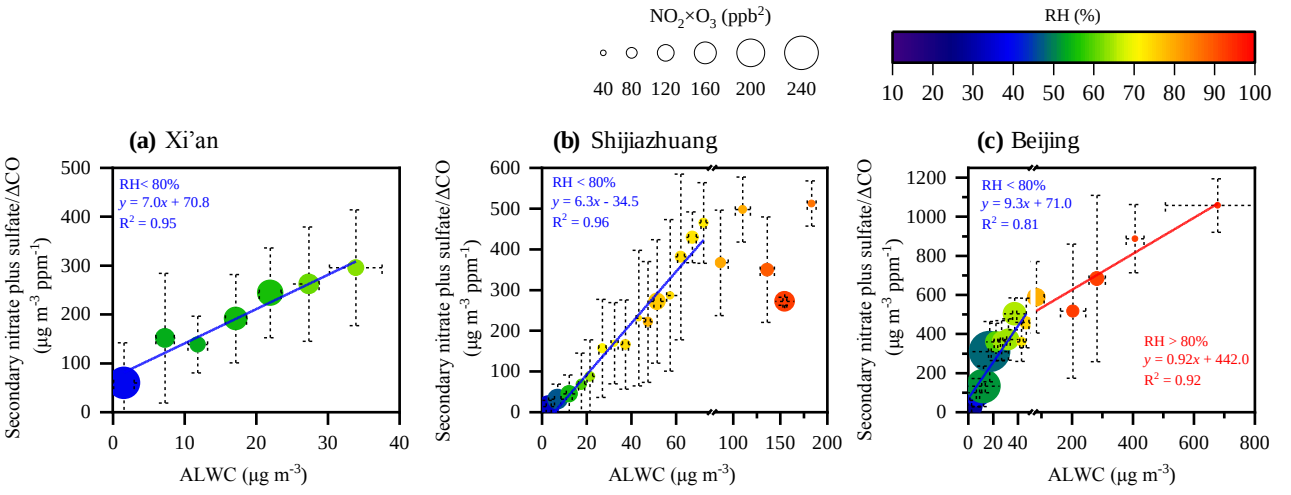

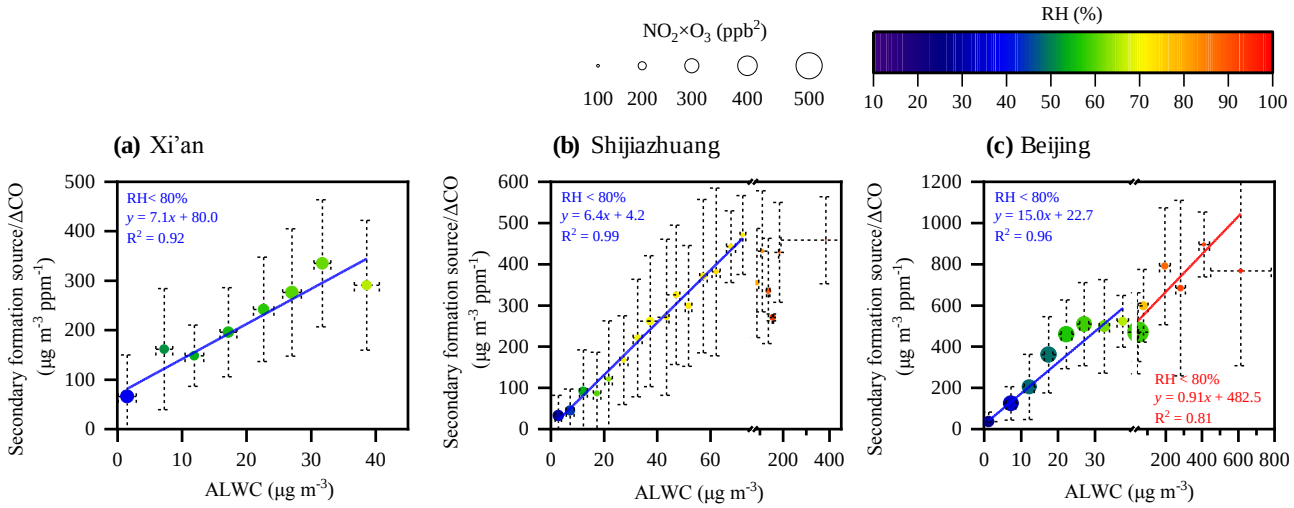

Figure 4. Correlation of ~~secondary nitrate plus sulfate~~secondary formation source/ΔCO and ALWC during ~~winter~~ sampling periods in (a) Xi'an, (b) Shijiazhuang, and (c) Beijing, respectively. The points and error bar represent the mean values and standard deviation values of ~~secondary nitrate plus sulfate~~secondary formation source/ΔCO and ALWC~~O~~* in each bin. In Xi'an, each bin is 5 μg m^{-3} (ΔALWC = 5 μg m^{-3}). In Shijiazhuang, each bin is 5 μg m^{-3} (ΔALWC = 5 μg m^{-3}) when ALWC ranged from 0 to 75μg m^{-3}, but 25 μg m^{-3} (ΔALWC = 25 μg m^{-3}) for ALWC ranged from 75 to 200 μg m^{-3} due to limitations in data. In Beijing, each bin is 5 μg m^{-3} (ΔALWC = 5 μg m^{-3}) when ALWC ranged from 0 to 50 μg m^{-3}, but 100 μg m^{-3} (ΔALWC = 100 μg m^{-3}) for ALWC ranged from 50 to 900 μg m^{-3} due to limitations in data.

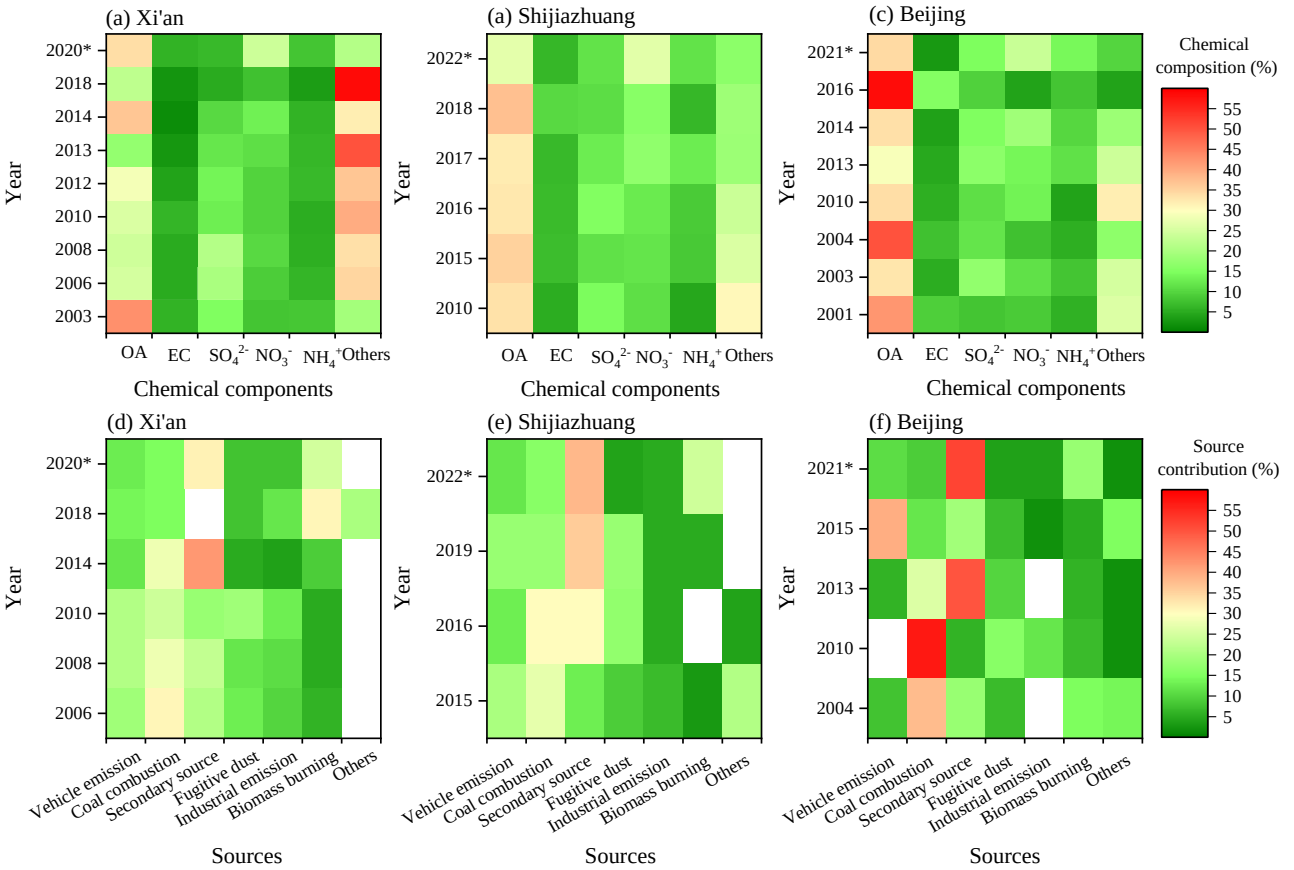

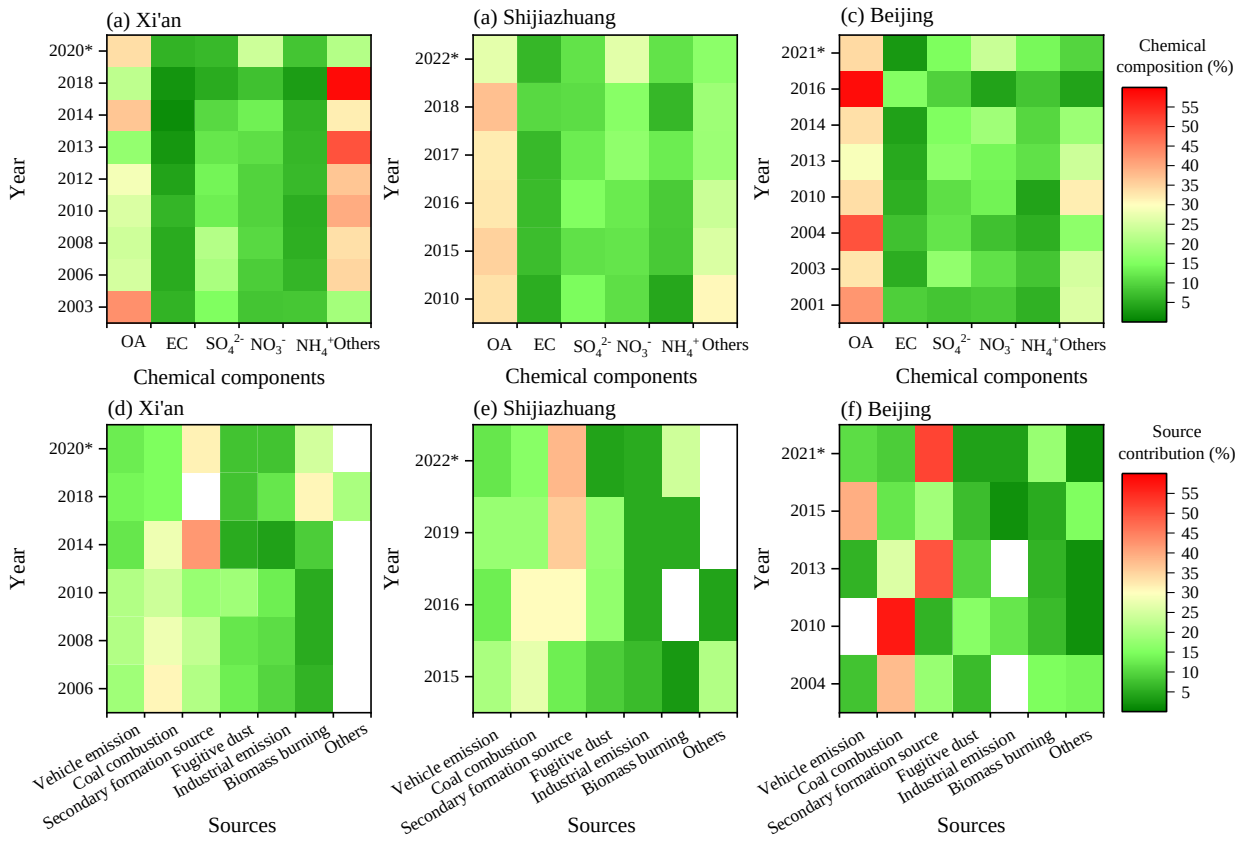

Figure 5. Summary of $PM_{2.5}$ and its composition (a, b, c) and source contribution (d, e, f) in Xi'an, Shijiazhuang, and Beijing in winter in past decades. Where * represents the result of this study, and the empty white area means no data. The data and references used for this figure are listed in Table ~~S6~~ S7 and ~~S7~~S8.

Supplement of

High-time-resolution chemical composition and source apportionment of $PM_{2.5}$ in northern Chinese cities: implications for policy

Yong Zhang[1,2,3], Jie Tian[1,2,4], Qiyuan Wang[1,2,3,4*], Lu Qi[5], Manousos Ioannis Manousakas[5], Yuemei Han[1,4], Weikang Ran[1,2], Yele Sun[6], Huikun Liu[1,2,4], Renjian Zhang[6], Yunfei Wu[6], Tianqu Cui[5], Kaspar Rudolf Daellenbach[5], Jay Gates Slowik[5], André S. H. Prévôt[5], Junji Cao[6*]

[1] State Key Laboratory of Loess and Quaternary Geology, Institute of Earth Environment, Chinese Academy of Sciences, Xi'an 710061, China
[2] National Observation and Research Station of Regional Ecological Environment Change and Comprehensive Management in the Guanzhong Plain, Shaanxi, Xi'an 710061, China
[3] University of Chinese Academy of Sciences, Beijing 100049, China
[4] Center for Excellence in Quaternary Science and Global Change, Xi'an 710061, China
[5] Laboratory of Atmospheric Chemistry, Paul Scherrer Institute (PSI), Villigen 5232, Switzerland
[6] Institute of Atmospheric Physics, Chinese Academy of Sciences, Beijing 100029, China

Correspondence: wangqy@ieecas.cn (Qiyuan Wang), jjcao@mail.iap.ac.cn (Junji Cao).

Text S1. Selcation of inputted HERM chemical species and its uncertainty calculation

Considering the validity and credibility of monitoring data, chemical species including OA, NO_3^-, SO_4^{2-}, NH_4^+, Cl^-, and BC were all selected to input HERM model for three pilot cities. For inorganic elements, Si, K, Ca, Cr, Mn, Fe, Ni, Cu, Zn, As, Se, Ba, and Pb in Xi'an and Beijing, and Si, K, Ca, Ti, Cr, Mn, Fe, Ni, Cu, Zn, As, Se, Ba, and Pb in Shijiazhuang were selected for source apportionment, respectively.

The uncertainty data of chemical species inputting HERM was calculated according to the recommendation in the PMF5.0 user guideline. If the measured chemical species concentration is greater than the minimum detection limit (MDL) provided, the uncertainty (Unc) calculation is based following equation:

$$Unc_i = \sqrt{(C_i \times E_i)^2 + (0.5 \times MDL_i)^2} \quad (1)$$

where C_i represents measured concertation for species i, E_i represents error fraction of species i. For online measured data, the error fraction was recommended to use 10% (Rai et al., 2020). If the measured concentration is less than or equal to the MDL provided, the Unc is calculated as the following equation:

$$Unc = \frac{5}{6} \times MDL \quad (2)$$

Text S2 Diagnostics of HERM solutions

In this study, factors numbering from two to ten were selected and run in the HERM software. Each factor solution was run thirty times with completely unconstrained profiles to explore the possible sources. The optimal factor number solution was determined by examining the ratio of Q and expected Q (Q_{exp}). The Q_{exp} in HERM was equal to (samples ×species – factors × (samples + species) + the number of constrained source profiles). As shown in Fig. S5, the value of Q/Q_{exp} decreased with the increase of the factor number, which suggests increasing the factor number could lead to a better explanation of the variance by HERM. However, the utility of increasing factors declined with the number of factors. Too many factors could cause splitting profiles, although the Q/Q_{exp} may be desirable (Liu et al., 2021; Salameh et al., 2018, 2016). Thus, the drops of Q/Q_{exp} ($\Delta Q/Q_{exp}$) were subsequently evaluated to choose the optimal solution factor number. As shown in Table S2, when the number of factors increases to more than six in Xi'an, the value of $\Delta Q/Q_{exp}$ shows a relatively stable change trend. A six-factor solution is preferable because $\Delta Q/Q_{exp}$ between the five-solution and six-solution is smaller than that between the six-solution and seven-solution (Liu et al., 2021). In addition, secondary ~~nitrate plus sulfate~~formation source and biomass burning were mixed when the factor number was five, and vehicle emission was split into two profiles when the factor number

was seven (Table S3). Therefore, the six-factor solution was determined as the optimal HERM solution for Xi'an. Similar criterias were used for Shijiazhuang and Beijing, six-factor and eight-factor solutions were determined as optimal HERM solutions, respectively.

Text S3 Estimation of secondary organic aerosol (SOA).

Due to lack of critical tracers of SOA, the sources of SOA cannot be individually resolved by receptor model. In this study, In this study, the secondary sources were mainly characterized by high EV values for inorganic aerosols such as SO_4^{2-} , NO_3^-, NH_4^+, but the medium EV values for OA (16~29%) were also presented on secondary sources in three pilot cities. This means that the SOA maybe mixed in with the factors of secondary sources. To verify this, the SOA concentrations we estimated by using a BC-tracer method (Wang et al., 2019) and then compared the results with those based on source apportionment. The SOA calculation by BC-tracer method was calculated as follow:

$$[SOA]_{BC\text{-}tracer} = [OA] - (OA/BC)_{pri} \times [BC] \quad \text{(S-1)}$$

where [ ] means mass concentration, $(OA/BC)_{pri}$ is the ratio of [OA] to [BC] in primary emission. The $(OA/BC)_{pri}$ ratios vary among sources, therefore, a minimum R squired (MRS) method was used to derive appropriate $(OA/BC)_{pri}$ values for three pilot cities. In previous studies (Srivastava et al., 2018; Wang et al., 2019), MRS method has been used to calculated the concertation of secondary organic carbon and brown carbon. More detailed information on the method and a validation of this approach can be found in Wang et al. (2019).

In addition, according to results of receptor model, SOA concentration can also be estimated as follow based on EV values of OA from secondary source factors.

$$[SOA]_{source\ apportionment} = [OA] \times EV\_OA \quad \text{(S-2)}$$

where EV_OA represents the EV values of OA in secondary sources factors resolved by HERM model.

As shown in Fig. S9, the $(OA/BC)_{pri}$ ratios were determined as 4.73 for Xi'an, 3.12 for Shijiazhuang and 7.6 for Beijing, respectively. Furthermore, the concentrations of SOA from three pilot cities were shown in Table R1 based two different methods. As we can see, the SOA concentrations estimated by EV values of OA are close to that by BC-tracer method for three pilot cities. This indicated SOA was mixed in secondary sources factors.

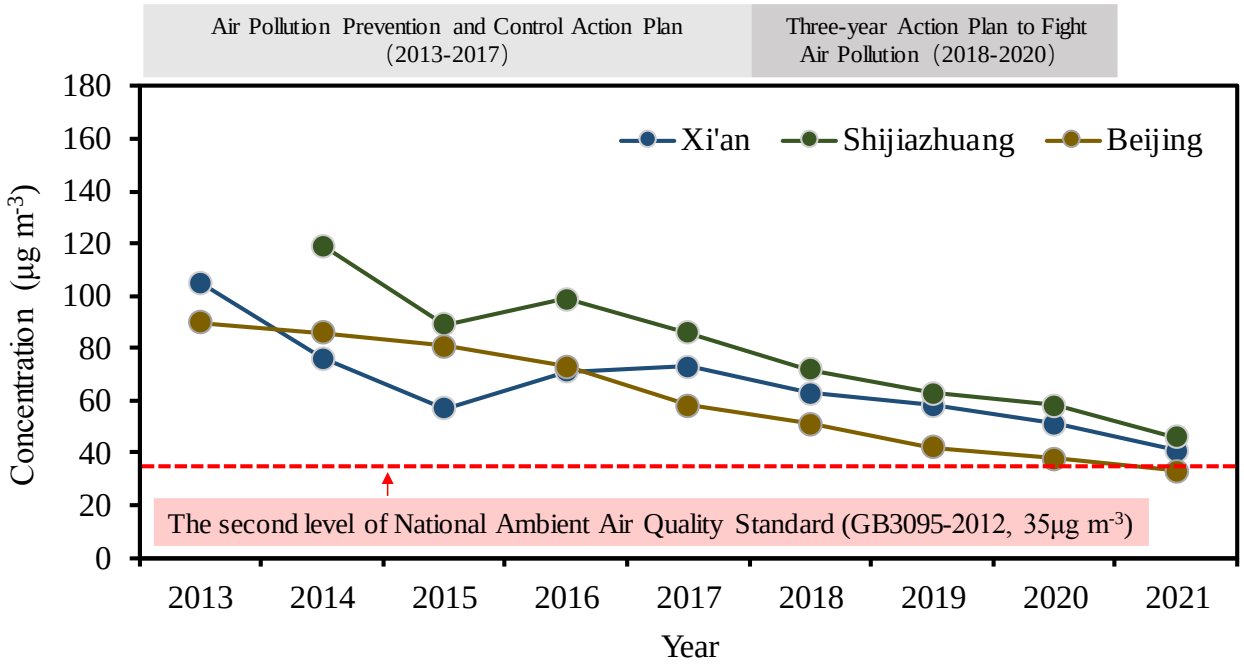

Figure S1. Annual average concentration of $PM_{2.5}$ from 2013 to 2021 in Xi'an, Shijiazhuang, and Beijing. (The data are from the website of the local Ecological Environment Bureau, Xi'an: http://xaepb.xa.gov.cn/, Shijiazhuang: https://sthjj.sjz.gov.cn/, Beijing: http://sthjj.beijing.gov.cn/). The red dotted line represents the second level of the National Ambient Air Quality Standard (GB3095-2012, 35 μg m^{-3})

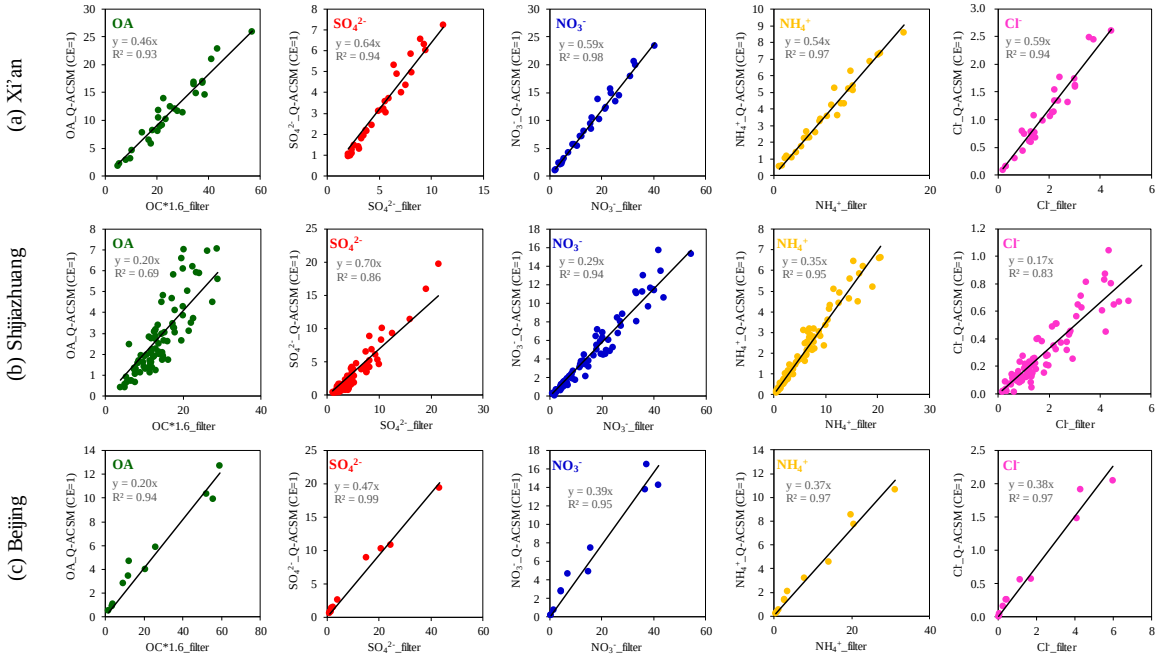

Figure S2. Correction of chemical components measured by Q-ACSM in different cities. During the campaigns, offline filter samples were simultaneously sampled for the correction. In summary, 29 offline samples in Xi'an, 83 offline samples in Shijiazhuang, and 10 offline samples in Beijing were sampled respectively.

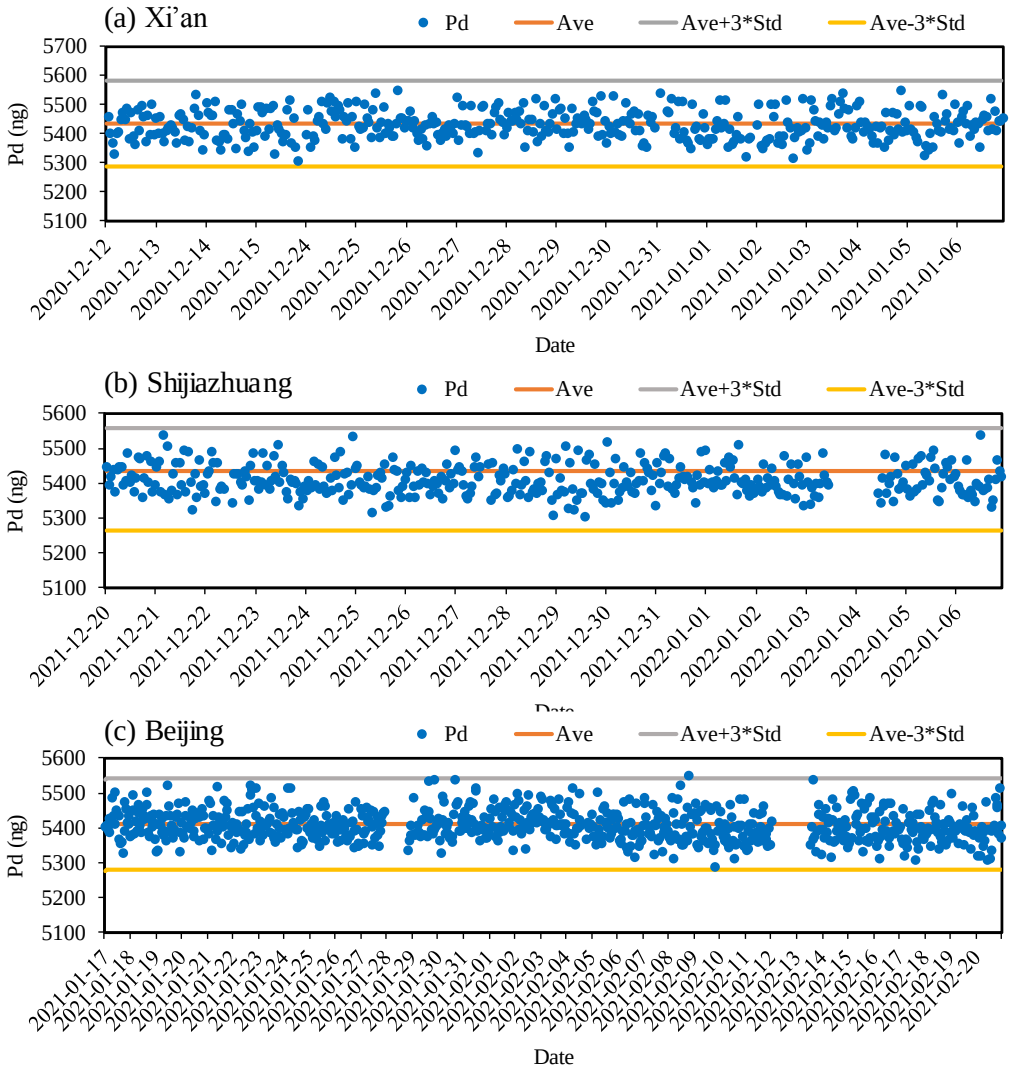

Figure S3. Concentration of the internal standard element (Pd) of Xact625 during sampling periods in (a) Xi'an, (b) Shijiazhuang, and (c) Beijing.

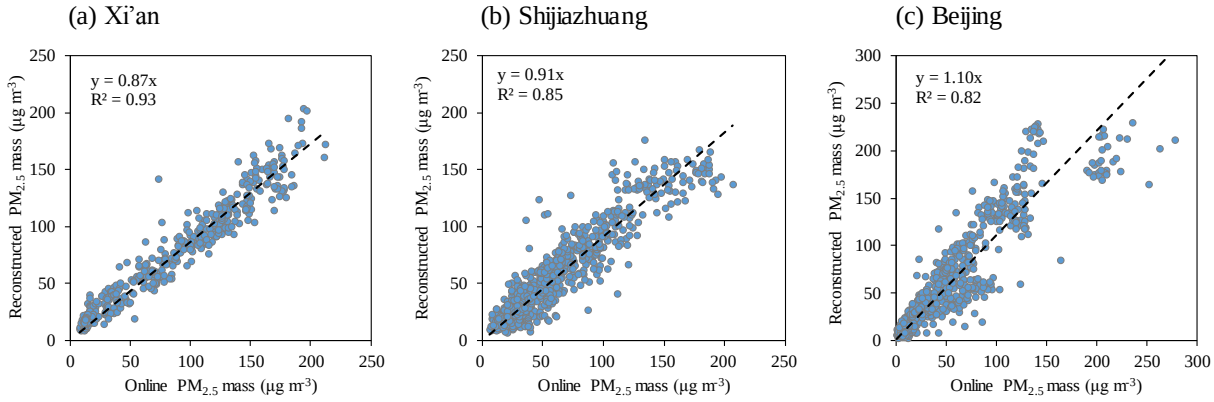

Figure S4. Correlation of online and reconstructed $PM_{2.5}$ concentration in (a) Xi'an, (b) Shijiazhuang, and (c) Beijing during the campaigns. The online $PM_{2.5}$ mass data in the X axis from national monitor stations near sampling sites.

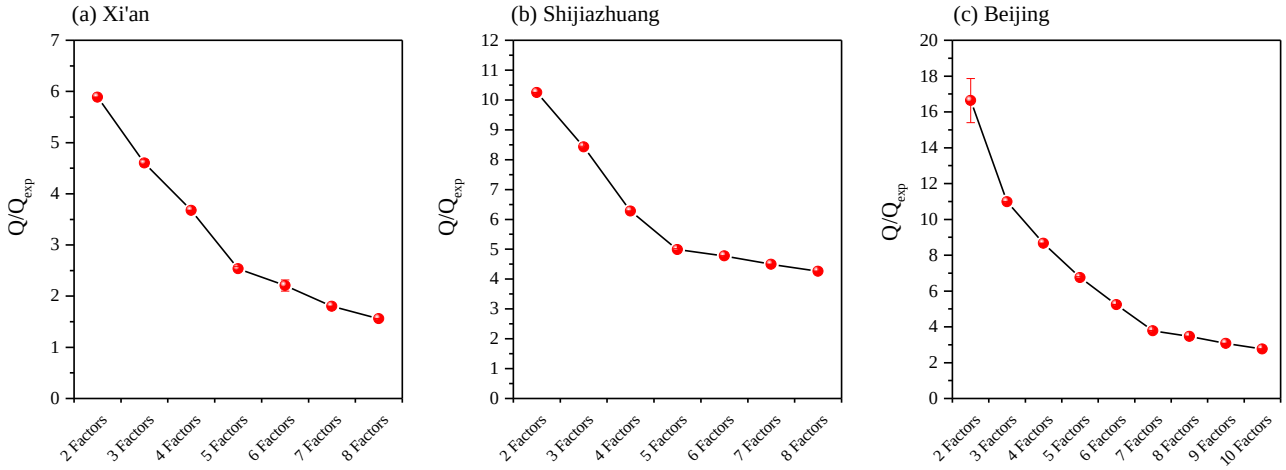

Figure S5. Values of Q/Q_{exp} for the unconstrained profile solutions with two to ten factors based on thirty runs in (a) Xi'an, (b) Shijiazhuang, and (c) Beijing, respectively.

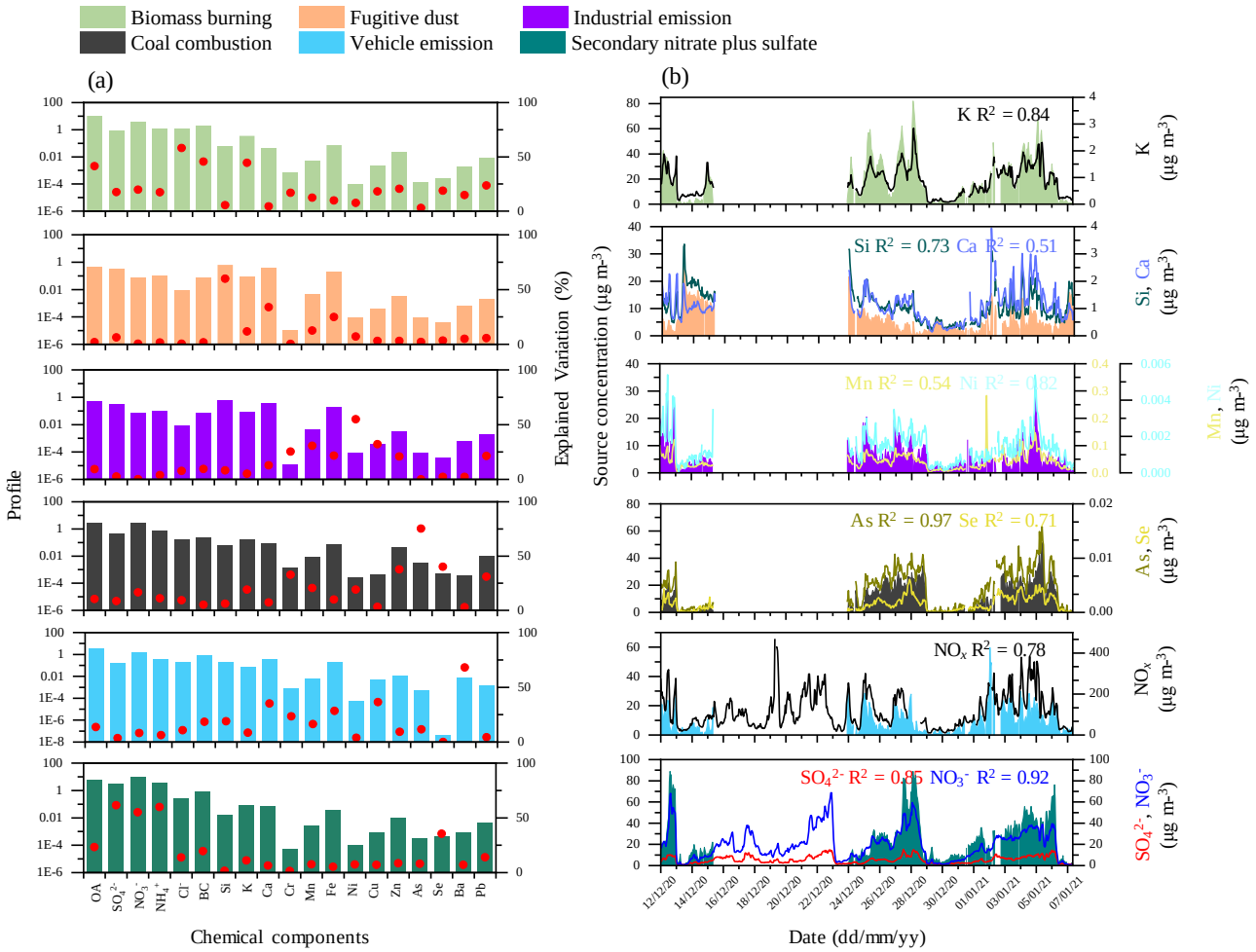
Biomass burning
Coal combustion
Fugitive dust
Vehicle emission
Industrial emission
Secondary nitrate plus sulfate
(a)
(b)
Profile
Explained Variation (%)
Source concentration (μg m-3)
K R2 = 0.84
Si R2 = 0.73 Ca R2 = 0.51
Mn R2 = 0.54 Ni R2 = 0.82
As R2 = 0.97 Se R2 = 0.71
NOx R2 = 0.78
SO42- R2 = 0.85 NO3- R2 = 0.92
K (μg m-3)
Si, Ca (μg m-3)
Mn, Ni (μg m-3)
As, Se (μg m-3)
NOx (μg m-3)
SO42-, NO3- (μg m-3)
OA
SO42-
NO3-
NH4+
Cl
BC
Si
K
Ca
Cr
Mn
Fe
Ni
Cu
Zn
As
Se
Ba
Pb
Chemical components
12/12/20
14/12/20
16/12/20
18/12/20
20/12/20
22/12/20
24/12/20
26/12/20
28/12/20
30/12/20
01/01/21
03/01/21
05/01/21
07/01/21
Date (dd/mm/yy)

91

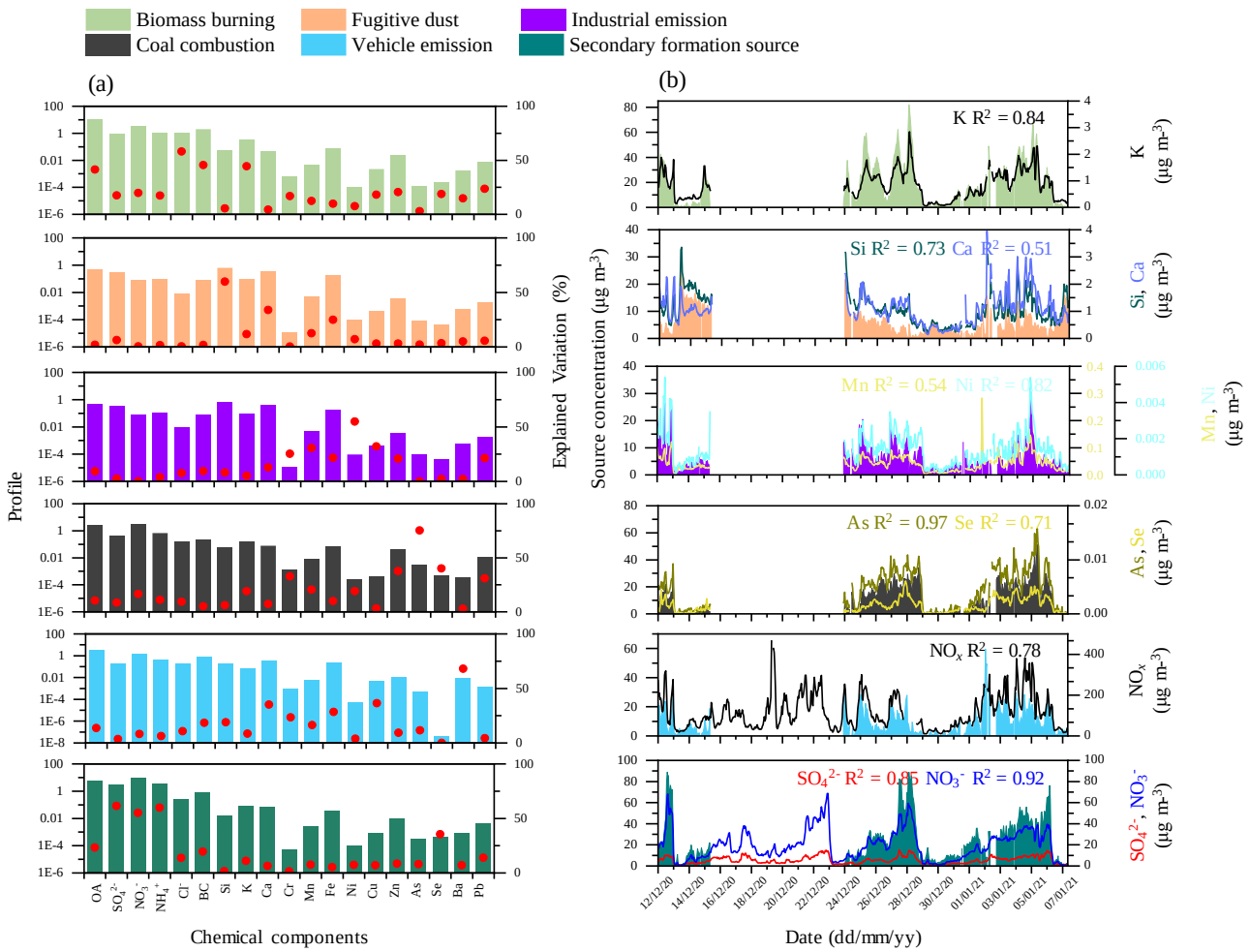

Figure S6. (a) Sources profiles obtained from HERM with a six-factor solution in Xi'an, the columns in each factor are the profile that displays the relative relation of the absolute values of variables. The red dot represents the explained variation (EV) in species for different factors. (b) Time series plots of sources concentration, including biomass burning, fugitive dust, industrial emission, coal combustion, vehicle emission, and secondary ~~nitrate plus sulfate~~formation source. The corresponding time trends of chemical tracers are also shown.

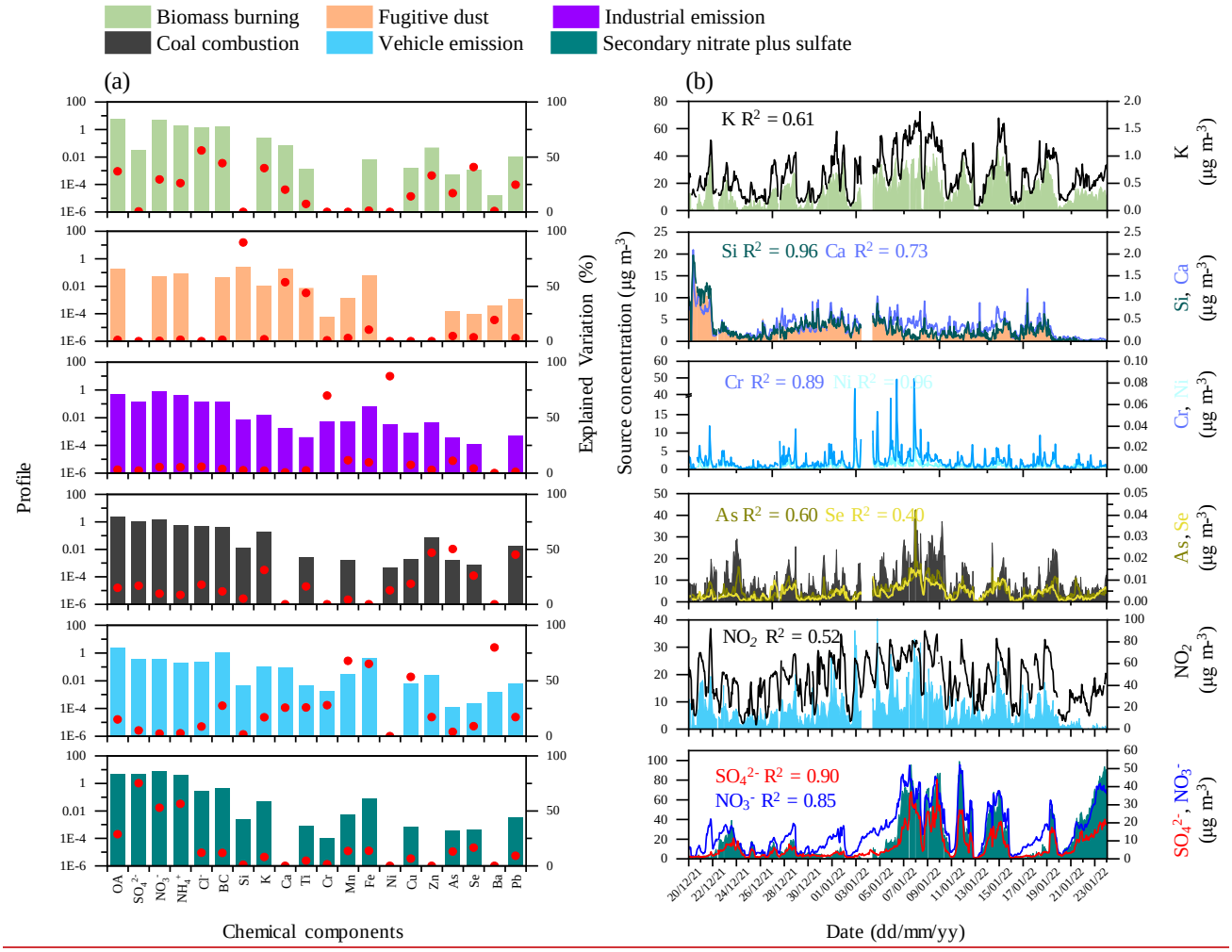
Biomass burning
Coal combustion
Fugitive dust
Vehicle emission
Industrial emission
Secondary nitrate plus sulfate
(a)
(b)
Profile
Explained Variation (%)
Source concentration (μg m-3)
Chemical components
Date (dd/mm/yy)
K R2 = 0.61
Si R2 = 0.96 Ca R2 = 0.73
Cr R2 = 0.89 Ni R2 = 0.86
As R2 = 0.60 Se R2 = 0.40
NO2 R2 = 0.52
SO42- R2 = 0.90
NO3- R2 = 0.85
K (μg m-3)
Si, Ca (μg m-3)
Cr, Ni (μg m-3)
As, Se (μg m-3)
NO2 (μg m-3)
SO42-, NO3- (μg m-3)
OA
SO42-
NO3-
NH4+
Cl-
BC
Si
K
Ca
Ti
Cr
Mn
Fe
Ni
Cu
Zn
As
Se
Ba
Pb

98

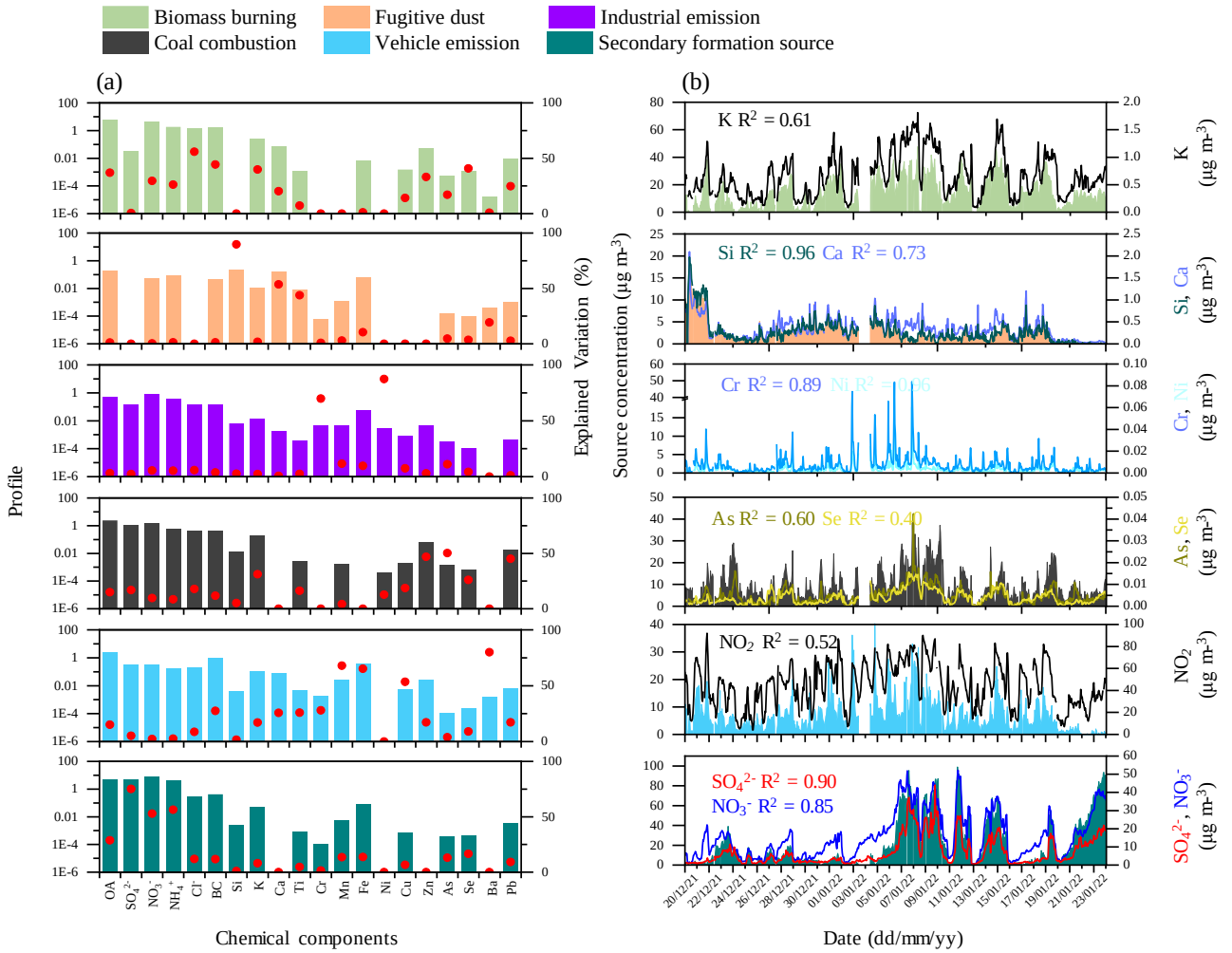

Figure S7. (a) Sources profiles obtained from HERM with a six-factor solution in Shijiazhuang, the columns in each factor are the profile that displays the relative relation of the absolute values of variables. The red dot represents the explained variation (EV) in species for different factors. (b) Time series plots of sources concentration, including biomass burning, fugitive dust, industrial emission, coal combustion, vehicle emission, and secondary ~~nitrate plus sulfate~~formation source. The corresponding time trends of chemical tracers are also shown.

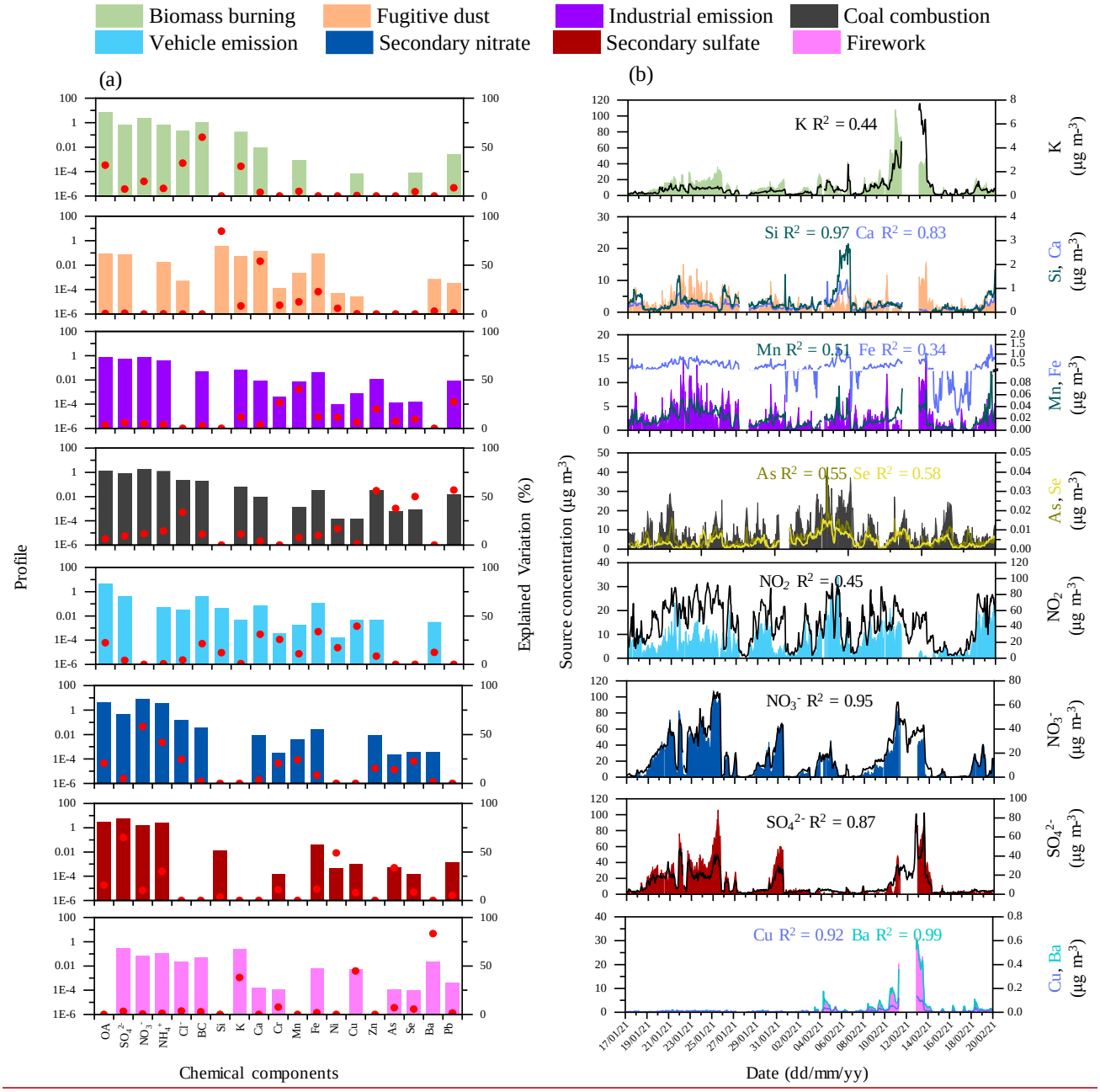
Biomass burning
Fugitive dust
Industrial emission
Coal combustion
Vehicle emission
Secondary nitrate
Secondary sulfate
Firework
(a)
(b)
Profile
Explained Variation (%)
Source concentration (μg m-3)
Chemical components
Date (dd/mm/yy)
K R2 = 0.44
Si R2 = 0.97 Ca R2 = 0.83
Mn R2 = 0.51 Fe R2 = 0.34
As R2 = 0.55 Se R2 = 0.58
NO2 R2 = 0.45
NO3- R2 = 0.95
SO42- R2 = 0.87
Cu R2 = 0.92 Ba R2 = 0.99
OA
SO42-
NO3-
NH4+
Cl-
BC
Si
K
Ca
Cr
Mn
Fe
Ni
Cu
Zn
As
Se
Ba
Pb

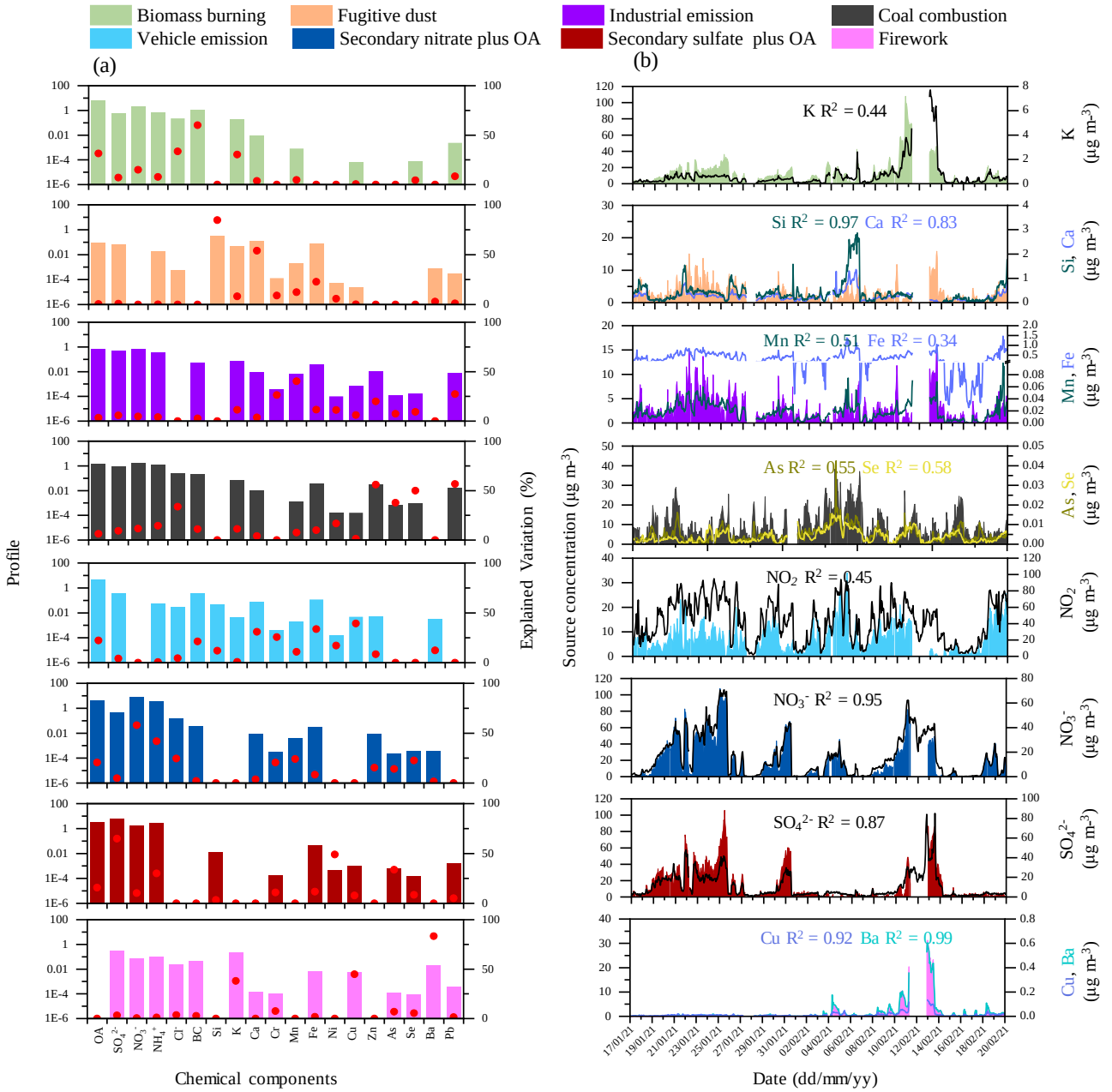

Figure S8. (a) Sources profiles obtained from HERM with an eight-factor solution in Beijing, the columns in each factor are the profile that displays the relative relation of the absolute values of variables. The red dot represents the explained variation (EV) in species for different factors. (b) Time series plots of sources concentration, including biomass burning, fugitive dust, industrial emission, coal combustion, vehicle emission, secondary nitrate plus OA, secondary sulfate plus OA, and firework. The corresponding time trends of chemical tracers are also shown.

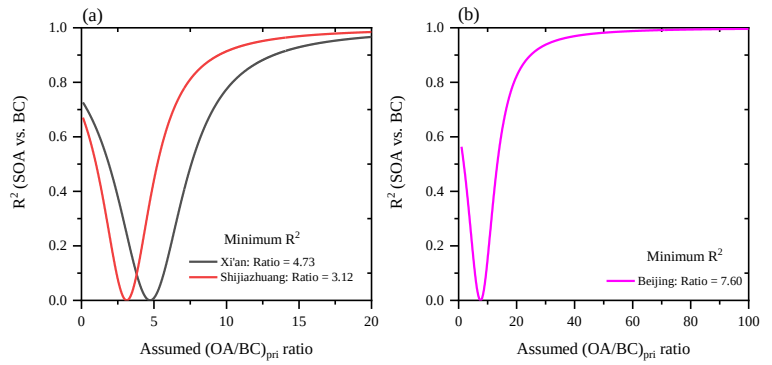

Figure S9. Coefficients of determination (R^2) for SOA versus BC mass concentration plotted against assumed ratios for OA to BC in primary emissions ($(OA/BC)_{pri}$) in Xi'an, Shijiazhuang and Beijing.

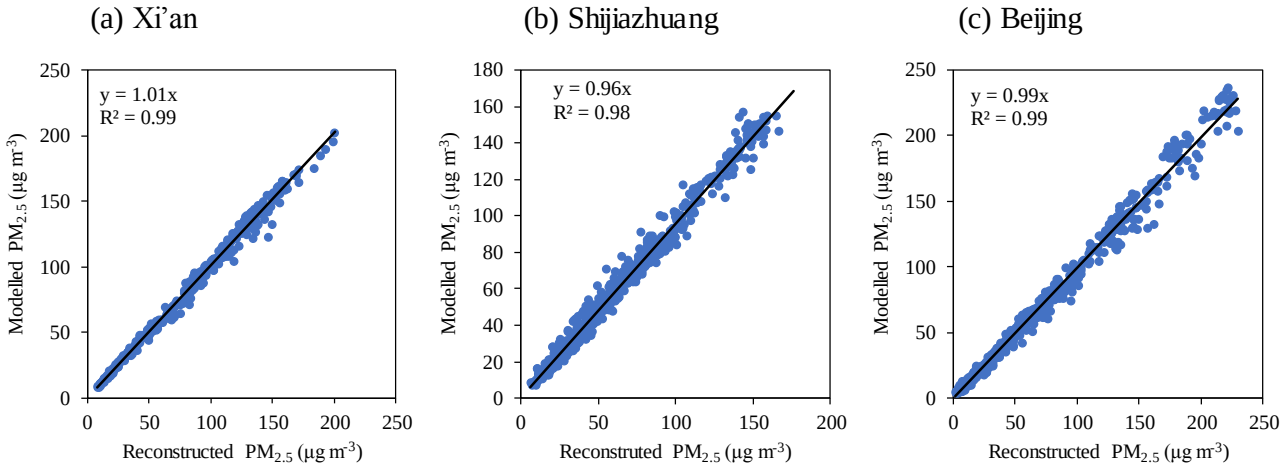

Figure ~~S9~~S10. Correlation between reconstructed $PM_{2.5}$ and modeled $PM_{2.5}$ mass concentrations derived by HERM in Xi'an, Shijiahuznag, and Beijing with optimal solutions

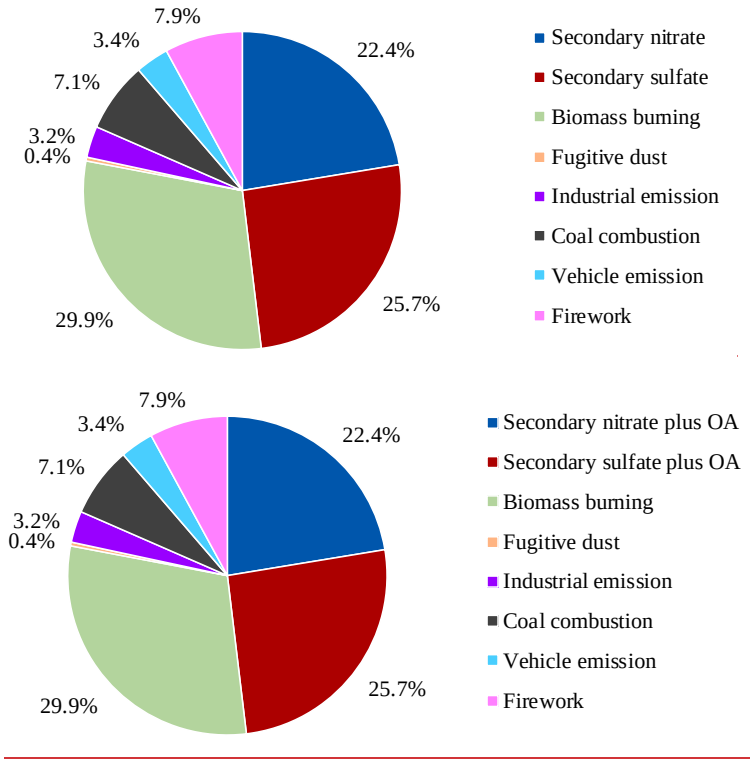

Figure ~~S10~~S11. Source contribution of $PM_{2.5}$ during Chinese Spring Festival (from New Year's Eve to January 3rd of the Lunar Calendar) in Beijing

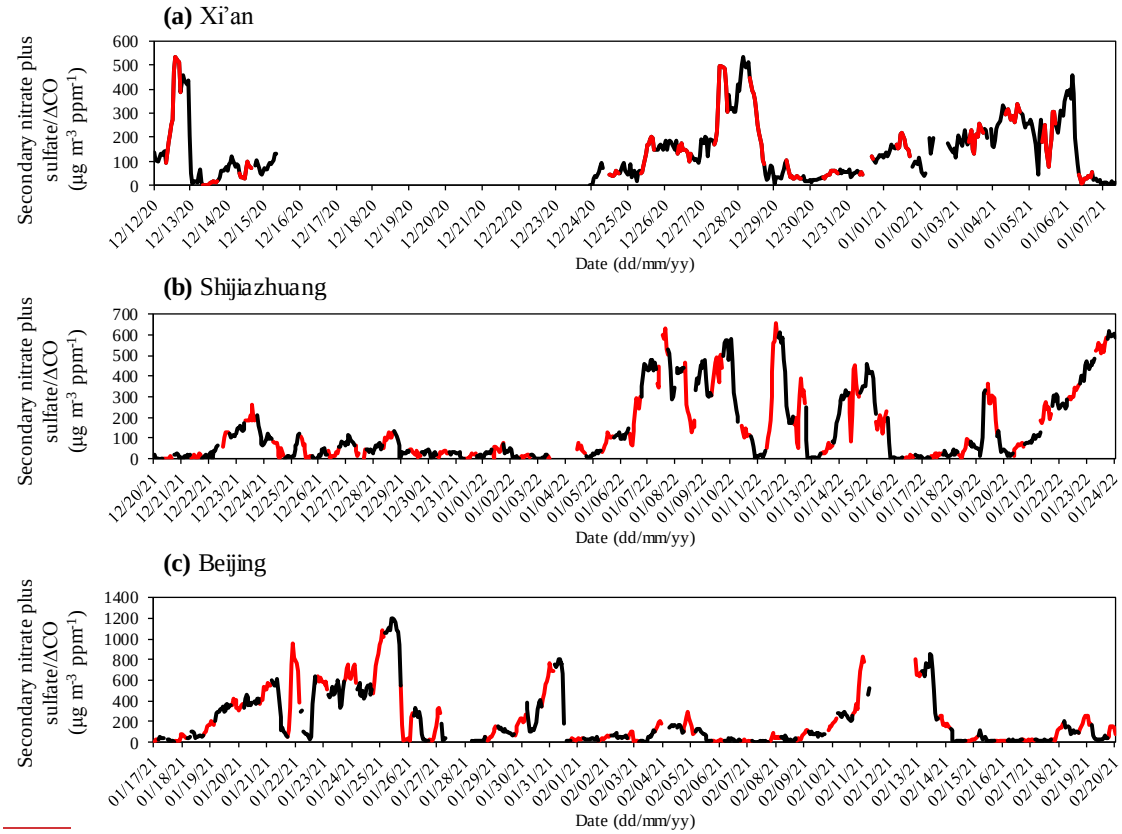
(a) Xi'an
Secondary nitrate plus sulfate/ΔCO (μg m-3 ppm-1)
Date (dd/mm/yy)
(b) Shijiazhuang
Secondary nitrate plus sulfate/ΔCO (μg m-3 ppm-1)
Date (dd/mm/yy)
(c) Beijing
Secondary nitrate plus sulfate/ΔCO (μg m-3 ppm-1)
Date (dd/mm/yy)

125

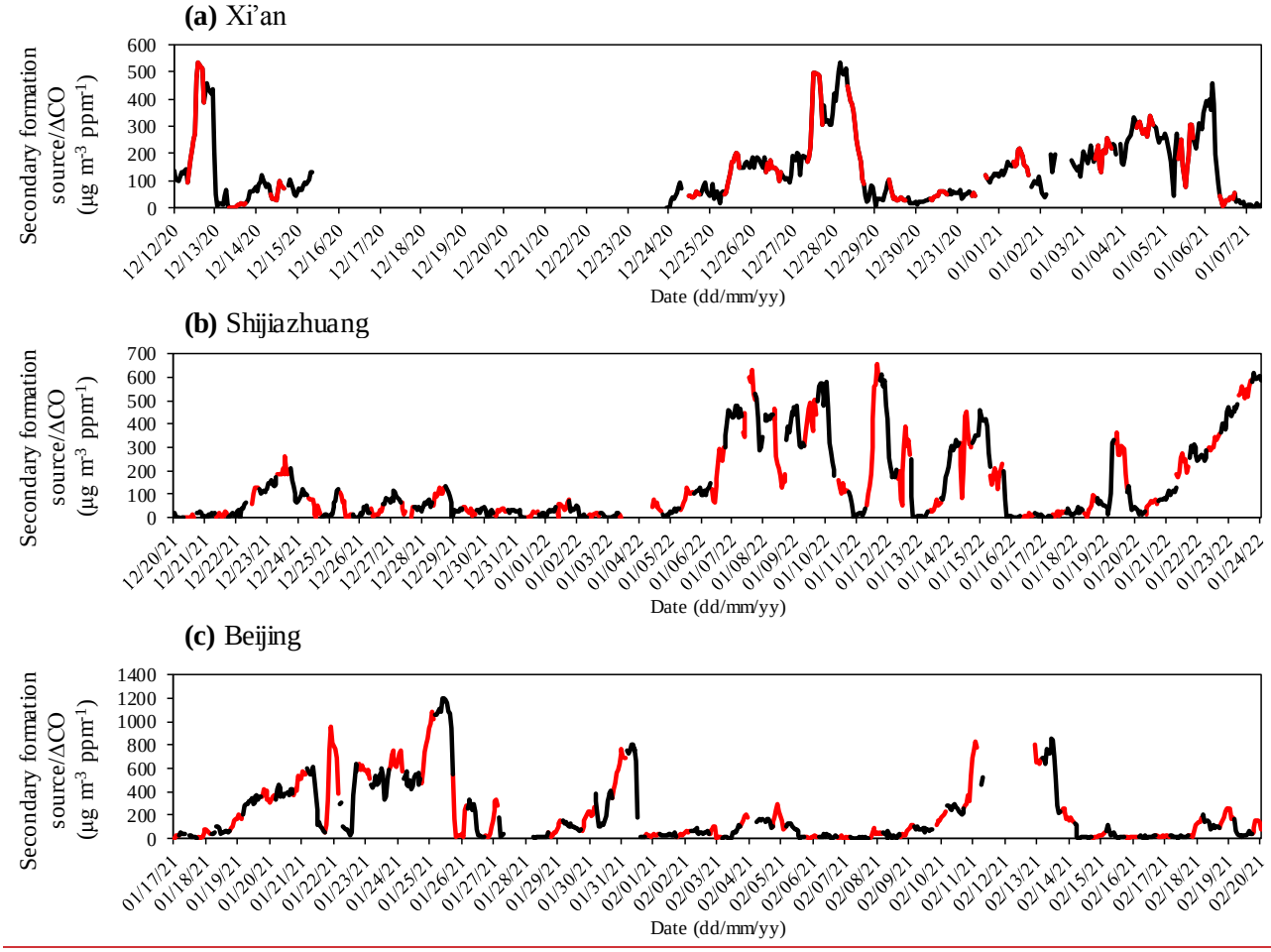
(a) Xi'an
Secondary formation source/ΔCO (μg m-3 ppm-1)
Date (dd/mm/yy)
(b) Shijiazhuang
Secondary formation source/ΔCO (μg m-3 ppm-1)
Date (dd/mm/yy)
(c) Beijing
Secondary formation source/ΔCO (μg m-3 ppm-1)
Date (dd/mm/yy)

126

Figure ~~S11~~S12. Time series plots of secondary ~~nitrate plus sulfate~~formation source/ΔCO in (a) Xi'an, (b) Shijiazhuang, and (c) Beijing. The red and black lines represent daytime (08:00-17:00 LST) and nighttime (18:00 - 07:00 the next day LST), respectively.

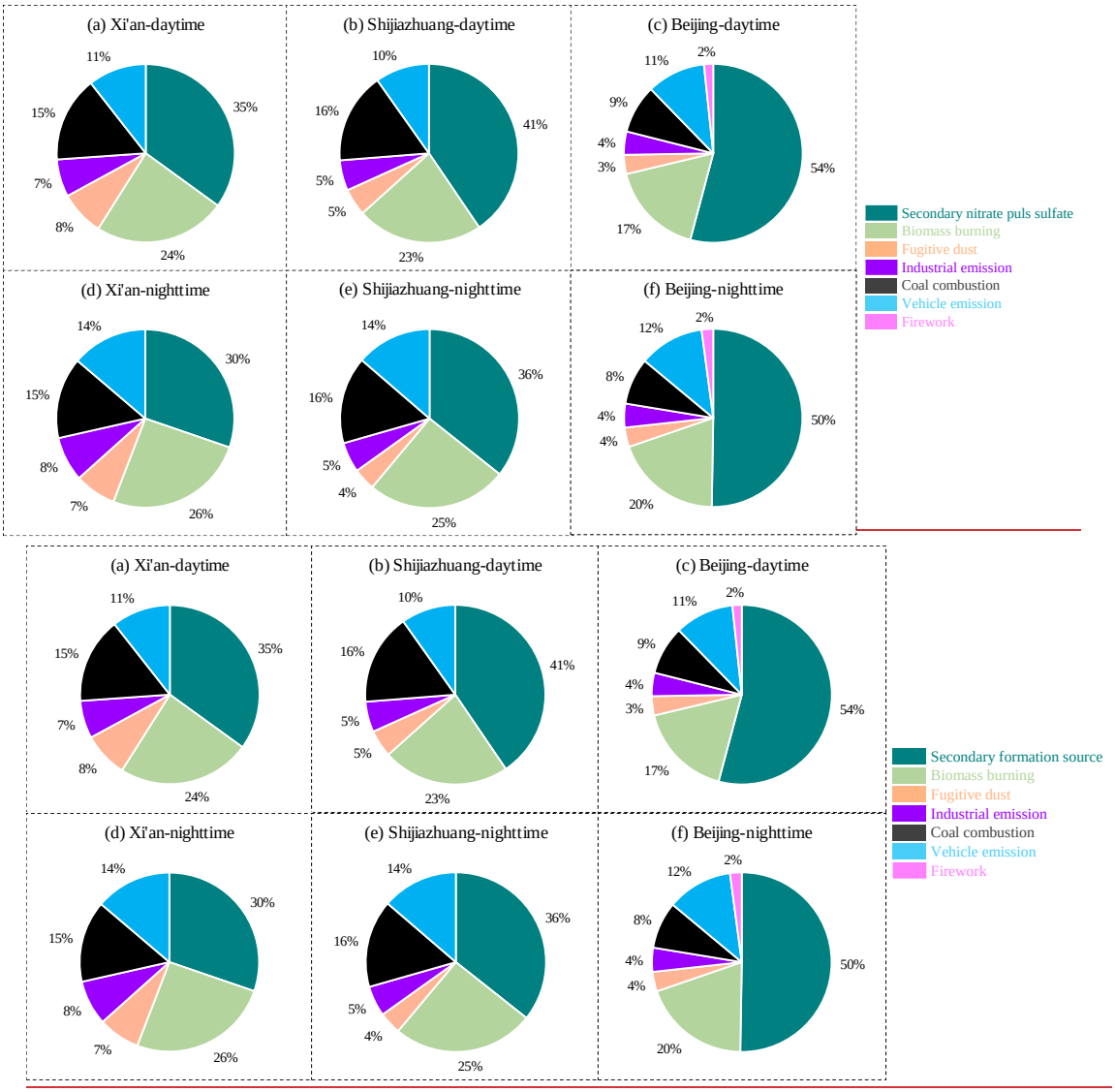

Figure ~~S12~~S13. Source contribution of $PM_{2.5}$ in three pilot cities during daytime and nighttime, respectively.

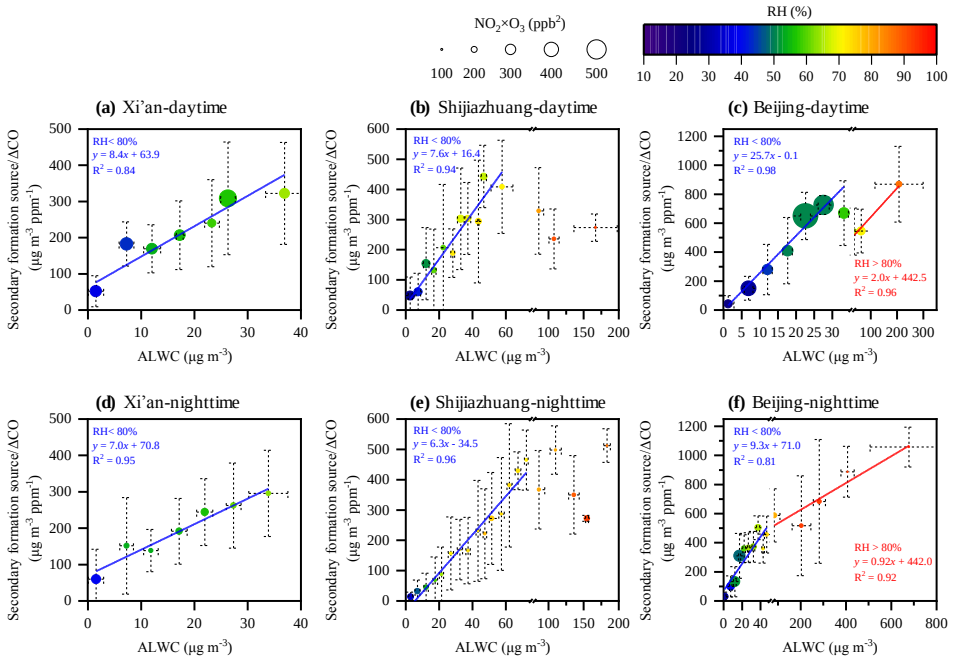

Figure S14. Correlation of secondary formation source/ΔCO and ALWC during daytime (08:00–17:00 LST, a–c) and nighttime (18:00–7:00 the next day LST, d–f) in Xi'an, Shijiazhuang, and Beijing, respectively. The points and error bar represent the mean values and standard deviation values of secondary formation source /ΔCO and ALWC in each bin. In Xi'an, each bin is 5 μg m^{-3} (ΔALWC = 5 μg m^{-3}). In Shijiazhuang, each bin is 5 μg m^{-3} (ΔALWC = 5 μg m^{-3}) when ALWC ranged from 0 to 75μg m^{-3}, but 25 μg m^{-3} (ΔALWC = 25 μg m^{-3}) for ALWC ranged from 75 to 200 μg m^{-3} due to limitations in data. In Beijing, during daytime, each bin is 5 μg m^{-3} (ΔALWC = 5 μg m^{-3}) when ALWC ranged from 0 to 40 μg m^{-3}, but 100 μg m^{-3} (ΔALWC = 100 μg m^{-3}) for ALWC ranged from 40 to 450 μg m^{-3} due to limitations in data. During nighttime, each bin is 5 μg m^{-3} (ΔALWC = 5 μg m^{-3}) when ALWC ranged from 0 to 50 μg m^{-3}, but 100 μg m^{-3} (ΔALWC = 100 μg m^{-3}) for ALWC ranged from 50 to 900 μg m^{-3} due to limitations in data.

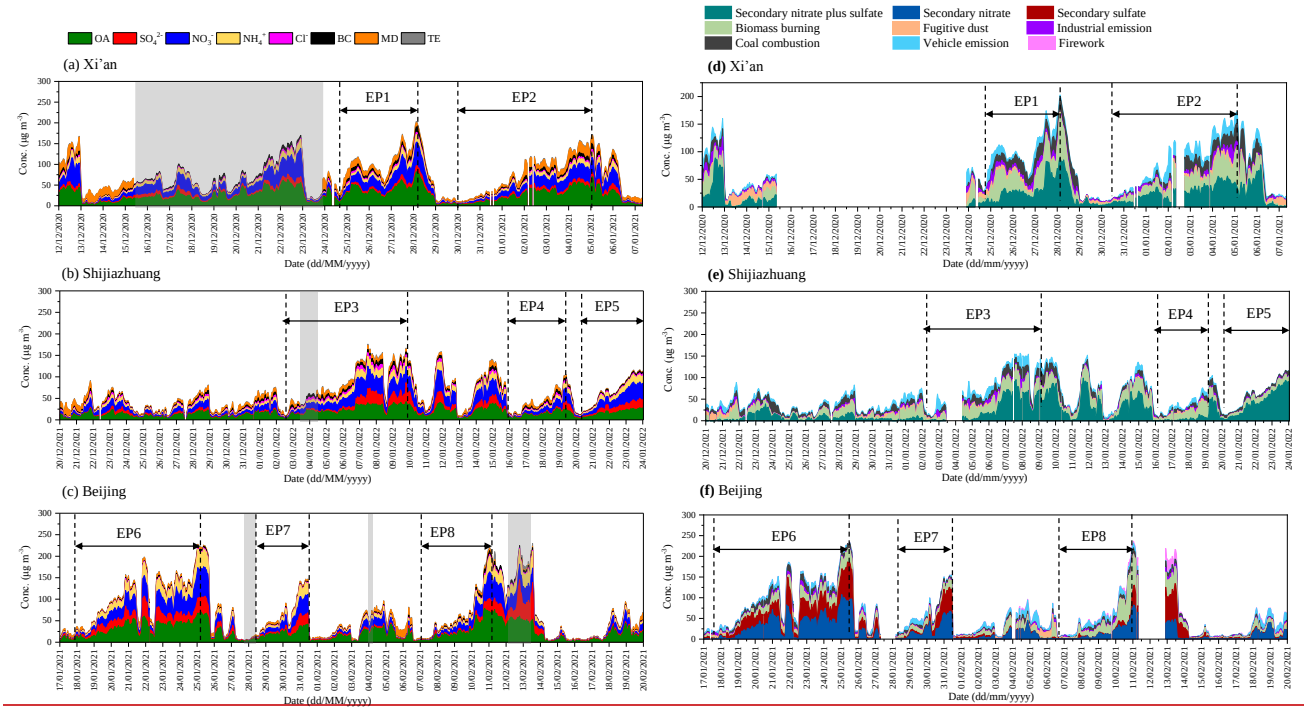

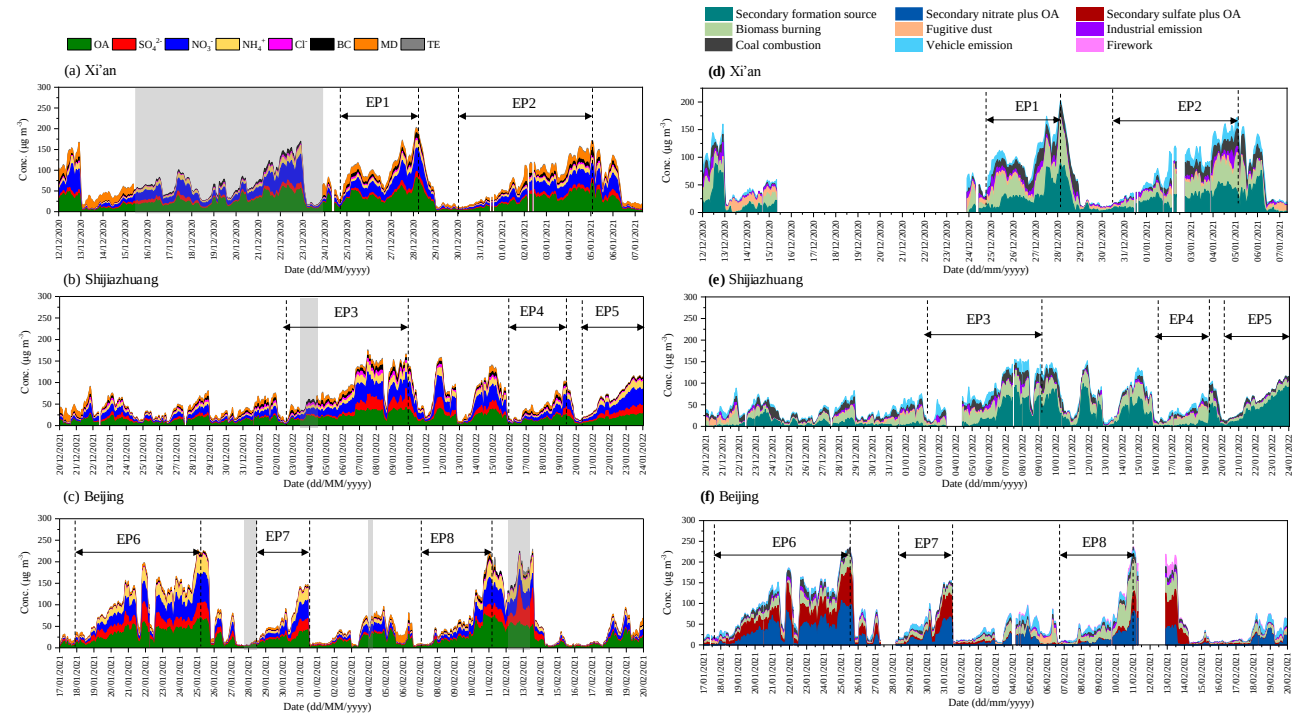

Figure ~~S13~~S15. The pollution episodes selection according to temporal variation of $PM_{2.5}$ chemical components (a-c) and source contribution (d-f) during the campaigns in Xi'an, Shijiazhuang, and Beijing, respectively. The gray shape parts were lack of MD values due to the out-of-order Xact625, and missing values in the time series owing to the out-of-order ACSM, AE33, and Xact625 at the same time.

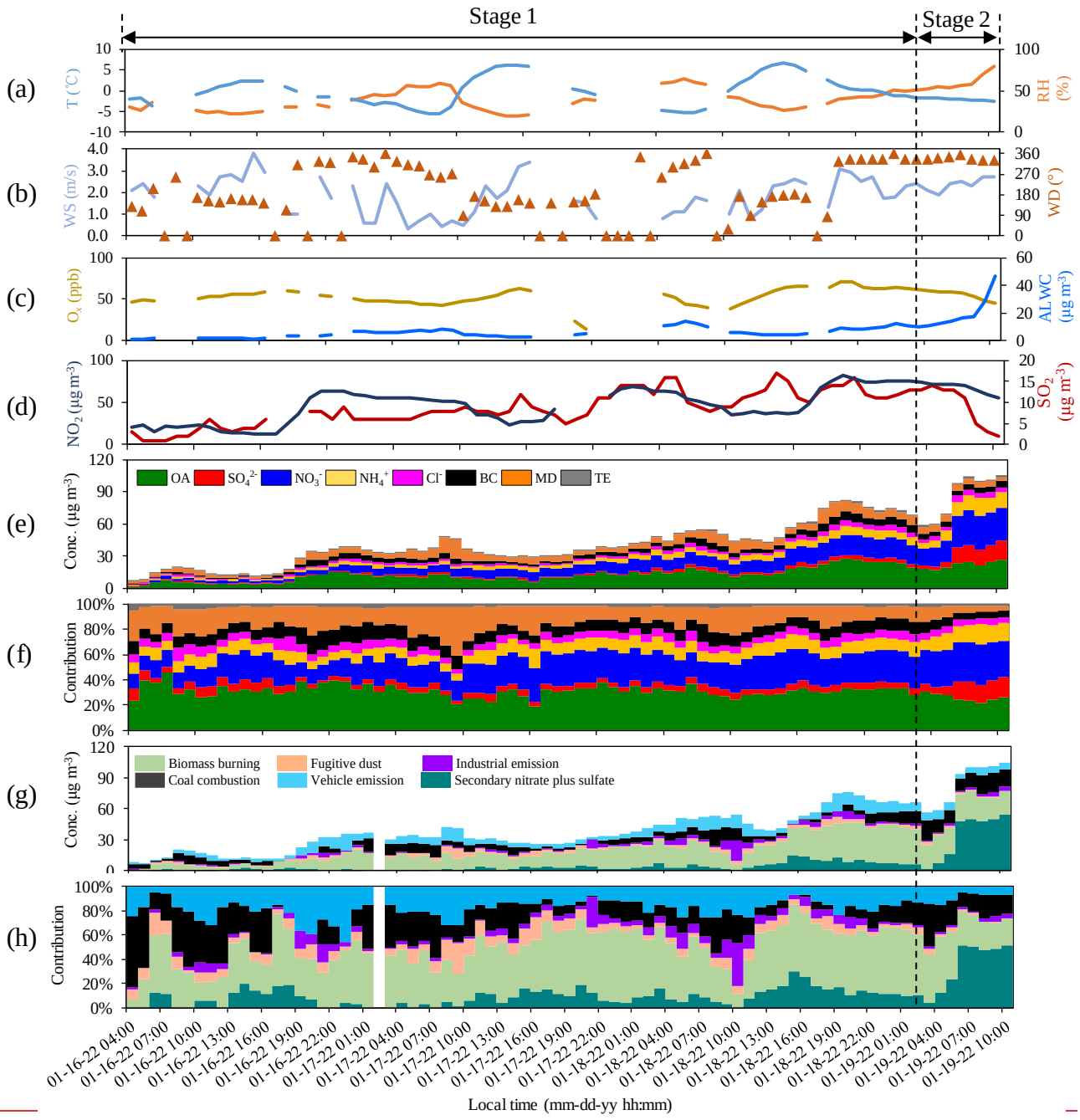
Stage 1
Stage 2
(a)
T (℃)
RH (%)
(b)
WS (m/s)
WD (°)
(c)
O_x (ppb)
ALWC (μg m^{-3})
(d)
NO_2 (μg m^{-3})
SO_2 (μg m^{-3})
(e)
Conc. (μg m^{-3})
OA
SO_4^{2-}
NO_3^-
NH_4^+
Cl^-
BC
MD
TE
(f)
Contribution
(g)
Conc. (μg m^{-3})
Biomass burning
Coal combustion
Fugitive dust
Vehicle emission
Industrial emission
Secondary nitrate plus sulfate
(h)
Contribution
01-16-22 04:00
01-16-22 07:00
01-16-22 10:00
01-16-22 13:00
01-16-22 16:00
01-16-22 19:00
01-16-22 22:00
01-17-22 01:00
01-17-22 04:00
01-17-22 07:00
01-17-22 10:00
01-17-22 13:00
01-17-22 16:00
01-17-22 19:00
01-17-22 22:00
01-18-22 01:00
01-18-22 04:00
01-18-22 07:00
01-18-22 10:00
01-18-22 13:00
01-18-22 16:00
01-18-22 19:00
01-18-22 22:00
01-19-22 01:00
01-19-22 04:00
01-19-22 07:00
01-19-22 10:00
Local time (mm-dd-yy hh:mm)

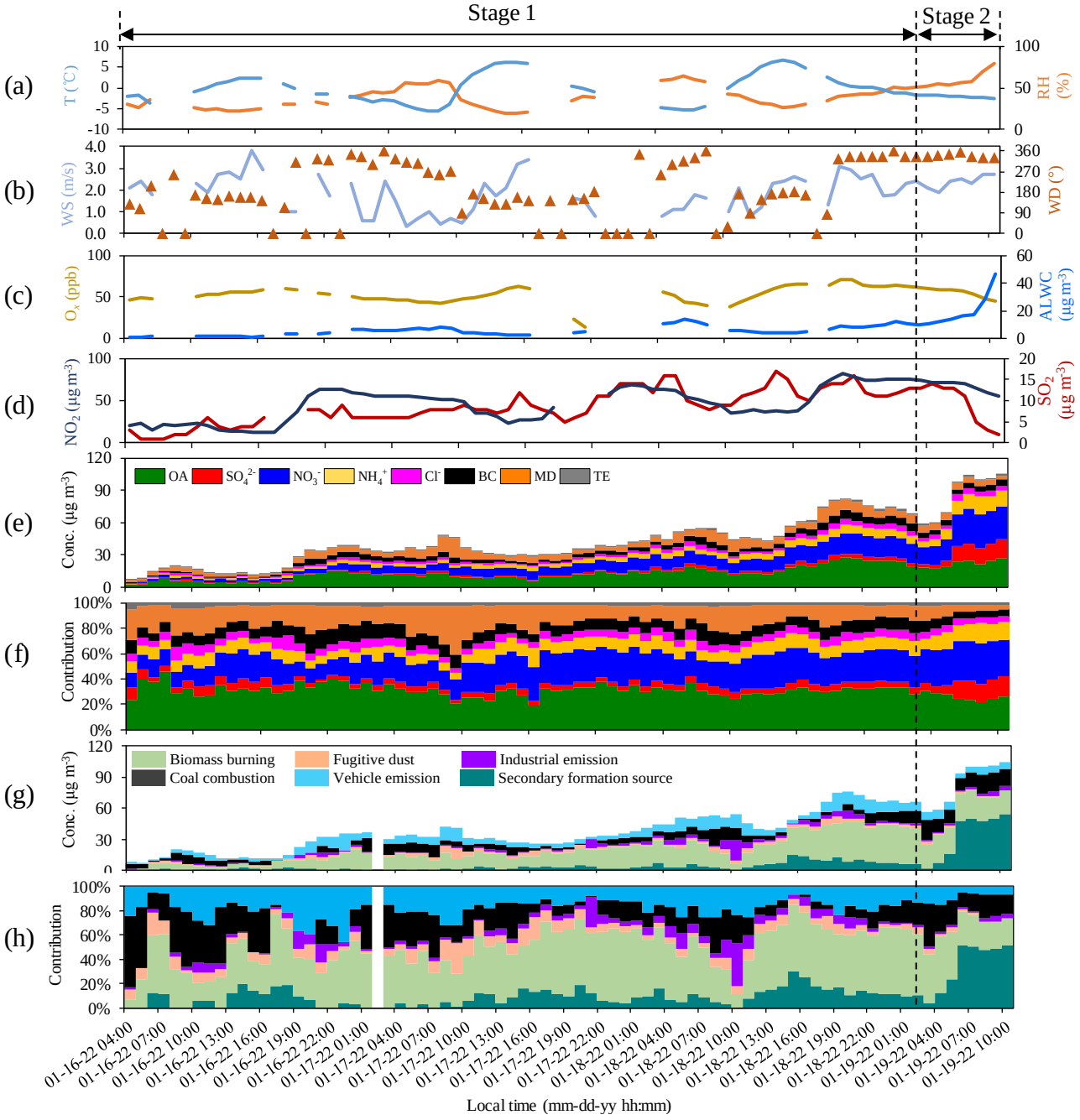

Figure S14.6 Time series of T and RH (a), WS and WD (b), O_x and ALWC (c), NO_2 and SO_2 (d), chemical components (e,f), and source contribution (g, h) of $PM_{2.5}$ during EP4 in Shijiazhuang.

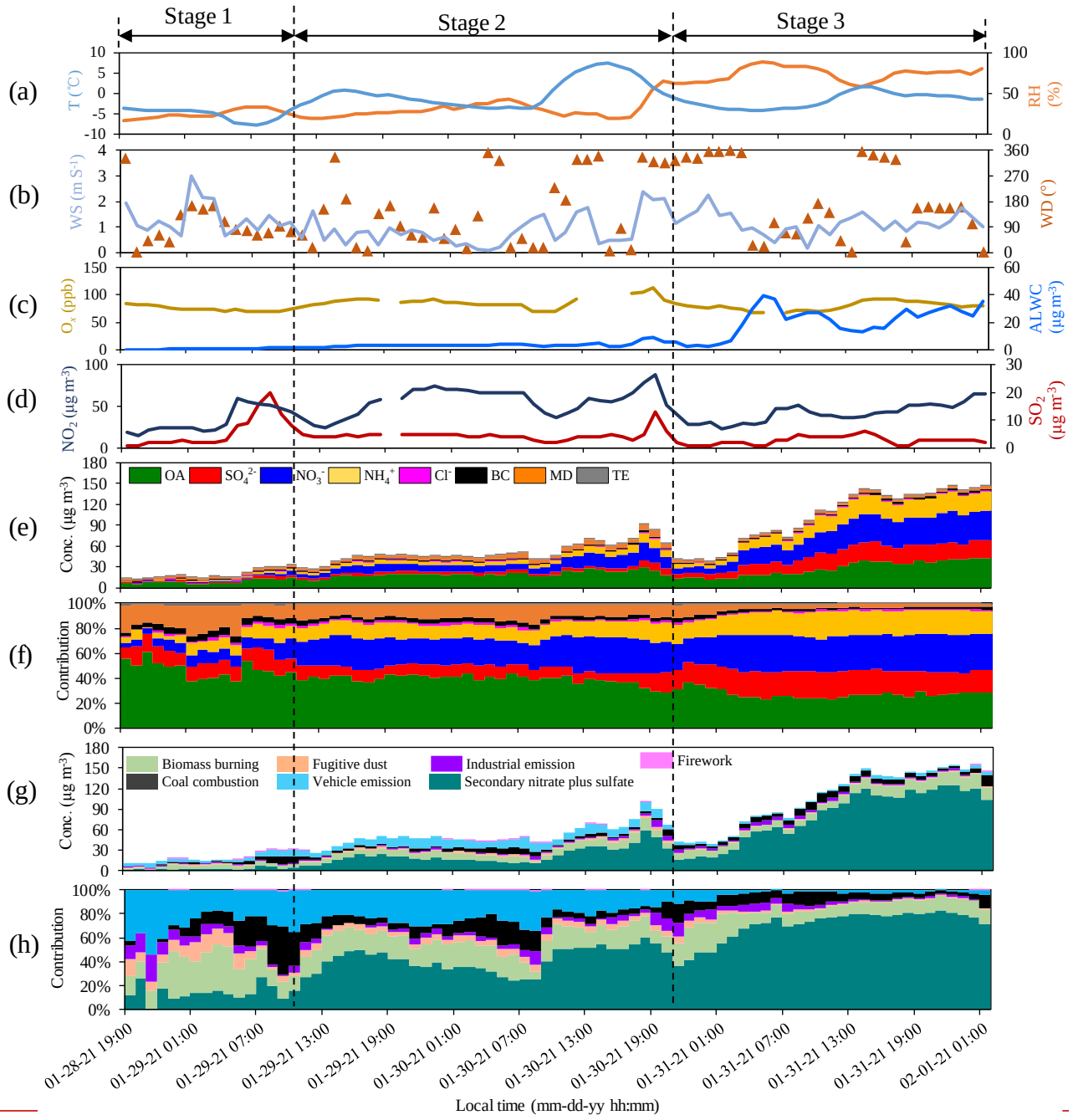
Stage 1
Stage 2
Stage 3
(a)
T (°C)
RH (%)
(b)
WS (m S-1)
WD (°)
(c)
Ox (ppb)
ALWC (μg m-3)
(d)
NO2 (μg m-3)
SO2 (μg m-3)
(e)
Conc. (μg m-3)
OA
SO4 2-
NO3 -
NH4 +
Cl-
BC
MD
TE
(f)
Contribution
(g)
Conc. (μg m-3)
Biomass burning
Coal combustion
Fugitive dust
Vehicle emission
Industrial emission
Secondary nitrate plus sulfate
Firework
(h)
Contribution
01-28-21 19:00
01-29-21 01:00
01-29-21 07:00
01-29-21 13:00
01-29-21 19:00
01-30-21 01:00
01-30-21 07:00
01-30-21 13:00
01-30-21 19:00
01-31-21 01:00
01-31-21 07:00
01-31-21 13:00
01-31-21 19:00
02-01-21 01:00
Local time (mm-dd-yy hh:mm)

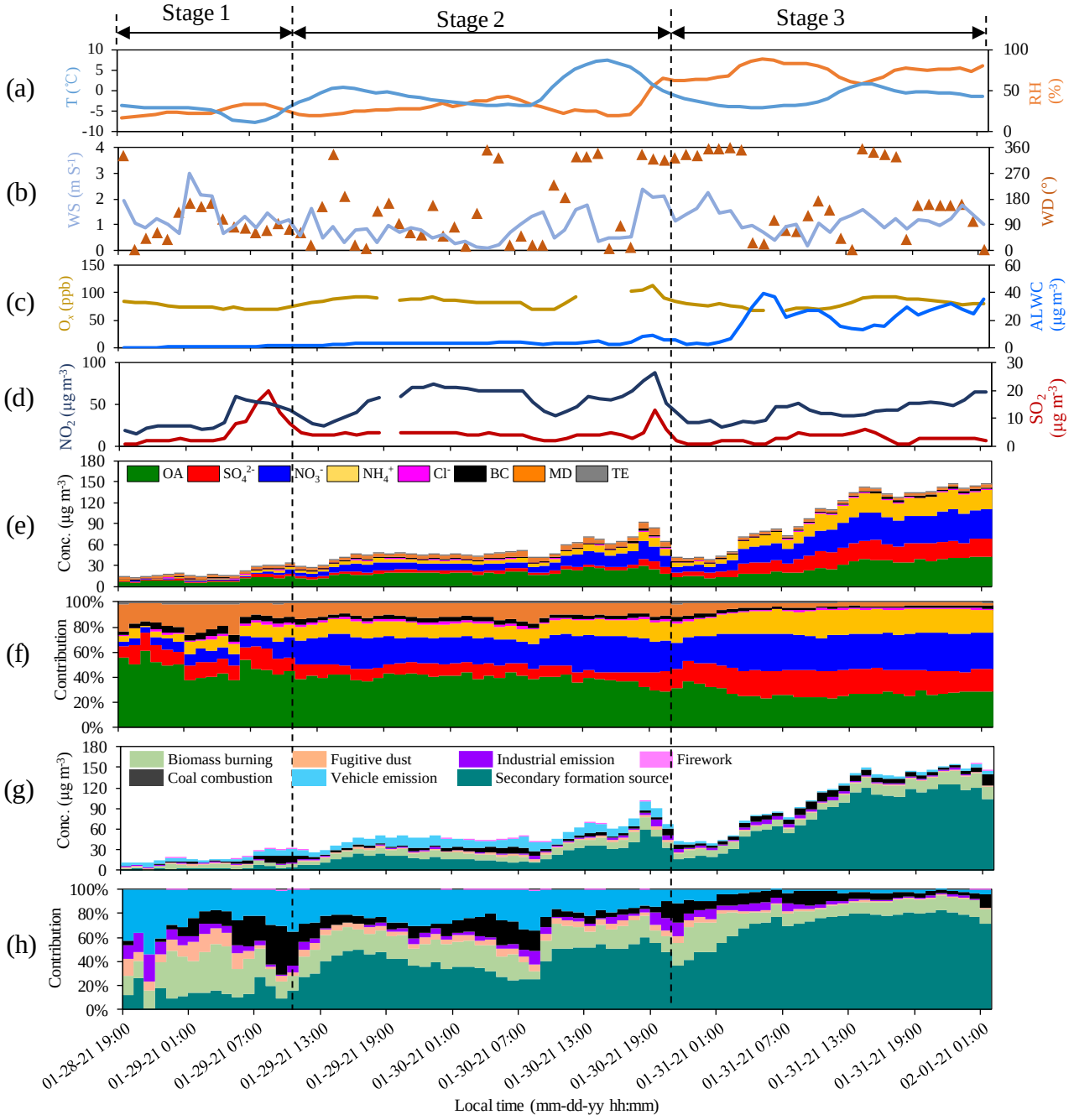

157

158 **Figure ~~S15~~S17.** Time series of T and RH (a), WS and WD (b), O_x and ALWC (c), NO_2 and SO_2 (d), chemical
159 components (e, f), and source contribution (g, h) of $PM_{2.5}$ during EP7 in Beijing

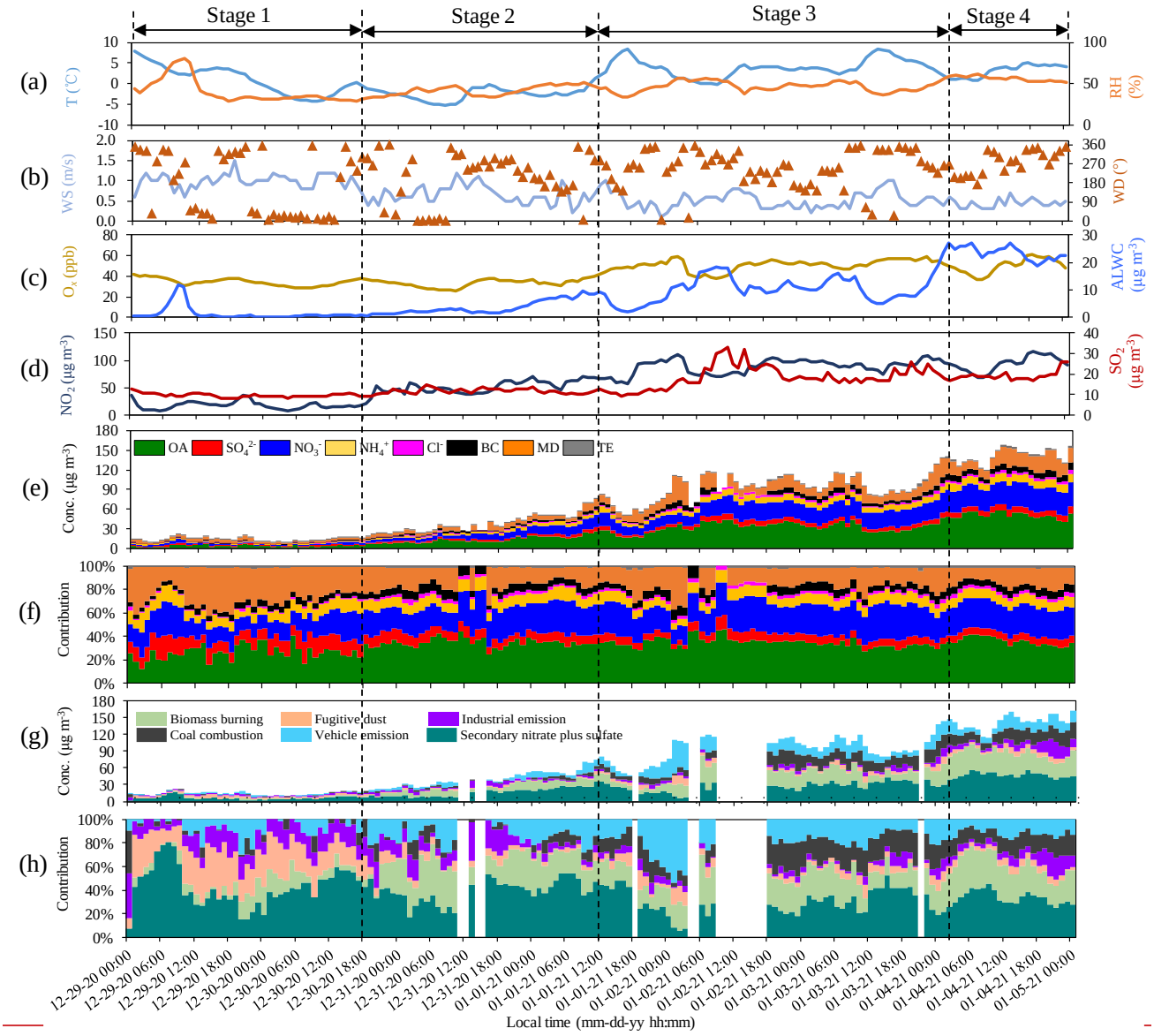
Stage 1
Stage 2
Stage 3
Stage 4
(a)
T (℃)
RH (%)
(b)
WS (m/s)
WD (°)
(c)
O_x (ppb)
ALWC (μg m^{-3})
(d)
NO_2 (μg m^{-3})
SO_2 (μg m^{-3})
(e)
Conc. (μg m^{-3})
OA
SO_4^{2-}
NO_3^-
NH_4^+
Cl^-
BC
MD
TE
(f)
Contribution
(g)
Conc. (μg m^{-3})
Biomass burning
Coal combustion
Fugitive dust
Vehicle emission
Industrial emission
Secondary nitrate plus sulfate
(h)
Contribution
12-29-20 00:00
12-29-20 06:00
12-29-20 12:00
12-29-20 18:00
12-30-20 00:00
12-30-20 06:00
12-30-20 12:00
12-30-20 18:00
12-31-20 00:00
12-31-20 06:00
12-31-20 12:00
12-31-20 18:00
01-01-21 00:00
01-01-21 06:00
01-01-21 12:00
01-01-21 18:00
01-02-21 00:00
01-02-21 06:00
01-02-21 12:00
01-02-21 18:00
01-03-21 00:00
01-03-21 06:00
01-03-21 12:00
01-03-21 18:00
01-04-21 00:00
01-04-21 06:00
01-04-21 12:00
01-04-21 18:00
01-05-21 00:00
Local time (mm-dd-yy hh:mm)

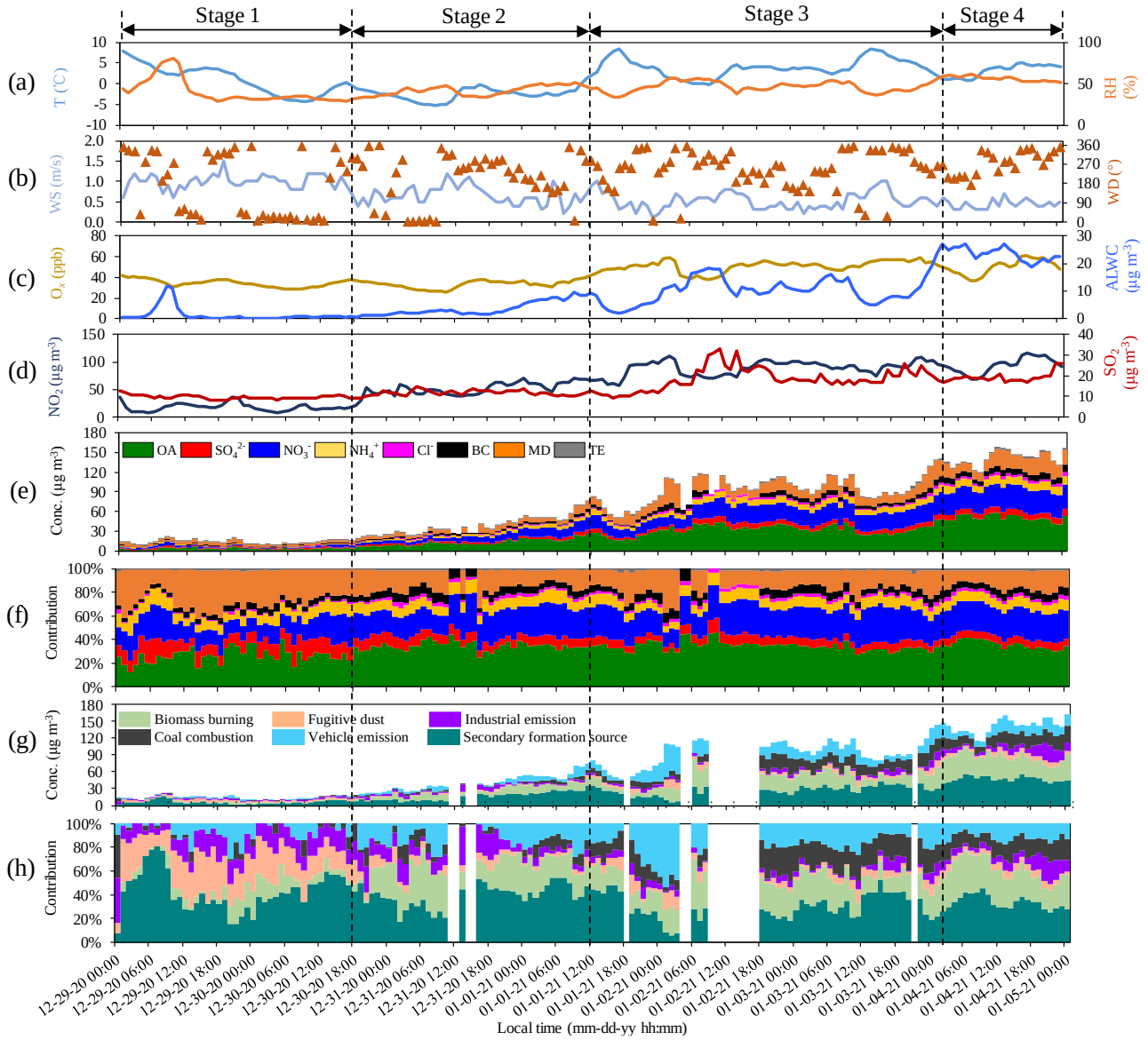

Figure ~~S16~~S18. Time series of T and RH (a), WS and WD (b), O_x and ALWC (c), NO_2 and SO_2 (d), chemical components (e, f), and source contribution (g, h) of $PM_{2.5}$ during EP2 in Xi'an.

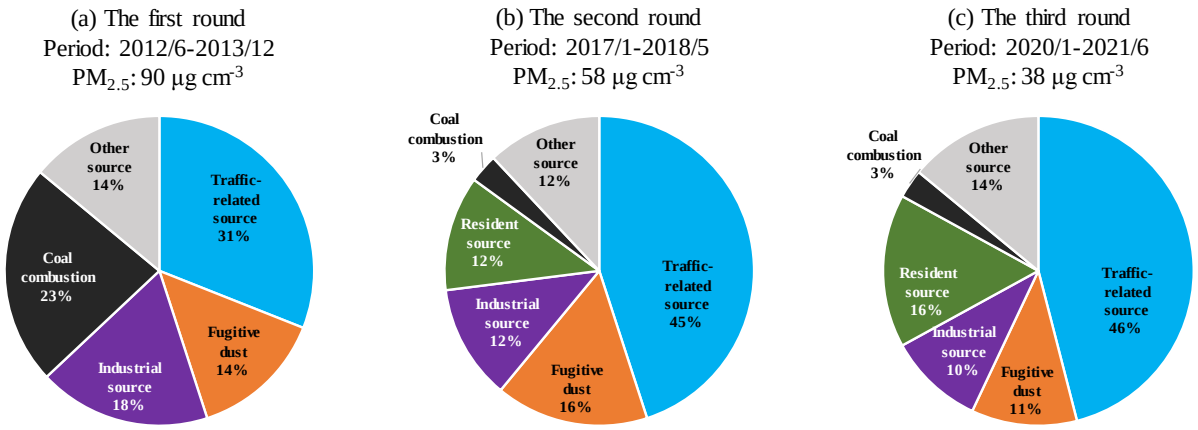

Figure S19. $PM_{2.5}$ sources apportionment in Beijing released by Beijing Municipal Ecology and Environment Bureau in the last decade (http://sthjj.beijing.gov.cn/so/s?tab=all&sourceCode=1100000122, in Chinese).

Table S1. Detailed information on complementary data for sampling sites

Sampling site	National Air Quality Monitoring Station	National Meteorological Station	complementary data
Xi'an	Gaoxinxiqu station, 1.1km from the sampling site	Haidian station, 7.6 km from the sampling site	hourly $PM_{2.5}$, NO_x, NO_2, CO, SO_2, O_3, WS, WD, T, RH
Shijiazhuang	Gaoxinqu station, 4.2 km from the sampling site	Shijiazhuang station, 23.8 km from the sampling site	hourly $PM_{2.5}$, NO_2, CO, SO_2, O_3, WS, WD, T, RH
Beijing	ChaoyangAotizhongxin station, 1.2 km from the sampling site	Jinghe station, 21.2 km from the sampling site	hourly $PM_{2.5}$, NO_2, CO, SO_2, O_3, WS, WD, T, RH

Note: WS: wind speed, WD: wind direction, T: temperature, RH: relative humidity.

Table S2. The $\Delta Q/Q_{exp}$[a] value with increasing factor number from two to ten of the runs in Xi'an, Shijiazhuang, and Beijing.

Parameter[b]	$\Delta Q/Q_{exp}$		
	Xi'an	Shijiazhuang	Beijing
F2-F3	1.3	1.8	5.7
F3-F4	0.9	2.2	2.3
F4-F5	1.1	1.2	1.9
F5-F6	0.4	0.3	1.5
F6-F7	0.3	0.3	1.5
F7-F8	0.2	0.2	0.3
F8-F9			0.4
F9-F10			0.3

[a] $\Delta Q/Q_{exp}$ means the difference of Q/Q_{exp} of two sequent factor numbers.

[b] Parameters represent the factor numbers (F) – (F+1).

Table S3. Sources diagnostics with increasing factor numbers from four to ten of the runs in Xi'an, Shijiazhuang, and Beijing.

Factor number	Sources identification		
	Xi'an	**Shijiazhuang**	**Beijing**
4	Secondary ~~nitrate plus sulfate~~formnation source mixed with biomass burning and coal burning mixed with industrial emission	i) Secondary ~~nitrate plus sulfate~~formation source mixed with primary sources including biomass burning and coal combustion ii) Biomass burning, coal combustion, and vehicle emission was also mixed	i) Secondary sources mixed with primary sources including biomass burning, coal combustion, and vehicle emission ii) Biomass burning and coal combustion was mixed
5	Secondary ~~nitrate plus sulfate~~foramtion source mixed with biomass burning	Biomass burning, coal combustion, and vehicle emissions were mixed	Secondary sulfate plus OA mixed with coal combustion and industrial emission; secondary nitrate plus OA mixed with biomass burning
6	Six individual sources were identified	Six individual sources were identified	Secondary sulfate plus OAmixed with coal combustion and secondary nitrate plus OA mixed with industrial emission
7	Vehicle emission was split into two profiles	Coal combustion was split into two profiles	Secondary sulfate plus OA mixed with coal combustion
8	Vehicle emission and industrial emission was split into two profiles, respectively.	Vehicle emission and coal combustion were split into two profiles, respectively.	Eight individual sources were identified
9			Coal combustion was split into two profiles
10			Coal combustion and biomass burning were split into two profiles, respectively.

Table S4. Average concentrations of reconstructed $PM_{2.5}$ and its chemical species in Xi'an, Shijiazhuang, and Beijing during the campaign* (μg m^{-3})

Chemical Species	Xi'an	Shijiazhuang	Beijing
Reconstructed $PM_{2.5}$	77 ± 47	60 ± 39	64 ± 57
OA	25.9 ± 18.0	16.0 ± 9.7	22.1 ± 18.1
SO_4^{2-}	5.2 ± 3.4	7.0 ± 7.6	9.6 ± 11.3
NO_3^-	18.5 ± 14.5	15.8 ± 12.5	15.2 ± 16.7
NH_4^+	6.2 ± 4.5	7.0 ± 5.5	9.2 ± 10.3
Cl^-	1.9 ± 1.5	2.8 ± 2.2	0.7 ± 0.8
BC	4.5 ± 3.2	3.9 ± 2.5	1.9 ± 1.8
MD[a]	13.2 ± 7.0	6.0 ± 4.0	4.8 ± 3.8
TE[b]	1.1 ± 0.7	1.0 ± 0.6	0.9 ± 1.5

* Data during Xact625 failure shown in Figure S2 was excluded to calculate average concentration of campaign

[a] MD means mineral dust, which is equal to 2.20Al + 2.49Si + 1.63Ca + 2.42Fe + 1.94Ti

[b] TE means trace elements which is equal to K + Cr + Mn + Ni + Cu + Zn + As +Se + Ba + Pb

Table S5. The nitrogen oxidation ratio (NOR) and sulfur oxidation ratio (SOR) in Xi'an, Beijing, and Shijiazhuang during the campaigns[a]

Parameters	Xi'an	Shijiazhuang	Beijing
NOR	0.15 ± 0.08	0.20 ± 0.11	0.16 ± 0.12
SOR	0.18 ± 0.08	0.36 ± 0.25	0.48 ± 0.23

[a] $NOR = n(NO_3^-)/(n(NO_3^-) + n(NO_2))$; $SOR = n(SO_4^{2-})/(n(SO_4^{2-}) + n(SO_2))$. where $n(NO_3^-)$, $n(NO_2)$, $n(SO_4^{2-})$, and $n(SO_2)$ are the molar concentrations of NO_3^-, NO_2, SO_4^{2-}, and SO_2, respectively.

Table S6. Average concentrations of SOA in Xi'an, Shijiazhuang, and Beijing during sampling periods estimated by BC-tracer method and source apportionment results (μg m^{-3})

SOA	Xi'an	Shijiazhuang	Beijing
$SOA_{\_BC\text{-}tracer}$	5.1 ± 5.8	4.2 ± 4.4	8.0 ± 9.0
$SOA_{\_source\ apportionment}$	6.0 ± 4.1	4.6 ± 2.8	8.2 ± 6.7

Table ~~S6~~S7. The concentration of $PM_{2.5}$ and its main chemical components during wintertime in Xi'an, Shijiazhuang, and Beijing in the last decades.

City	Year	$PM_{2.5}$	OA[a]	EC	SO_4^{2-}	NO_3^-	NH_4^+	Others	References
		μg m^{-3}	μg m^{-3}	μg m^{-3}	μg m^{-3}	μg m^{-3}	μg m^{-3}	μg m^{-3}	
Xi'an	2003	356	153.3	21.5	53.8	29.2	29.6	68.9	Cao et al., 2012
	2006	230	57.4	11.4	45.9	20.6	14.2	80.0	Xu et al., 2016
	2008	199	48.3	9.9	42.5	20.8	11.0	66.9	Xu et al., 2016
	2010	233	60.0	14.7	30.6	22.9	12.3	92.8	Xu et al., 2016
	2012	196	56.3	8.2	27.0	19.2	13.3	71.9	Zhang et al., 2015
	2013	263	45.8	7.1	31.7	29.2	17.1	132.5	Niu et al., 2016
	2014	156	57.4	2.5	16.2	20.6	9.4	49.7	Dai et al., 2018
	2018	189	42.1	4.9	9.7	14.5	6.6	111.0	Wang et al., 2022
	2020*	77	25.9	4.5	5.2	18.5	6.2	16.2	This study
Shijiazhuang	2010	227	75.6	12.2	33.2	25.3	10.5	70.2	Zhao et al., 2013
	2015	232	82.0	16.3	26.6	27.4	19.8	59.7	Huang et al., 2017
	2016	193	63.2	13.5	29.5	24.0	17.0	45.8	Liu et al., 2019
	2017	97	31.2	6.5	12.5	16.5	12.5	17.8	Liu et al., 2019
	2018	96	35.8	10.1	10.5	15.3	6.3	18.0	Zhang et al., 2020
	2022*	60	16.0	3.9	7.0	15.8	7.0	9.8	This study
Beijing	2001	122	51.5	11.3	9.9	10.7	7.1	31.5	Duan et al., 2006
	2003	116	38.2	6.2	20.0	13.1	9.4	29.1	Cao et al., 2012
	2004	107	53.8	8.3	12.7	8.3	6.0	17.9	Song et al., 2007
	2010	127	42.9	7.1	14.2	17.1	5.2	40.5	Zhao et al., 2013
	2013	132	38.5	6.4	21.9	18.5	15.1	31.6	Tao et al., 2015
	2014	138	46.4	5.2	21.0	26.0	14.1	25.3	Ma et al., 2017
	2016	130	75.7	20.2	12.3	5.5	10.5	5.3	Xu et al., 2018
	2021*	64	22.1	1.9	9.6	15.2	9.2	6.4	This study

* study was conducted on online monitoring equipment, and the rest studies were researched on filter sampling experiments.

[a] Assumption of OA = 1.6 × OC for the filter-based sampling experiments

Table ~~S7~~S8. The concentration of $PM_{2.5}$ and its source contribution during wintertime in Xi'an, Shijiazhuang, and Beijing in the last decades.

City	Year	$PM_{2.5}$	Vehicle emission	Coal combustion	Secondary formation source	Fugitive dust	Industrial emission	Biomass burning	Others	References
		μg m^{-3}	μg m^{-3}	μg m^{-3}	μg m^{-3}	μg m^{-3}	μg m^{-3}	μg m^{-3}	μg m^{-3}	
Xi'an	2006	392	74.5	121.5	82.3	51.0	39.2	23.5		Xu et al., 2016
	2008	199	41.8	55.7	45.8	23.9	21.9	10.0		Xu et al., 2016
	2010	233	48.9	55.9	41.9	44.3	30.3	11.7		Xu et al., 2016
	2014	169	20.3	47.3	71.0	8.5	6.8	15.2		Dai et al., 2020
	2018	189	26.5	28.4		15.1	22.7	58.6	37.8	Wang et al., 2022
	2020*	77	10.0	11.6	24.6	6.2	6.2	19.3		This study
Shijiazhuang	2015	232	46.4	62.6	30.2	20.9	16.2	7.0	48.7	Huang et al., 2017
	2016	181	23.5	54.3	54.3	30.8	9.1		7.2	Liu et al., 2018
	2019	119	21.4	21.4	42.8	21.4	6.0	6.0		Diao et al., 2021
	2022*	60	7.2	9.6	22.8	2.4	3.0	14.4		This study
Beijing	2004	107	8.6	40.7	19.3	7.5		16.1	15.0	Song et al., 2007
	2010	139		79.2	8.3	22.2	16.7	9.7	2.8	Zhang et al., 2013
	2013	159	9.5	41.3	79.5	15.9		9.5	3.2	Huang et al., 2014
	2015	125	48.8	15.0	23.8	8.8	2.5	6.3	18.8	Huang et al., 2017
	2021*	64	7.0	5.8	33.3	2.6	2.6	11.5	1.3	This study

* study was conducted on online monitoring equipment, and the rest studies were researched on filter sampling experiments.

References:

Cao, J.-J., Shen, Z.-X., Chow, J. C., Watson, J. G., Lee, S.-C., Tie, X.-X., Ho, K.-F., Wang, G.-H., and Han, Y.-M.: Winter and summer $PM_{2.5}$ chemical compositions in fourteen Chinese cities, J. Air Waste Manage., 62, 1214–1226, https://doi.org/10.1080/10962247.2012.701193, 2012.

Chen, L., Lowenthal, D., Watson, J., Koracin, D., Kumar, N., Knipping, E., Wheeler, N., Craig, K., Reid, S.: Toward effective source apportionment using positive matrix factorization: experiments with simulated $PM_{2.5}$ data. J. Air Waste Manage., 60(1), 43–54, https://doi.org/10.3155/1047-3289.60.1.43, 2010.

Dai, Q., Bi, X., Liu, B., Li, L., Ding, J., Song, W., Bi, S., Schulze, B. C., Song, C., Wu, J., Zhang, Y., Feng, Y., and Hopke, P. K.: Chemical nature of $PM_{2.5}$ and PM_{10} in Xi'an, China: Insights into primary emissions and secondary particle formation, Environ. Pollut., 240, 155–166, https://doi.org/10.1016/j.envpol.2018.04.111, 2018.

Dai, Q., Hopke, P. K., Bi, X., and Feng, Y.: Improving apportionment of $PM_{2.5}$ using multisite PMF by constraining G-values with a prioriinformation, Sci. Total Environ., 736, 139657, https://doi.org/10.1016/j.scitotenv.2020.139657, 2020.

Diao, L., Zhang, H., Liu, B., Dai, C., Zhang, Y., Dai, Q., Bi, X., Zhang, L., Song, C., and Feng, Y.: Health risks of inhaled selected toxic elements during the haze episodes in Shijiazhuang, China: Insight into critical risk sources, Environ. Pollut., 276, 116664, https://doi.org/10.1016/j.envpol.2021.116664, 2021.

Duan, F., He, K., Ma, Y., Yang, F., Yu, X., Cadle, S., Chan, T., and Mulawa, P.: Concentration and chemical characteristics of $PM_{2.5}$ in Beijing, China: 2001–2002, Sci. Total Environ., 355, 264–275, https://doi.org/10.1016/j.scitotenv.2005.03.001, 2006.

Huang, R.-J., Zhang, Y., Bozzetti, C., Ho, K.-F., Cao, J.-J., Han, Y., Daellenbach, K. R., Slowik, J. G., Platt, S. M., Canonaco, F., Zotter, P., Wolf, R., Pieber, S. M., Bruns, E. A., Crippa, M., Ciarelli, G., Piazzalunga, A., Schwikowski, M., Abbaszade, G., Schnelle-Kreis, J., Zimmermann, R., An, Z., Szidat, S., Baltensperger, U., Haddad, I. E., and Prévôt, A. S. H.: High secondary aerosol contribution to particulate pollution during haze events in China, Nature, 514, 218–222, https://doi.org/10.1038/nature13774, 2014.

Huang, X., Liu, Z., Liu, J., Hu, B., Wen, T., Tang, G., Zhang, J., Wu, F., Ji, D., Wang, L., and Wang, Y.: Chemical characterization and source identification of $PM_{2.5}$ at multiple sites in the Beijing–Tianjin–Hebei region, China, Atmos. Chem. Phys., 17, 12941–12962, https://doi.org/10.5194/acp-17-12941-2017, 2017.

Liu, B., Cheng, Y., Zhou, M., Liang, D., Dai, Q., Wang, L., Jin, W., Zhang, L., Ren, Y., Zhou, J., Dai, C., Xu, J., Wang, J., Feng, Y., and Zhang, Y.: Effectiveness evaluation of temporary emission control action in 2016 in winter in Shijiazhuang, China, Atmos. Chem. Phys., 18, 7019–7039, https://doi.org/10.5194/acp-18-7019-2018, 2018.

Liu, G., Xin, J., Wang, X., Si, R., Ma, Y., Wen, T., Zhao, L., Zhao, D., Wang, Y., and Gao, W.: Impact of the coal banning zone on visibility in the Beijing-Tianjin-Hebei region, Sci. Total Environ., 692, 402–410, https://doi.org/10.1016/j.scitotenv.2019.07.006, 2019.

Liu, H., Wang, Q., Ye, J., Su, X. li, Zhang, T., Zhang, Y., Tian, J., Dong, Y., Chen, Y., Zhu, C., Han, Y., and Cao, J.: Changes in Source-Specific Black Carbon Aerosol and the Induced Radiative Effects Due to the COVID-19 Lockdown, Geophys. Res. Lett., 48, https://doi.org/10.1029/2021GL092987, 2021.

Ma, Q., Wu, Y., Tao, J., Xia, Y., Liu, X., Zhang, D., Han, Z., Zhang, X., and Zhang, R.: Variations of Chemical Composition and Source Apportionment of $PM_{2.5}$ during Winter Haze Episodes in Beijing, Aerosol Air Qual. Res., 17, 2791–2803, https://doi.org/10.4209/aaqr.2017.10.0366, 2017.

Niu, X., Cao, J., Shen, Z., Ho, S. S. H., Tie, X., Zhao, S., Xu, H., Zhang, T., and Huang, R.: $PM_{2.5}$ from the Guanzhong Plain: Chemical composition and implications for emission reductions, Atmos. Environ., 147, 458–469, https://doi.org/10.1016/j.atmosenv.2016.10.029, 2016.

Rai, P., Furger, M., Slowik, J. G., Canonaco, F., Fröhlich, R., Hüglin, C., Minguillón, M. C., Petterson, K., Baltensperger, U., and Prévôt, A. S. H.: Source apportionment of highly time-resolved elements during a firework episode from a rural freeway site in Switzerland, Atmos. Chem. Phys., 20, 1657–1674, https://doi.org/10.5194/acp-20-1657-2020, 2020.

Salameh, D., Pey, J., Bozzetti, C., El Haddad, I., Detournay, A., Sylvestre, A., Canonaco, F., Armengaud, A., Piga, D., Robin, D., Prevot, A. S. H., Jaffrezo, J.-L., Wortham, H., and Marchand, N.: Sources of $PM_{2.5}$ at an urban-industrial Mediterranean city, Marseille (France): Application of the ME-2 solver to inorganic and organic markers, Atmos. Res., 214, 263–274, https://doi.org/10.1016/j.atmosres.2018.08.005, 2018.

Salameh, T., Sauvage, S., Afif, C., Borbon, A., and Locoge, N.: Source apportionment vs. emission inventories of non-methane hydrocarbons (NMHC) in an urban area of the Middle East: local and global perspectives, Atmos. Chem. Phys., 16, 3595–3607, https://doi.org/10.5194/acp-16-3595-2016, 2016.

Shrivastava, M., Cappa, C., Fan, J., Goldstein, A., Guenther, A., Jimenez, J., Kuang, C., Laskin, A., Martin S., Ng, N., Petaja, T., Pierce, J., Rasch, P., Roldin, P., Senfeld, J., Shiling, J., Smith, J., Thornton, J., Volkamer, R., Wang, J., Worsnop, D., Zaveri, R., Zelenyuk, A., Zhang, Q.: secondary organic aerosol: Implications for global climate forcing. Rev. Geophys., 55, 509–559. https://doi.org/10.1002/2016RG000540, 2017.

Song, Y., Tang, X., Xie, S., Zhang, Y., Wei, Y., Zhang, M., Zeng, L., and Lu, S.: Source apportionment of $PM_{2.5}$ in Beijing in 2004, J. Hazard. Mater., 146, 124–130, https://doi.org/10.1016/j.jhazmat.2006.11.058, 2007.

Tao, J., Zhang, L., Gao, J., Wang, H., Chai, F., and Wang, S.: Aerosol chemical composition and light scattering during a winter season in Beijing, Atmos. Environ., 110, 36–44, https://doi.org/10.1016/j.atmosenv.2015.03.037, 2015.

Wang, Q.; Han, Y.; Ye, J.; Liu, S.; Pongpiachan, S.; Zhang, N.; Han, Y.; Tian, J.; Wu, C.; Long, X.; Zhang, Q.; Zhang, W.; Zhao, Z.; Cao, J.: High Contribution of secondary brown carbon to aerosol light absorption in the southeastern margin of Tibetan Plateau. Geophys. Res. Lett. 46, 4962−4970, https://doi.org/10.1029/2019GL082731, 2019.

Wang, Z., Wang, R., Wang, J., Wang, Y., McPherson Donahue, N., Tang, R., Dong, Z., Li, X., Wang, L., Han, Y., and Cao, J.: The seasonal variation, characteristics and secondary generation of $PM_{2.5}$ in Xi'an, China, especially during pollution events, Environ. Res., 212, 113388, https://doi.org/10.1016/j.envres.2022.113388, 2022.

Xu, H., Cao, J., Chow, J. C., Huang, R.-J., Shen, Z., Chen, L. W. A., Ho, K. F., and Watson, J. G.: Inter-annual variability of wintertime $PM_{2.5}$ chemical composition in Xi'an, China: Evidences of changing source emissions, Sci. Total Environ., 545–546, 546–555, https://doi.org/10.1016/j.scitotenv.2015.12.070, 2016.

Xu, X., Zhang, H., Chen, J., Li, Q., Wang, X., Wang, W., Zhang, Q., Xue, L., Ding, A., and Mellouki, A.: Six sources mainly contributing to the haze episodes and health risk assessment of $PM_{2.5}$ at Beijing suburb in winter 2016, Ecotoxicol. Environ. Saf., 166, 146–156, https://doi.org/10.1016/j.ecoenv.2018.09.069, 2018.

Zhang, Q., Shen, Z., Cao, J., Zhang, R., Zhang, L., Huang, R.-J., Zheng, C., Wang, L., Liu, S., Xu, H., Zheng, C., and Liu, P.: Variations in $PM_{2.5}$, TSP, BC, and trace gases (NO_2, SO_2, and O_3) between haze and non-haze episodes in winter over Xi'an, China, Atmos. Environ., 112, 64–71, https://doi.org/10.1016/j.atmosenv.2015.04.033, 2015.

Zhang, R., Jing, J., Tao, J., Hsu, S.-C., Wang, G., Cao, J., Lee, C. S. L., Zhu, L., Chen, Z., Zhao, Y., and Shen, Z.: Chemical characterization and source apportionment of $PM_{2.5}$ in Beijing: seasonal perspective, Atmos. Chem. Phys., 13, 7053–7074, https://doi.org/10.5194/acp-13-7053-2013, 2013.

Zhang, W., Liu, B., Zhang, Y., Li, Y., Sun, X., Gu, Y., Dai, C., Li, N., Song, C., Dai, Q., Han, Y., and Feng, Y.: A refined source apportionment study of atmospheric $PM_{2.5}$ during winter heating period in Shijiazhuang, China, using a receptor model coupled with a source-oriented model, Atmos. Environ., 222, 117157, https://doi.org/10.1016/j.atmosenv.2019.117157, 2020.

Zhao, P. S., Dong, F., He, D., Zhao, X. J., Zhang, X. L., Zhang, W. Z., Yao, Q., and Liu, H. Y.: Characteristics of concentrations and chemical compositions for $PM_{2.5}$ in the region of Beijing, Tianjin, and Hebei, China, Atmos. Chem. Phys., 13, 4631–4644, https://doi.org/10.5194/acp-13-4631-2013, 2013.